UNIVERSITA' DEGLI STUDI ROMA TRE

DIPARTIMENTO DI SCIENZE

Scuola di Dottorato di Ricerca in

SCIENZE DEI MATERIALI, NANOTECNOLOGIE E SISTEMI COMPLESSI

XXXII° CICLO

Correlation between calcium signaling and ATP release mediated by connexin hemichannels in different mouse models of disease

Flavia Mazzarda

Relatori:

Prof. Fabio Mammano

Prof. Fabio Bruni

”Oh tell me Lord how could it be,
That though our cells make ATP,
It’s not all used for energy,
But sometimes is secreted free.
It puzzles you, it puzzles me,
While Geoffrey Burnstock smiles with glee
At the many roles of ATP.”

Samuel C. Silverstein, 1989

Acknowledgments

Foremost, I would like to express my special thanks and gratitude to my supervisors Prof. Fabio Mammano who gave me the opportunity to be part of this project and for his constant support, and to Prof. Fabio Bruni for his support and immense knowledge. Besides my supervisors, I would like to thank Anna Maria Salvatore for introducing me in the research world and for the stimulating discussions.

Secondly, I would like to thank all the people that work in EMMA, in particular Marcello Raspa, Fabrizio Bonaventura, Ilaria Losso, Alessandro Grop and Simone Manghisi for their technical support and constant helpfulness.

My sincere gratitude also goes to my friends and fellow labmates: Chiara Peres, Gaia Ziraldo, Veronica Zorzi e Chiara Nardin. I learned a lot from each of them.

Last but not the least, I would like to thank my family: my parents Giacomo e Cristiana and my sister Emilia, without them all this would not be possible and Alex, who always believes in me.

Funding: this work was partially supported by grants to prof. Fabio Mammano: National Research Council of Italy (CNR), Grant No.DSB.AD008.370.003\TERABIO-IBCN; Italian Ministry of Health, Project Code RF-2011-02348435 (Principal Investigator: Prof. Francesco Di Virgilio, University of Ferrara).

Table of Contents

Summary

The hypothesis that adenosine triphosphate (ATP) is used as a messenger for cell-to-cell communication, formulated in the 1990', is now widely accepted [1]. Recent studies pointed out that the alteration of the mechanisms of ATP release, with the consequent alteration of calcium (Ca^{2+}) signaling, could lead to numerous diseases [2]. The understanding of the relation between Ca^{2+} signaling and ATP release is fundamental for the development of new therapeutic strategies. In this thesis, we focused on the study of purinergic signaling in the developing cochleae and tumor microenvironment (TME).

During pre-hearing stages of development in mice, periodic transient elevations of cytosolic free Ca^{2+} concentration occur spontaneously in the greater epithelial ridge (GER) and propagate as intercellular Ca^{2+} waves invading variable portions of the GER [3]. Prior works indicate that intercellular Ca^{2+} waves in the GER rely on the interplay between inositol-1,4,5-trisphosphate (IP3), generated intracellularly, and ATP, released extracellularly. A vast body of data supports the hypothesis that, in the developing cochlea, ATP is released through connexin hemichannels [4], however a direct proof is still lacking.

To test this hypothesis, we generated ATP cell-based biosensors (ATP- BCs) stably expressing P2Y2 purinergic receptors (P2Y2R) and sensitive to ATP in the nM range. We also designed and built a closed microfluidic chamber (10 µl max. volume) to put in close contact the cochlea with the ATP-BCs plated on the transparent roof of the chamber and facing the fluid interior of the chamber. These ATP-BCs sited at less than 100 µm from the surface of a cochlear organotypic culture plated on the chamber bottom. After loading both biosensor cells and cochlea with Ca^{2+}-selective dyes, this architecture and the multi-photon microscope allowed us to monitor Ca^{2+} responses in ATP-BCs during propagation of stimulated Ca^{2+} waves in the GER of the cochlea underneath. Ca^{2+} signals disappeared on both cochlea and ATP-BCs upon replacing ARL67156 (100 µM, an inhibitor of ectonucleotidases) with apyrase (40 U/ml, an enzyme that catalyzes the sequential hydrolysis of ATP) in the extracellular medium, confirming that ATP mediated Ca^{2+} wave propagation in the GER. To determine the source of the released ATP, we tested cochlear organotypic cultures from two different mutant mice with global deletion of pannexin 1 ($Panx1^{-/-}$), and of connexin 30 ($Cx30^{-/-}$). Using the microfluidic chamber, we determined that Ca^{2+} signals in the ATP-BCs were the same irrespective of whether they faced $Panx1^{-/-}$ or age-matched $Panx1^{+/+}$ cochlear cultures. In contrast, Ca^{2+} signals were strongly depressed in presence of $Cx30^{-/-}$ cultures. Together, these results validate our working hypothesis and confirm that connexin hemichannels are the major players of ATP release process that mediates Ca^{2+} wave propagation in the GER.

We also explored the possibility of using ATP-BCs to detect extracellular ATP in the tumor microenvironment with promising results. Replacing the fluid trapped between the ATP-BCs and the tumor with a solution containing apyrase, the responses of ATP-BCs were abolished showing that our tool is one of the few probes suitable for the *in vivo* detection of extracellular ATP [5].

Finally, we investigated the role of the P2X7 purinergic receptor (P2X7R) in tumor angiogenesis through micro-computed tomography (micro-CT). For this purpose, we inoculated parental B16-F10 or B16-F10 P2X7R-silenced (shRNA P2X7R) cells in wild type (WT) and P2X7 knock out (KO) mice and we compared the micro-CT measurements after the perfusion with Microfil compound. The data

suggests that tumors derived from inoculation of B16 WT cells in WT mice are more angiogenic compared with the others, thus supporting the hypothesis that this receptor is involved in the release of the vascular endothelial growth factors (VEGF) [6].

1. Introduction

1.1 ATP as signaling molecule

The proposal that purine nucleotides are extracellular signaling molecules, as well as an intracellular energy sources, was first reported by Drury and Szent-Gyorgyi [7]. Although the term 'purinergic' signaling was introduced in 1972 [8], this concept was not well accepted until the 1990's when receptor subtypes for purines and pyrimidines were cloned and characterized. Two families of purinergic receptors have been defined to date, namely P1 and P2 receptors (Figure 1.1) [1]. P1 receptors belong to the superfamily of seven transmembrane receptors which are subdivided into A1, A2A, A2B and A3 receptor subtypes [1]. These receptors bind extracellular adenosine with different affinities [9]. The P2 receptor family is subdivided in two subfamilies, namely P2X and P2Y [10, 11, 12]. P2X receptors are ligand-gated ion channels of which seven subtypes have been characterized (P2X1–7) [13, 14]; P2Y receptors are seven transmembrane receptors of which eight subtypes have been identified (P2Y1, 2, 4, 6, 11–14) [11, 15, 16]. Ligands for these receptors and their affinities are reported in Figure 1.1. Purinoreceptors are widely distributed throughout living cells and tissues [12].

ATP fulfills all requirements for a true extracellular messenger: it is present in minute amounts (nmol/l) in the extracellular space under physiological conditions and, on the contrary, it is stored intracellularly to very high amounts (from 5 to 10 mmol/l).

Subtype	Physiologic ligands	Subtype	Physiologic ligands	Subtype	Physiologic ligands
P1 receptors		*P2 receptors*		*P2Y*	
A_1	Ado (EC_{50}: 0.18–0.53 μM) Inosine (EC_{50}: 290 μM)	*P2X*		$P2Y_1$	ADP (EC_{50}: 8 μM)
		$P2X_1$	ATP (EC_{50}: 0.05–1 μM)		
A_{2A}	Ado (EC_{50}: 0.56–0.95 μM) Inosine (EC_{50}: 50 μM)			$P2Y_2$	UTP (EC_{50}: 0.14 μM) = ATP (EC_{50}: 0.23 μM)
		$P2X_2$	ATP (EC_{50}: 1–30 μM)		
A_{2B}	Ado (EC_{50}: 16.2–64.1 μM)	$P2X_3$	ATP (EC_{50}: 0.3–1 μM)		
		$P2X_4$	ATP (EC_{50}: 1–10 μM)	$P2Y_4$	UTP (EC_{50}: 2.5–2.6 μM) ≫ ATP, UDP
A_3	Ado (EC_{50}: 0.18–0.53 μM) Inosine (EC_{50}: 0.03–2.5 μM)	$P2X_5$	ATP (EC_{50}: 1–10 μM)	$P2Y_6$	UDP (EC_{50}: 0.3 μM) ≫ UTP (EC_{50}: 6 μM)
		$P2X_6$	ATP (EC_{50}: 1–12 μM)	$P2Y_{11}$	ATP (EC_{50}: 17 μM)
		$P2X_7$	ATP (EC_{50}: 100–780 μM)		
				$P2Y_{12}$	ADP (EC_{50}: 0.07 μM)
				$P2Y_{13}$	ADP (EC_{50}: 0.06 μM) > ATP (EC_{50}: 0.26 μM)
				$P2Y_{14}$	UDP-glucose (EC_{50}: 0.1–0.5 μM)

Figure 1.1: Physiological ligands and affinities of purinergic receptors: adapted from Ref. [9].

This trans-plasma membrane concentration gradient may cause large responses when ATP is released. Furthermore, ATP is water soluble which permits rapid diffusion through the aqueous tissue interstitium. Finally ATP is quickly degraded by extracellular ecto-nucleotide enzymes that terminate

its signaling action to avoid overstimulation. Thus, ATP molecules in the extracellular compartment are finely controlled by enzymes catalyzing their conversion (Figure 1.2) [17, 18, 19]. These so-called ecto-enzymes are located on cell surfaces or may be found in soluble form in the interstitial medium or in body fluids. The currently known ectoenzymes, which are involved mainly in the breakdown of extracellular ATP, include four families that partially share tissue distribution and substrate specificity: (1) the ectonucleoside triphosphate diphosphohydrolase (E-NTPDase) family (that includes CD39), (2) the ectonucleotide pyrophosphatase/phosphodiesterase (E-NPP) family, (3) the alkaline phosphatases, and (4) the ecto-5'-nucleotidase (e.g. CD73).

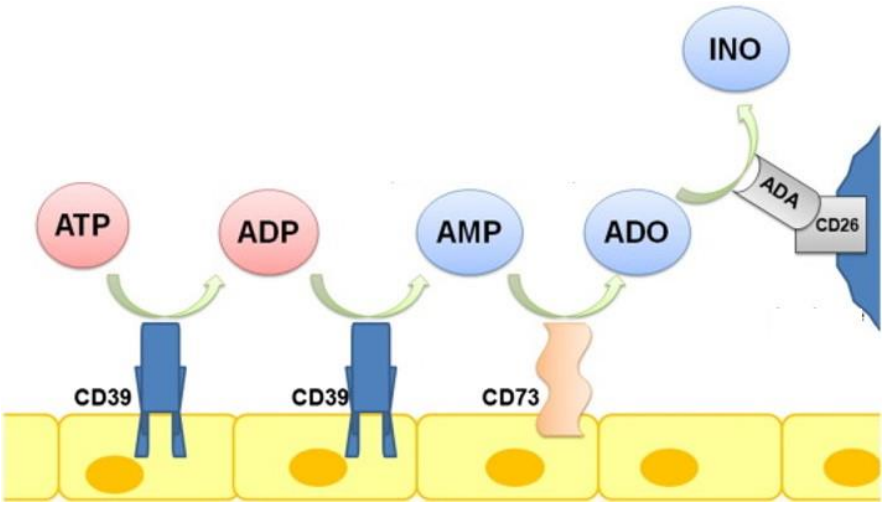

Figure 1.2: Extracellular ATP metabolism: adapted from Ref. [20]. ATP = adenosine triphosphate, ADP = adenosine diphosphate, AMP = adenosine monophosphate, ADO = adenosine, INO = inosine; CD39, CD73, CD26 and ADA are ecto-nucleotide enzymes.

At present, ATP purinergic signaling is recognized as a widespread mechanism for cell-to-cell communication in living organisms. In particular, this molecule is fundamental for peripheral and central nervous systems [21] but it is also a powerful extracellular messenger to non-neuronal cells, including secretory, exocrine and endocrine, endothelial, immune, musculo-skeletal and inflammatory cells [12] and is involved in a series of cellular pathways such as proliferation, differentiation, migration and death in development and regeneration [22]. Particularly in the immune system, ATP and its breakdown product adenosine perform an important modulator role of the immune responses on both immune and non-immune cells. [23, 24].

More recently, the focus has been on the pathophysiology and therapeutic potential of both P1 [25, 26, 27, 28, 29] and P2 [2, 30, 31, 32] receptors. Reviews focused on different aspects of purinergic pathophysiology are also available, including inflammatory and immune disorders [33, 34, 35]; cancer [36, 37]; P2X7 receptors as therapeutic targets [38] and pain [39].

1.2 ATP release conduits and mechanisms

The mechanism of ATP release is incompletely characterized, despite the many pathways (connexins, pannexins, ABC transporters and secretory granules) identified in different cell types [40]. Here we summarized some of these mechanisms reported in Figure 1.3.

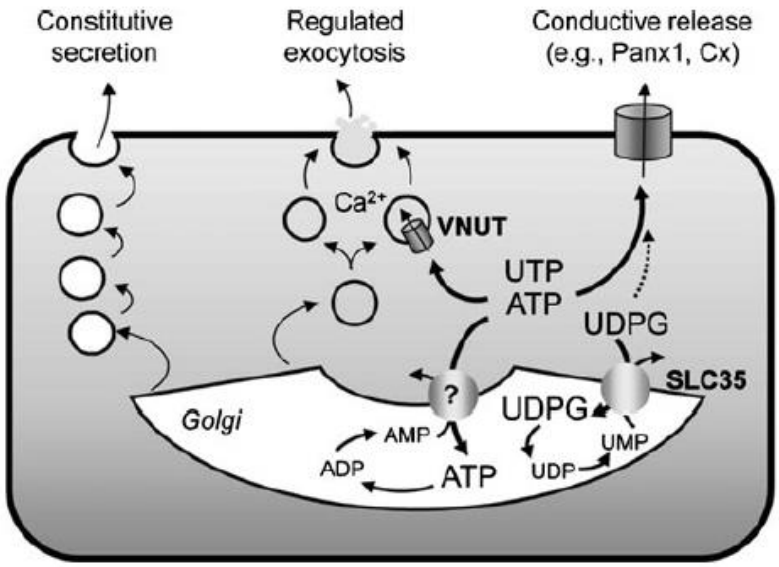

Figure 1.3: Potential pathways for nucleotide release: from Ref. [40]. Several candidate ATP conducting channels, including connexins (Cx) and pannexin 1 (Panx1) efflux cytosolic ATP out of the cells. Vesicular nucleotide transporter (VNUT) transports ATP into granules and vesicles competent for Ca^{2+} regulated exocytosis. ATP enters the secretory pathway via endoplasmic reticulum/Golgi resident solute carrier-like transporters (SLC35).

Connexin hemichannels

Connexins (Cx) are a large family of homologous vertebrate proteins that post-translationally oligomerize into hexameric structures [41, 42]. Once trafficked to the plasma membrane, a connexin hexamer (also known as connexon) can function as an independent channel, also called hemichannel, and mediates the movement of molecules such as ions, nucleotides or small metabolites between the cytosolic compartment and the extracellular milieu [43]. Alternatively, one connexon can dock head-to-head with another compatible connexon located on an adjacent cell, forming a direct cell-cell communication conduit named intercellular gap junction channel (IGJC) [44, 45]. More than 20 human connexin isoforms have been identified, with predicted molecular masses ranging from 23 to 62 kDa [46, 47].

Most connexin hemichannels exhibit permeability to ATP and small dyes (e.g., propidium and ethidium iodide and Lucifer Yellow). Opening of connexins can be induced by membrane depolarization, typically in the 40–60 mV range [48]. Ionized calcium (Ca^{2+}) destabilizes the open state of the hemichannels keeping the opening probability very low at normal extracellular concentration (around 1.8 mM). Conversely, reduction of extracellular Ca^{2+} to levels below 0.5 mM promotes the opening of most connexin hemichannel isoforms (i.e. Cx26, Cx32, Cx43, Cx46, Cx50) [49, 50, 51, 52, 53].

The involvement of connexin hemichannels in the release of ATP was first suggested by Nedergaard and co-workers [54], who observed that lowering the extracellular Ca^{2+} concentration promoted the

uptake of the fluorescent probe propidium iodide in cells overexpressing human Cx32 or Cx43, as well as ATP release from the same cells. The cytosolic free Ca^{2+} ($[Ca^{2+}]_c$) also plays a role in hemichannel gating. Indeed, De Vuyst et al. [55, 56] reported a bell-shaped dependence for ATP release and propidium iodide uptake with a peak at $[Ca^{2+}]_c \sim 500nM$ in cells overexpressing Cx32 and Cx43. It is currently thought that intracellular Ca^{2+} triggers connexin hemichannel opening via multiple (and only partially characterized) signaling steps [57]. Moreover, ATP release mediated by open hemichannels has been linked to a variety of pathophysiological responses in connexin-deficient mice, such as ischemia and epilepsy [58, 59], deafness [43, 60], skin disorder [61] and impaired activation of the immune system [62, 63]. Summarizing, physiological, pharmacological and genetic evidences support the hypothesis that connexin hemichannels contribute to ATP release in a variety of cell types.

Pannexin channels

Pannexins are a class of proteins forming plasma membrane channels (named pannexons) that, akin connexin hemichannels, are permeable to small dyes and ATP [64]. Despite the lack of homology between connexin and pannexin primary amino acid sequences, they strikingly share a similar structure and membrane topology. However, unlike connexons, pannexons in mammalian cells do not assemble into gap junctions [65].

Pannexin1 (Panx1), which requires 6 subunits to form a functional channel [66], is the most thoroughly characterized member of the pannexin family [67, 68, 69] (which includes also Panx2 and Panx3). Panx1 distribution is widespread and, in most cell types and tissues, is broadly shared with that of connexins [67]. Moreover, permeability profiles, channel conductance and pharmacological characteristics of connexins and pannexins partially overlap [70], with the notable differences that Panx1 channels are insensitive to changes of the extracellular Ca^{2+} concentration [71].

A number of studies support the notion that Panx1 is involved in the regulated release of ATP from viable mammalian cells proved through pharmacological inhibitors [40, 72] or through mutant mouse models [40, 73]. Clearly, the opening of such as a large, non-selective channel as Panx1 may collapse the ion gradients across the cell plasma membrane, resulting in cell death. Indeed, ATP release via pannexins is associated to hypotonic cell swelling and apoptosis [73, 74, 75, 76]. More recently, it has been proposed from Qiu and Dahl [77] that ATP release acts as negative feedback on Panx1, binding to and preventing deleterious long-lasting opening of the channel. An alternative possibility is that Panx1 interacts with a different ATP/dye channel or transporter such as P2X7 receptors, as suggested in Refs. [71, 78].

To date, because of controversial publications and cell-specific responses, the correlation between Panx1 and ATP release remains unclear in most tissues.

One of the object of this thesis is to shed light on the role of Panx1 in the particular environment of the developing cochlea and the hearing acquisition. Due to conflicts in published results the physiological function of Panx1 expressed in the mammalian inner ear [79, 80, 81] remains unclear. Panx1, which is predominantly expressed in the supporting cells of the organ of Corti (responsible for sound transduction), has been claimed to dominate ATP release in the cochlea [82]. Specifically Chen and co- workers [82] reported that ATP release was reduced (by ~8-fold) in Foxg1- Cre-Panx1 mice compared to WT siblings. Oddly, these mice also exhibited hearing loss, as determined by auditory brainstem response (ABR) measurements. In contrast, three other mouse strains that are proven

global knockouts of Panx1 (including the Panx1$^{-/-}$ mice [43, 83] used in this study) did not exhibit any measurable auditory phenotype [43, 83, 84]. Moreover, intercellular Ca^{2+} signaling (ICS) in organotypic cultures from Panx1$^{-/-}$ mice was indistinguishable from those of wild type controls [83]. However, a formal proof that clearly establishes a direct spatial and temporal correlation between Ca^{2+} events on cochlear non-sensory cells and the Panx1 involvement in the ATP release is missing.

P2X7 receptors/channels

In 1997, Rassendren et al. [85] cloned the human gene for P2X7 purinergic receptor. P2X7 is an ATP-gated plasma membrane ion channel that has been consistently implicated in cytotoxicity. It is known that the functional P2X7 receptor is generated by the homotrimeric assembly of P2X7 subunits. Upon transient stimulation with ATP, P2X7 behaves like a cation-selective channel permeable to sodium (Na^+), potassium (K^+) and Ca^{2+}. However, sustained stimulation drives (as yet poorly understood) a transition that leads to formation of a nonselective pore permeable to aqueous solutes of molecular mass up to 900 Da [86].

Data in astrocyte by Suadicani and co-workers [87] and in bone cells by Brandao-Bruch and co-workers [88] support a role for P2X7 in the release of ATP. Other studies extended the notion to the immune system [89] and the tumor microenvironment [90], however the mechanism of ATP release from the P2X7R is incompletely characterized [91].

Vesicular release

It has been long known that ATP, neurotransmitters and other extracellular signaling molecules are packed in specialized granules in neuroendocrine tissues and released from cells via regulated exocytosis [92, 93]. In addition, ATP release has been associated with regulated exocytosis in pancreatic acinar cells, goblet epithelial cells, mast cells, pancreatic β islets, and other exocrine/endocrine tissues [91].

The complex process of exocytosis is schematized in Figure 1.4. It involves primarily a solute carrier (SLC) 17A9, a member of the SLC17 family of ion transporters [94] that was recently characterized as a vesicular nucleotide transporter (named VNUT) whose function is to uptake the ATP into the vesicles [95, 96]. ATP release is regulated by Ca^{2+} that triggers the fusion of the vesicle with the plasma membrane [97, 98].

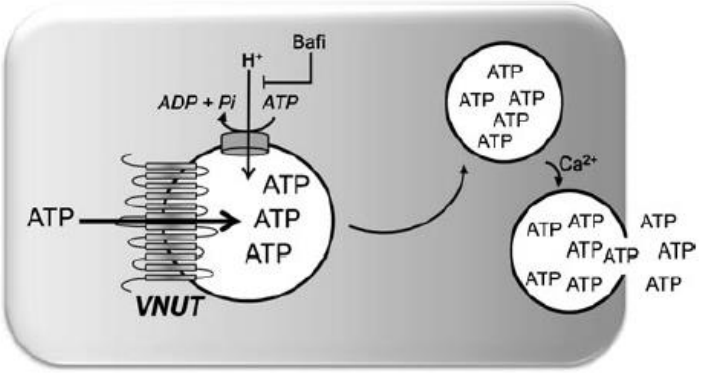

Figure 1.4: Schematic representation of vesicular nucleotide transporter (VNUT): from [40]. VNUT transports ATP to the lumen of secretory granules, using the electrochemical gradient provided by proton pump V-ATPase. ATP containing granules are secreted via Ca^{2+}-regulated exocytosis.

1.3 Ca^{2+} signaling stimulated by ATP release

ATP-mediate signaling and Ca^{2+} signaling are profoundly interdependent and these two signaling pathways are essential for most cellular responses and secretions. Ca^{2+} concentration is kept in sub-micromolar range in the cytosol, whereas it is thousand times higher in the extracellular space [99]. On the contrary, cytosolic ATP concentration is generally between 1–10 mM, whereas the extracellular concentration does not exceed 1–10 nM [100]. To keep a low level cytosolic Ca^{2+} concentration, cells restrict Ca^{2+} signals in space (in cells Ca^{2+} is stored in intracellular compartment such as endoplasmic reticulum (ER)) and time (an extended influx of Ca^{2+} in the cytoplasm is toxic [101] and can lead to apoptosis [102]). ATP as an energy source is required to keep low the cytosolic Ca^{2+} concentration [103]. On the other hand, ATP molecules are often released by Ca^{2+}-regulated exocytosis (as mentioned in the previous section) to promote intercellular communication [97, 98]. ATP effects are mediated by the extended family of purinoceptors linked to Ca^{2+} signaling (summarized in Figure 1.5). Generation of Ca^{2+} signals seems to be the general consequence of purinoceptors activation. All P2X receptors (inotropic receptors) are permeable to Ca^{2+} and their activation leads to an increase in intracellular Ca^{2+} from extracellular sources [104, 105]. P2Y receptors (metabotropic receptors), instead, may lead to increases in intracellular Ca^{2+} from intracellular sources, depending on their subtype. Indeed some of these receptors (P2Y1, P2Y2, P2Y4, P2Y11) are coupled, via G proteins, to phospholipase C that produces IP3 and diacylglycerol promoting Ca^{2+} release from the endoplasmic reticulum via IP3-gated receptors (Figure 1.6). The ATP-induced Ca^{2+} signaling mediated through the metabotropic route seems to be almost universal in non-excitable cells such as immune cells [106], epidermal keratinocytes [22] and inner ear cells [3, 107].

Receptor Subunit	Signal Transduction
$P2X_1$	$I_{Na/K/Ca^{2+}}$
$P2X_2$	$I_{Na/K}$
$P2X_3$	$I_{Na/K/Ca^{2+}}$
$P2X_4$	$I_{Na/K}$
$P2X_5$	$I_{Na/K/Ca^{2+}}$
$P2X_6$	$I_{Na/K/Ca^{2+}}$
$P2X_7$	$I_{Na/K}$, pore formation
Receptor Subtype	**Signal Transduction**
$P2Y_1$	PLCβ/IP_3 Ca^{2+}
$P2Y_2$	PLCβ/IP_3 Ca^{2+}
$P2Y_4$	PLCβ/IP_3 Ca^{2+}
$P2Y_6$	PLCβ/IP_3 Ca^{2+}
$P2Y_{11}$	PLCβ/IP_3 Ca^{2+} Adenylate cyclase
$P2Y_T$/$P2Y_{12}$	IP_3 Ca^{2+} Adenylate cyclase

PLCβ, phospholipase Cβ; IP_3, inositol 1,4,5-trisphosphate;

Figure 1.5: Signal transduction of pathways associated with P2 receptor: adapted from Ref. [108].

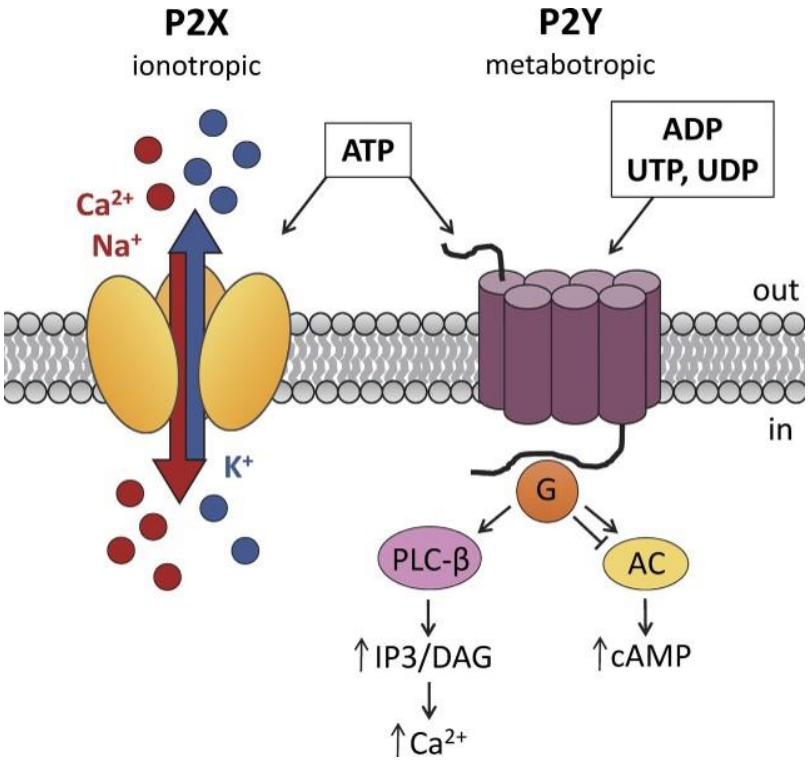

Figure 1.6: Purinergic signaling: from Ref. [109]. P2X receptors are trimeric ion channels in which each subunit consists of two membrane-spanning domains. Binding of ATP to P2X channels causes a conformational change that opens the pore and allows Ca^{2+} and/or Na^{+} to enter and K^{+} to leave the cell. P2Y receptors consist of seven transmembrane domains and are G protein–coupled receptors. Binding of ATP (or ADP, UTP, or UDP) to P2Y receptors activates different G protein signaling pathways, depending on the specific G protein associated with the receptor.

In this thesis, we exploited the tight coupling between P2Y purinergic receptors and Ca^{2+} signaling. We generate cell-based biosensors sensitive to small (nM) variations of ATP concentration in the extracellular milieu thanks to the overexpression of P2Y2 receptor (P2Y2R) on plasma membrane of HEK293T cells. The Ca^{2+} released within these cells from the ER following ATP binding to P2Y2Rs, was visualized with a fluorescent calcium indicator, preventively loaded into the cells. Thus, our ATP biosensor cells encoded fluctuations in the extracellular ATP concentration into corresponding modulation of Ca^{2+}-dependent fluorescence emission that could be easily detected in a suitable confocal microscope. Exemplary application of the technology is provided for the inner ear in mouse cochlear organotypic culture and for tumor microenvironment in live mice. Usually extracellular ATP is measured in the cell supernatant by using the standard bioluminescence luciferine/luciferase assays. However, this technique provides only an indirect estimate of the level that ATP can reach at sites of release close to the plasma membrane and, more importantly, does not allow real-time or *in vivo* measurement of the extracellular ATP concentration. Thus, our powerful probes allow monitoring of ATP kinetics in the extracellular space.

2. Aims of this work

In this thesis we investigated purinergic signaling in two different environments: developing cochlea cultures and melanoma. Part of this thesis was also dedicated to the generation and characterization of a powerful new tool for the detection of extracellular ATP based on live-cell biosensors. We combined multi-photon imaging with (i) ATP biosensor cells and novel microfluidic chamber, for measurements in cochlea cultures, and with (ii) ATP biosensor cells and a dorsal skinfold chamber for the tumor microenvironment, with the specific aim to:

1. investigate the role of connexin hemichannels and pannexin channels in ATP release in cochlear oraganotypic cultures of two different transgenic mice (pannexin 1 knock out and connexin 30 knock out);

2. characterize the enhancement of ATP-dependent Ca^{2+} signaling in cochlear non-sensory cells of $Cx30^{A88V/A88V}$ mutant mice;

3. validate the possibility of using ATP biosensor cells for *in vivo* measurements of extracellular ATP in tumor microenvironment;

Moreover, through micro-computed tomography we investigated the role of the P2X7 purinergic receptor in tumor angiogenesis.

3. Generation and characterization of ATP biosensor cells

3.1 Introduction to live cell-based biosensors

A biosensor is a device that measures biological or chemical reactions by generating signals proportional to the concentration of an analyte in the reaction. In cell-based biosensors, whole cells serve as the molecular recognition element and are employed in applications such as disease monitoring, drug discovery, detection of pollutants and in biomedical research. A typical biosensor consists of the following components:

- *Analyte*: A substance of interest that needs detection. For instance, in this thesis, the analyte is adenosine triphosphate (ATP).

- *Bioreceptor*: A molecule that specifically binds the analyte. In this specific case the bioreceptor is the G-protein-coupled P2Y2 purinergic receptor (P2Y2R) express in the cells after lentiviral infection (see Section 3.2.2).

- *Transducer*: The transducer is an element that converts the biological binding in a detectable signal. As a transducer, we used intracellular calcium indicators (e.g. Fluo-8) loaded in the cells in order to detect ATP-P2Y2R binding. As shown in the Figure 1.6 (see Section 1.3), extracellular ATP binds P2Y2 receptors and it activates a canonical transduction cascade that ends with Ca^{2+} release from the endoplasmic reticulum (ER) and raises the cytplasmatic concentration of Ca^{2+} ions [110] which bind the fluorescent calcium indicator. The subsequent conformational change of the transducer leads to the enhancement of the emitted fluorescence detectable through a fluorescence microscope.

Biosensors utilizing live cells have attracted a great deal of attention in the last 20 years because of high specificity and sensitivity to their targets [111, 112]. Since ATP is fundamental for cell-cell communication (as widely discuss in the Introduction), the deep understanding of its molecular pathways as second messenger, its involvement in diseases [35, 36] and its relation with Ca^{2+} signaling [100], could lead to the development of new therapeutic strategies. For elucidate the mechanism of ATP release, in this chapter, we introduced and characterized a novel ATP biosensor based on live cells (ATP-BCs) capable to detect low concentrations of ATP (nM) in the extracellular environment.

3.2 Materials and Methods

3.2.1 Spinning Disk Confocal Microscopy

The spinning disk confocal microscope, used in this work to characterized Ca^{2+} signals stimulated in ATP-BCs, was previously designed and built in the laboratory. The system is schematized in Figure 3.1 and described in detail in Ref. [113].

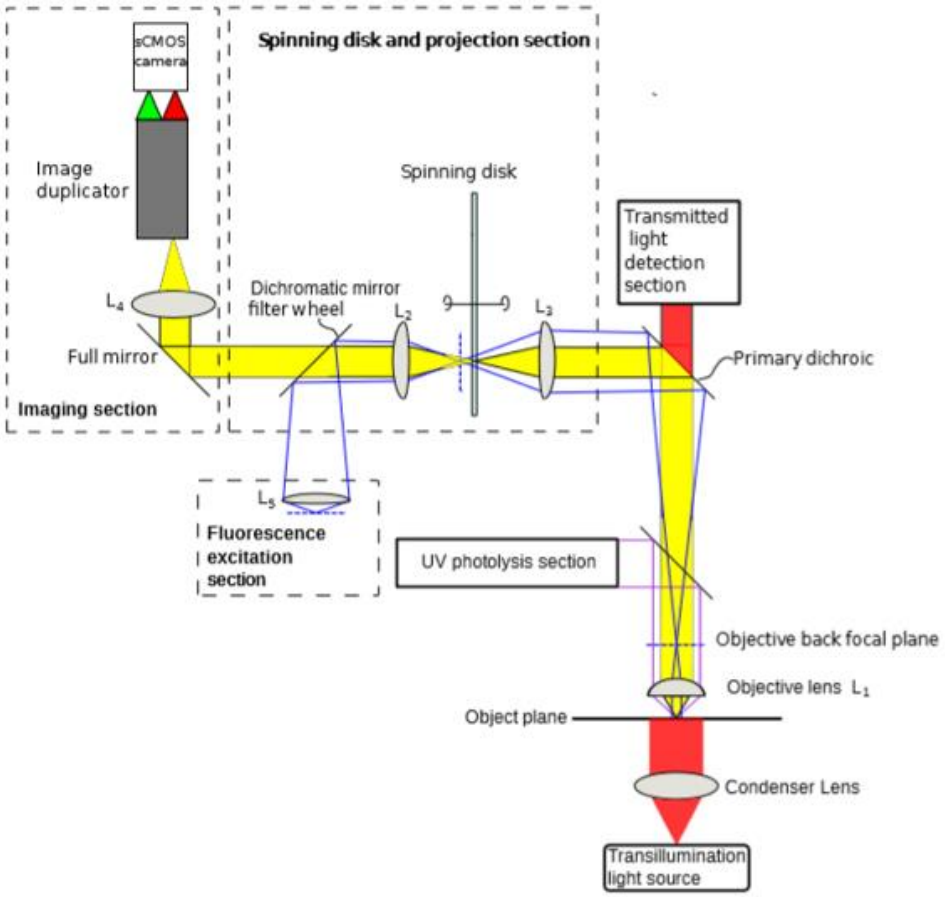

Figure 3.1: Schematic description of the spinning disk confocal microscope used in these studies: adapted from [113]. L1: Nikon Fluor (60X, 1 N.A.) water immersion objective lens; L2, L3: achromatic doublets; L4: microscope projection lens.

The microscope was coupled with a pneumatic PicoPump (PV820, World Precision Instruments Inc.) for the rapid delivery of the ATP by pressure through a microcapillary in a limited area under a 60X water immersion objective (Nikon Fluor, N.A. 1.00) and with a peristaltic pump (Harvard Apparatus, Cat.N. P-70) when global change of the extracellular solution was requested. The two configurations are shown in Figure 3.2.

Green fluorophores, such as Fluo-8 (AAT Bioquest, Cat.N. 21091), were loaded into the cells and excited by a 488 nm diode laser (COMPACT-150G-488-SM. World Star Tech). Excitation light was conveyed towards the objective by a triband dichroic mirror (FF395/527/610-Di01, Semrock) and focused on the sample. The emission signal, collected with the same objective, was filtered by triband

filter (FF425/527/685-25, Semrock) followed by a green band pass filter (ET535/30M, Chroma) located in front of a cooled s-CMOS camera (PCO.edge, PCO GmBH).

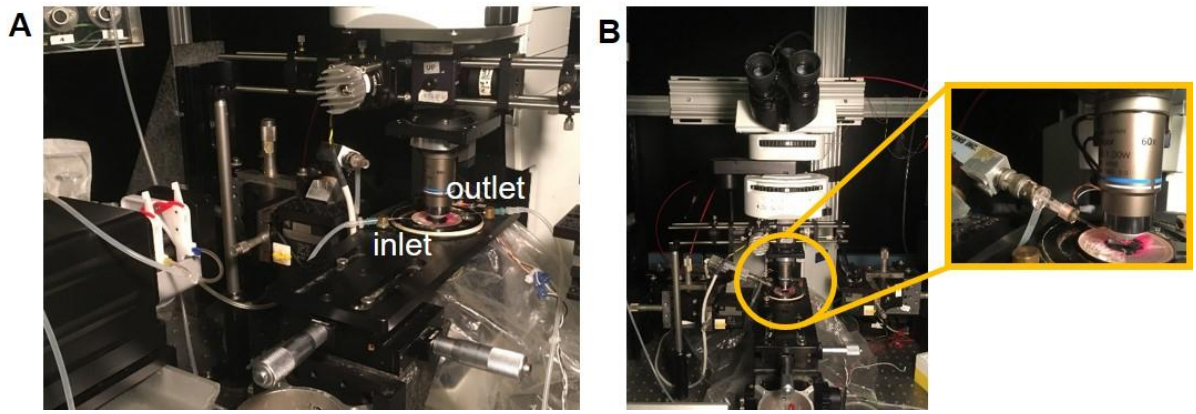

Figure 3.2: Different configurations used to deliver solutions under the spinning disk microscope: (A) Peristaltic pump, with tubing and sample-holder, used for overall solutions changes. (B) Pneumatic PicoPump (puffer system) for the rapid delivery of small fluid quantities in the limited area under the objective.

3.2.2 Generation of ATP biosensor cells (ATP-BCs)

To generate ATP-BCs stably expressing the P2Y2 receptors, two different cell lines were tested: Human embryonic kidney cells (HEK293T, purchased from American Type Culture Collection, ATCC, Cat.N. CRL-3216) and Chinese hamster ovary cells (CHO, purchased from ATCC, Cat.N. CCL-61). Both cell lines were tested to decide which was more adapted to detect low concentrations of ATP in the extracellular medium.

Lentivirus is a common tool used to generate cell lines stably expressing a gene of interest. The technique used to obtain the plasmid vectors, shown in the Figure 3.3 A, was the Gibson Assembly [114], whereby the P2Y2R cDNA (kindly provided from Marta Fumagalli of the laboratory of Molecular and Cellular Pharmacology of Purinergic Transmission, University of Milan) was ligated in the pUltra-hot empty vector (a kind gift from Malcolm Moore obtained from Addgene, plasmid #24130). pUltra-hot is a bicistronic vector for the simultaneous expression of two distinct proteins from the same RNA transcript driven by the Ubiquitin (Ubc) promoter. The first (constant) protein is mCherry, a red fluorescence protein that helps to distinguish infected from not infected cells, and the second (variable) protein was the P2Y2R, selected among the P2 family of G-Protein coupled receptors for its high sensitivity for extracellular ATP [9].

Viral vectors were purified from bacteria using a plasmid purification maxi kit (Qiagen, Cat.N. 12965). Thereafter, a standard protocol of lentiviral production and infection was used [115], as schematized in Figure 3.3 B. HEK293T cells were used as packaging cells for the production of lentivirus. Packaging refers to the preparation of competent virus from DNA vectors. The vector pUltra-hot-P2Y2R containing the cDNA of interest (transfer vector), the envelop vector (pMD2.G, a gift from Didier Trono, Addgene plasmid #12259) and the packaging vectors (psPAX2, a gift from Didier Trono, Addgene plasmid #12260) were transiently transfected into HEK293T cells. After (at least) 48 hours, the virus-containing supernatant was harvested and concentrated. If the transfer vector expresses a

fluorescent coding protein, as in this case, a high percentage of fluorescent packaging cells indicates a correspondingly high percentage of virus producing cells.

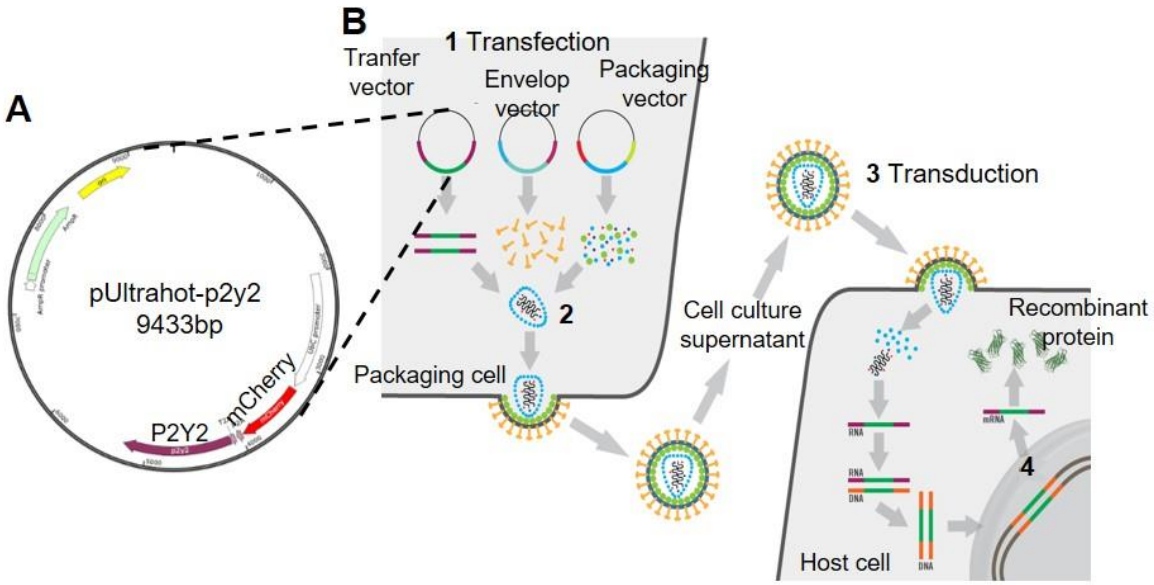

Figure 3.3: Diagram of pUltra-hot-P2Y2R plasmid vector and overview of recombinant lentivirus particles and infection of target cells: (A) circular double-stranded DNA molecule. Plasmid vectors were obtained by fusing the pUltra-hot empty vector with P2Y2R cDNA using the Gibson assembly method [114]. (B) adapted from "TransIT-Lenti for High Titer Lentivirus Production", Mirus Bio. (//www.mirusbio.com/applications/high-titer- virus-production/lentivirus-production). (1) Schematic description of packaging cell transfection; (2) Virus is assembled and released into the supernatant; (3) Target cells are transduced with recombinant lentivirus particles. (4) Transcription and translation result in the production of the protein encoded by the gene of interest.

To generate ATP-BCs, HEK293T cells or CHO cells were infected with the lentivirus described above 24 hours after plating at 30% confluence. Sequa-brene (Sigma-Aldrich, Cat.N. S2667) was added to the lentivirus vial to enhance viral transduction efficiency. Sequa-brene concentration ranged from 4 µg/ml (for the infection of HEK293T) to 16 µg/ml (for the infection of CHO). Lentiviral vectors reached full integration 48 hours after exposing the cells to the infection, as reported by red fluorescence of the mCherry proteins co-expressed with the P2Y2Rs.

Once generated through lentiviral infection, the biosensor cell lines, either HEK293T-mCherry-P2Y2R or CHO-mCherry-P2Y2R, are maintained in DMEM/F12 containing 10% heat inactivated FBS, 1% penicillin/streptomycin (Sigma-Aldrich, Cat.N. 15070063), 1% L-glutamine (Sigma-Aldrich, Cat.N. 25030024) and 1% sodium pyruvate (Sigma-Aldrich, Cat.N. 11360070). Cell cultures were maintained at 37°C under controlled atmosphere of CO_2 (5%). For the imaging, cells were plated on 12 mm round glass coverslips pre-treated with Laminin (2.5 µg/cm^2 Sigma-Aldrich, Cat.N. 11243217001) to promote cell adhesion and were incubated for 30 min at 37°C with membrane-permeable AM ester derivatives of Fluo-8 (5 µM) supplemented with pluronic F-127 (0.1% w/v, Sigma-Aldrich, Cat.N. P2443) and sulfinpyrazone (250 µM, Sigma-Aldrich, Cat.N. S9509) to prevent dye sequestration and secretion. Two

extracellular solutions, differing only in the concentration of free calcium ions, were used for imaging namely:

- High Calcium Solution (HCS) containing in mM: 138 NaCl, 5 KCl, 2 $CaCl_2$, 0.4 NaH_2PO_4, 10 Hepes, 6 D-glucose, pH7.3;

- Low Calcium Solution (LCS) containing in mM: 138 NaCl, 5 KCl, 0.02 $CaCl_2$, 0.4 NaH_2PO_4, 10 Hepes, 6 D-glucose, pH7.3.

Where specified HCS or LCS were supplemented with Ionomycin (Sigma- Aldrich. Cat.N. 13909), ARL67156 (Sigma-Aldrich, Cat.N. A265), Probenecid (Sigma-Aldrich, Cat.N. P8761), DIDS (Sigma-Aldrich, Cat.N. D3514), Fast Green FCF (Sigma-Aldrich, Cat.N. F7252). Fluo-8 loaded ATP-BCs were transferred on the stage of the spinning disk microscope, images were acquired at 4 frames per second. Alternatively, ATP-BCs were imaged under a multi-photon microscope (see Section 4.2.1 for detailed description). In this case the Fluo-8 dye was excited at 920 nm by focusing pulsed light from a Ti:Sa laser. Fluorescence emission was filtered through a band-pass filter (ET460/50m-2p, Chroma Technology) placed in front of a non-descanned GaAsP detector. Images were acquired at 5 frames per second.

3.2.3 Data analysis and statistics

Image processing and data analysis were carried out by the open source ImageJ software and using Matlab environment (release 2011, The MathWorks Inc). Ca^{2+} signals were quantified as pixel-by-pixel relative changes of fluorescence emission intensity, i.e., $\Delta F(t)/F_0$ (where t is time, $\Delta F(t) = F(t) - F_0$, F(t) is fluorescence at time t and F_0 is the fluorescence at the onset of the recording).

For data analysis, normality of distribution was assayed using the Kolmogorov–Smirnov test. Statistical comparisons of means were made by two-tailed analysis of variance (ANOVA) and post-hoc comparison by Tuckey's test (Tukey, 1949) using Matlab. The Mann-Whitney U-test was used for data that were not normally distributed and/or had dissimilar variance. Mean values are quoted ± standard error of the mean (s.e.m.), where p = p-values < 0.05 indicate statistical significance.

3.3 Results

3.3.1 Dose-Response Curve of ATP-BCs

In order to validate the suitability of the ATP biosensor cells (ATP-BCs) engineered to express P2Y2 receptors, cells were loaded with fluorescent calcium indicator (e.g. Fluo-8) selective for calcium ions (Ca^{2+}). Indeed, Ca^{2+} and ATP are strongly related, as already discussed in the Introduction. We used the spinning disk confocal microscope (see Material and Methods, Section 3.2.1) to quantify fluorescence intensity changes of ATP-BCs loaded with Fluo-8 and excited at 488 nm. Cells were stimulated by using a PicoPump ("puffer") system to deliver ATP through a glass micro-capillary (Figure 3.4 A,B,D,E) at concentrations ranging from 0.01 nM to 1 µM for the HEK293T-P2Y2R cells and from 0.01 nM to 500 µM for the CHO-P2Y2R cells.

To determine the dissociation constant (K_d), i.e. the ATP concentration that produces a 50% maximal response, the maximum intensity of the cells fluorescence in the field of view were extrapolated from the curves shown in Figure 3.4 A,B,D,E. The data were fitted with the Hill equations as reported in

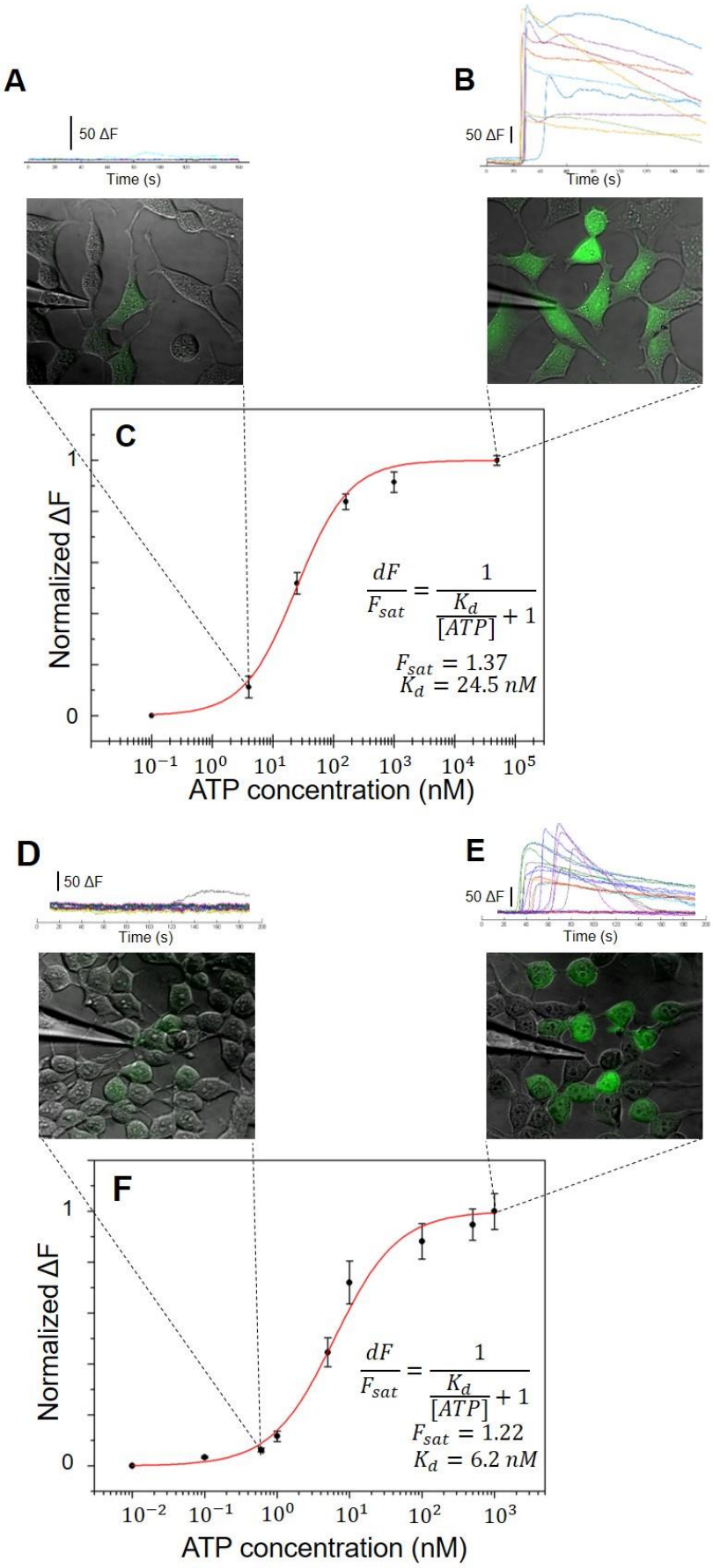

Figure 3.4: (Caption on the following page)

Figure 3.4: Calibration curve of CHO-P2Y2R and HEK293T-P2Y2R biosensor cells: (A,B,D,E) The traces at the top show representative Ca^{2+} responses evoked in biosensor cells by ATP stimulation at concentration of 4 nM (A), 500 µM (B) 1 nM (D) or 1 µM (E). Traces were generated as pixel averages of fluorescence changes in regions of interest (ROIs) encompassing responding cells. Images show the pipette of the puffer system for the rapid delivery of ATP solution on the plated biosensor cells loaded with Fluo-8. Each image is the merge of a bright-field image and a fluorescence emission image. (C,F) Normalized fluorescence intensity changes (mean and s.e.m. of three independent experiments) due to Ca^{2+} responses stimulated by different ATP concentrations. The fitting curve was obtained by Hill dose-response equation reported in the figure.

Figure 3.4 C,F. Data fitting permitted us to estimate the saturation concentration values (C_{sat}) and the values of the K_d. HEK293T-P2Y2R cells showed higher affinity (C_{sat} = 500 nM, K_d=6.2 nM) for ATP molecules compared to CHO-P2Y2R cells (C_{sat} = 100 µM, K_d=24.5 nM) suggesting the better suitability of HEK293T-P2Y2R cells as biosensors.

During the acquisition of Ca^{2+} evoked signals from ATP-BCs, dose-dependent oscillation responses were detected (Figure 3.5 A) in accord with the theoretical prediction of Ref. [116]. Specifically, Ca^{2+} responses exhibit an oscillatory character at 1 nM and 10 nM of ATP concentration (five recordings for each concentration). Self-sustained Ca^{2+} oscillations were elicited for ATP concentrations up to 1 µM (the value of saturation concentration for the HEK293T biosensors). Cytosolic Ca^{2+} concentration returned to baseline after 20 seconds from the washout showing the reversibility of the process [117].

Control experiments were also carried out to better characterize the ATP-BCs and to confirm that signals described above were indeed due to the binding of ATP molecules to specific P2Y2 receptors. In particular, parental HEK293T cells stimulated with 100 nM ATP did not respond (Figure 3.5 B) indicating low expression levels of endogenous P2 receptors [118]. We also determined that HEK293T-P2Y2R cells did not respond to constant pressure of the vehicle alone (Figure 3.5 C, data from three independent experiments). Stimulation with the Ca^{2+} ionofore ionomycin (10 µM), confirmed that Fluo-8 was correctly loaded into the cells (Figure 3.5 D).

We next looked for the effects of repeated ATP application on the same pool of P2Y2R-expressing cells to test for the occurrence of receptor desensitization [116]. This information is crucial to be aware of the sensitivity of the biosensors. The chosen ATP concentration was around the half of the maximal fluorescence intensity (10 nM). The area under the curves shown in Figure 3.6 A, which represents the time integral of the Ca^{2+} fluorescence intensity, decreased gradually and linearly with successive stimuli for up to 6 consecutive measurements. The corresponding fluorescent curves were displayed in Figure 3.6 B.

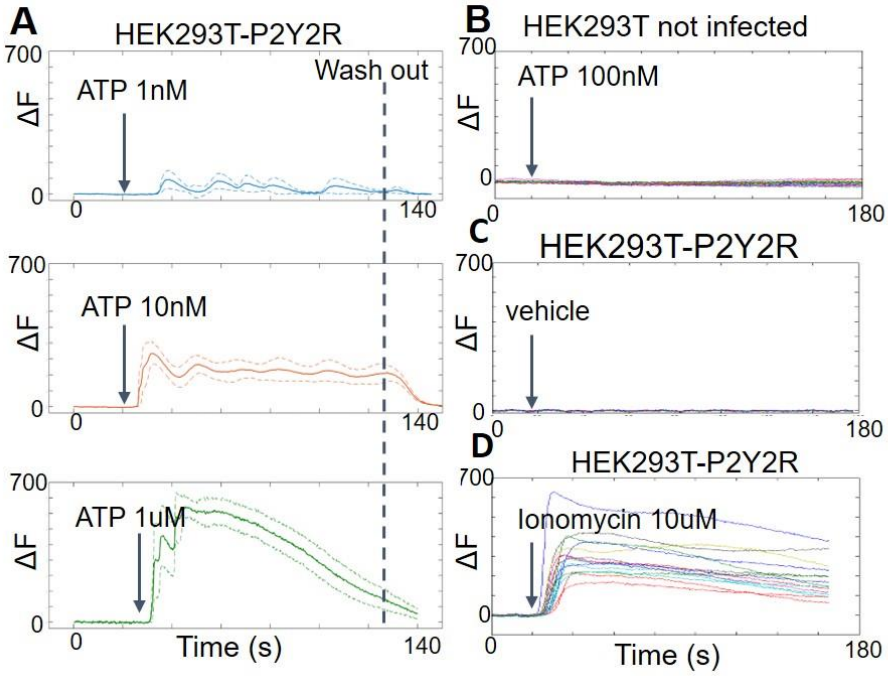

Figure 3.5: Ca^{2+} responses evoked in HEK293T-P2Y2R cells by different stimuli: (A) Fluorescence traces from HEK293T-P2Y2R cells were computed as pixel signal average within ROIs encompassing each individual cells. Shown are mean ΔF fluorescence traces (solid lines) ± s.e.m. (dashed lines) for n= 5 cells in each condition. Vertical dashed line marks the onset of perfusion for the wash out process. (B,C,D) Representative curves of control experiment used to determine the effective selectivity of the ATP-BCs. Black arrows mark the onset of focal drug delivery with the pneumatic PicoPump (puff stimulation).

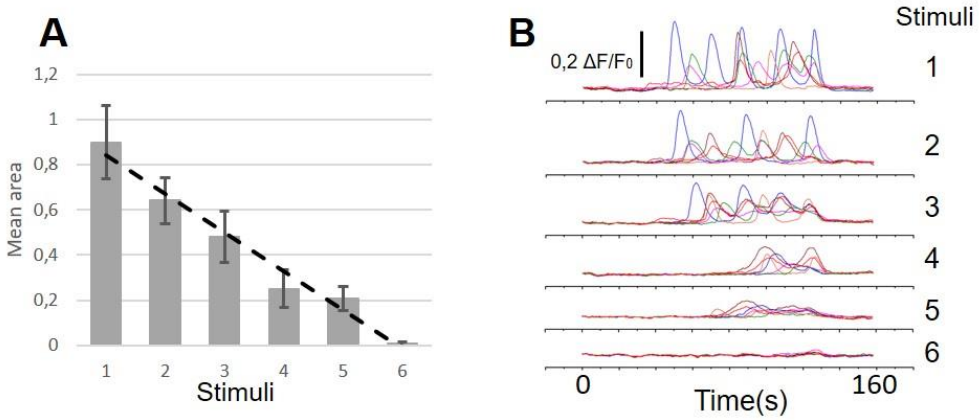

Figure 3.6: Run-down effect: (A) The histogram displays the mean area under the $\Delta F/F_0$ Ca^{2+} signals shown in (B) as a function of repeated ATP stimuli at a concentration of 10 nM. Shown are the mean and s.e.m for n = 6 cells. The dashed line indicates a descending linear trend. (B) Traces generated as pixel average from n = 6 cells under the effect of six consecutive stimuli at 10 nM ATP concentration.

3.3.2 Pharmacological modulation of ATP-BCs responses

In the previous section, we described the modulation of Ca^{2+} in response to the specific binding of ATP molecules to P2Y2 receptors. Here, we focused on the selectivity of the ATP-BCs testing the effect of compounds that mediate channels, such as connexons or pannexons, and their interaction with the P2Y2 receptors.

The signal transduction pathway describes the series of intermediate actions between the binding of ATP to the receptor and the final physiological effect. Since these pathways can be very complex, biosensor responses to compounds must be characterized and the possible interactions with drugs or solutions must be taken into account.

For this purpose, cells are seeded onto 12 mm round glass coverslips treated with Laminin (2.5 µg/cm^2) and loaded with Fluo-8 (5 µM) following the protocol explained in Section 3.2.2. Samples were then transferred on the stage of the spinning disk confocal microscope (see Section 3.2.1 for the microscope setup) and during the measurements, cells were perfused at a constant flow rate of 1 ml/min with HCS supplemented with one of the following compound: 1) ARL67156 (100 µM), an inhibitor of ecto-ATPases [119] which is crucial for the detection of low concentrations of ATP; 2) Probenecid (1 mM), an inhibitor of pannexin1 (Panx1) channels [120, 121]; 3) Fast Green FCF (10 µM), a well-known inhibitor of the ionotropic P2X7 receptor that also selectively inhibits Panx1 channels [120]; 4) DIDS (50 µM), an inhibitor of pannexin1 channels that binds also P2X7 purinergic receptors in the same site of ATP [122]. As shown in Figure 3.7, we monitored the occurrence of spontaneous cytosolic Ca^{2+} transients in ATP-BCs perfusing either with inhibitors (ARL67156, Probenecid, Fast Green FCF, DIDS) or with ATP (100 nM). Statistical analysis was performed on the mean area underlying the fluorescence curves and reveled significant difference between the pooled data ($p < 0.001$, ANOVA) showing that none of the compounds interfere with the ATP-dependent Ca^{2+} responses of our ATP-BCs.

Similarly, we tested ATP-BCs responses to HCS+ATP (100 nM) after 10 minutes incubation with the previously tested drugs (used at same concentrations as before). Data analysis indicates that neither Probenecid nor ARL67156 affected ATP-BCs responses to ATP (Figure 3.8 A). Conversely, Fast Green FCF and DIDS reduced the ATP-dependent responses of the ATP-BCs, possibly by interfering with the pathway that links ATP binding to Ca^{2+} release from the ER of the ATP-BCs [123] (Figure 3.8 A). Furthermore, as reported in Figure 3.8 B, the area under the curves of Ca^{2+}-dependent Fluo-8 fluorescence emission changes were significantly different for Fast Green FCF and for DIDS vs. 100 nM ATP alone ($p < 0, 001$, t-test), but not for Probenecid and ARL67156 ($p = 0{,}2851$, $p = 0{,}4104$, respectively; Student's t test). Together, these results indicate that Fast Green or DIDS cannot be used as pharmacological inhibitor when the presence of ATP in the extracellular medium is assayed by ATP-BCs.

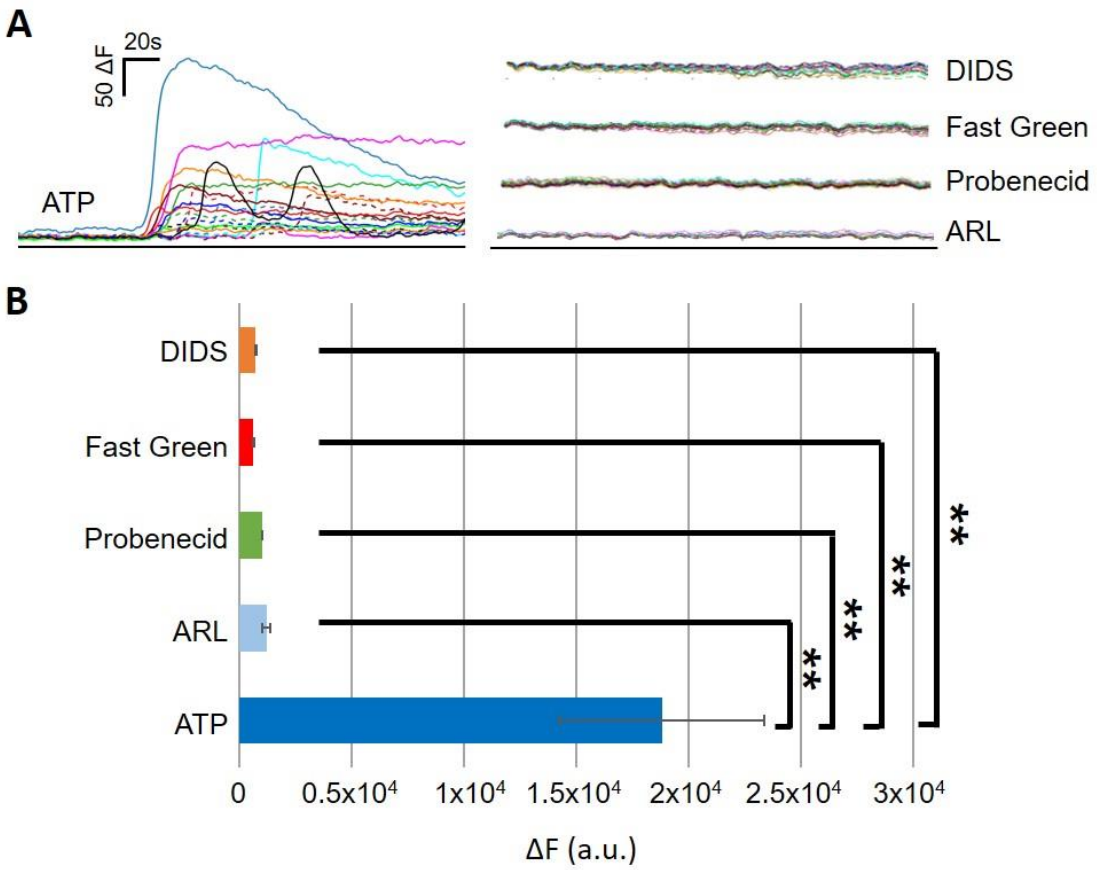

Figure 3.7: Response of ATP-BCs to perfusion with connexins and pannexins inhibitors and an ecto-ATPases inhibitor (ARL67156): (A) Representative Ca^{2+} traces computed as pixel fluorescence average within each ROIs encompassing a biosensor cell subject to a constant flow rate (1 ml/min) of an extracellular medium containing 100 nM ATP (left) and of 50 µM DIDS, 10 µM Fast Green FCF, 1 mM probenecid and 100 µM ARL (right). (B) Histogram shows mean area under the curves displayed in (A). Data shown are the mean and s.e.m. for n=2 independent experiment (**p < 0, 001, Student t test).

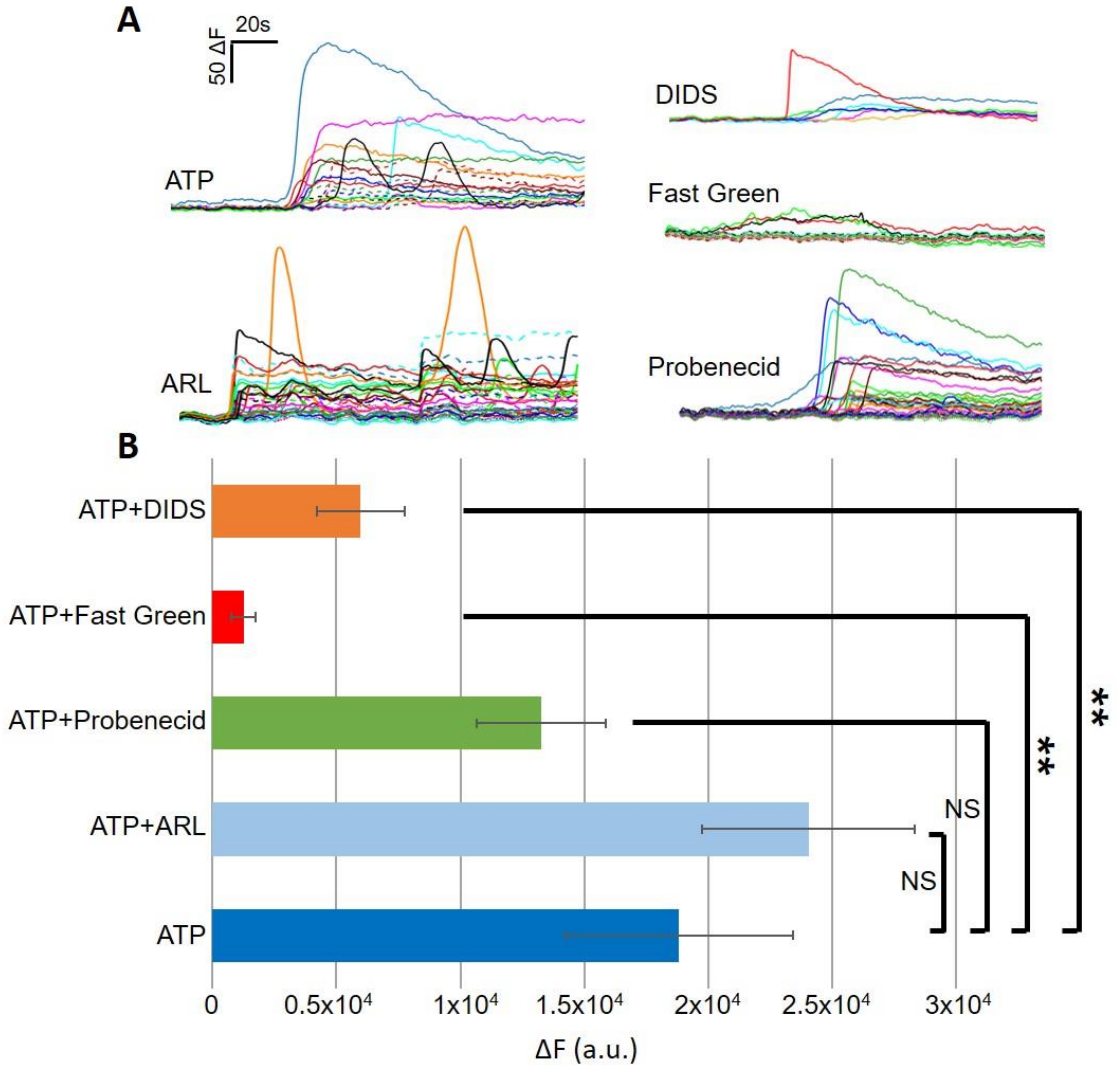

Figure 3.8: Response of ATP-BCs to 100 nM ATP after 10 minutes incubation with different inhibitors: (A) Representative Ca^{2+} traces computed as fluorescence emission averages within each ROIs encompassing a biosensor cell during perfusion of a 2 mM Ca^{2+} solution supplemented with 100 nM ATP, 100 µM ARL (left) and with 50 µM DIDS, 10 µM Fast Green FCF and 1 mM Probenecid (right) at 1 ml/min flow rate. (B) Histogram shows mean area under the curves displayed in (A). Data shown are the mean and s.e.m. for n=2 independent experiment (**p < 0, 001, p = 0,4104 (for ATP vs. ATP+ARL), p = 0,2851 (for ATP vs. ATP+Probenecid), Student t test).

3.3.3 Design and construction of a microfluidic chamber to detect ATP release using ATP-BCs

As mentioned, we generated ATP-BCs to investigate the correlation between Ca^{2+} signaling in a specific pathophysiological condition (such as tumor microenvironments or developing cochlea) and paracrine release of ATP. To this end, a microfluidic chamber was designed to put in close contact ATP-BCs with the sample of interest while performing Ca^{2+} imaging simultaneously in ATP-BCs and the tissue of interest. The Plexiglass parts of the chamber (part 1 and 3 reported in Figure 3.9) were intended to ease the rapid enclosure of the chamber without damaging the samples and were kindly fabricated by Imagensis Group. The Polydimethylsiloxane sample holder (PDMS) (part 2 in Figure 3.9), instead was kindly fabricated by IFN-CNR. As shown in Figure 3.9, the PDMS included the microfluidic channels (used for the incoming and outcoming fluids) and the sample placements. The lower enclosure was designed to host the sample of interest (e.g. cochlear organotypic cultures) plated onto 5 mm glass coverslip; the upper enclosure was designed to accommodate ATP-BCs plated on 12 mm glass coverslip (pre-coated with Laminin).

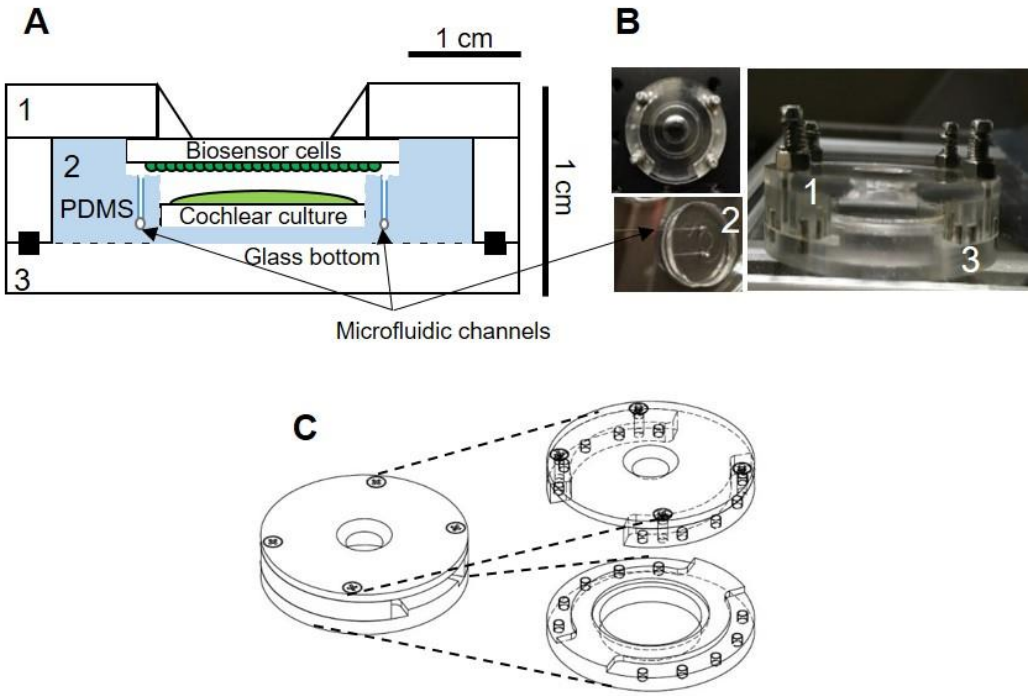

Figure 3.9: Microfluidic chamber architecture: (A) Schematic representation of a frontal cross section of the microfluidic chamber. Note the different scale bars in the vertical and horizontal directions. Numbers represent the 3 parts into which the microfluidic chamber can be divided. (B) Left: top view of the chamber and the PDMS used to hold samples and microfluidic channels. Right: side view of the whole microfluidic chamber. (C) CAD drawing of the chamber.

By mean of this architecture, it was possible to set the ATP-BCs few microns apart from the sample of interest to prevent ATP degradation and diffusion and maximizing the probability of ATP sensing by the ATP-BCs. The distance between the two focal plane of the sample and of the ATP-BCs, ranged from few tens of µm to few thousands of µm.

A recirculating fluid flow system allowed for the introduction of chemical agents into the chamber. As shown in Figure 3.10 B, the system circulates fluid between a media reservoir and the chamber using a peristaltic pump with 0.8 mm inner diameter (ID) silicone tube sets. In order to minimize fluid volume and to connect the tubes with the PDMS, smaller diameter stainless steel tubing (0.12 mm ID) were used. Connections to the chamber were made by direct insertion of these thin steel tubes into the PDMS. This structure also reduces the effective volume of the chamber to 10 µl, whereas the total fluid volume in the system was 200 µl.

3.3.4 Analysis of ATP-BC responses in the microfluidic chamber

Since mechanical stress could induce metabolic and/or morphological changes [124, 125], ATP-BCs loaded with Fluo-8 were enclosed alone in the closed microfluidic chamber and probed under different flow rates (from 0.05 ml/min to 1.6ml/min). As reported in Figure 3.10 A, we measured the variation in fluorescence intensity (ΔF) vs the initial fluorescence with fluid at rest ($F_{0@REST}$). Enhancement of fluorescence occurred abruptly when the flow rate exceeded 0.2 ml/min. Therefore, for the rest of these experiments we used a flow rate of 0.1 ml/min which did not induce any visible morphological change (nor increase the fluorescence) suggesting that at this rate the fluid shear stress did not affect the Ca^{2+}-response of the ATP-BCs in the microfluidic chamber.

Next, to determine the time constant necessary to completely replace fluids in the tubes (T_t) and in the chamber (T_c) at flow rate of 0.1ml/min, we monitored over time the effect of introducing a fluorescein solution (120 µM) in the chamber (Figure 3.10 B). Time constants were calculated from the intercepts between a linear interpolation of the most sharply rising curve segment and the two asymptotic lines (Figure 3.10 B). Their values were 66 s for inflow and 54 s to reach steady state, respectively.

As a further control, ATP-BCs in the microfluidic chamber were perfused at the flow rate of 0.1 ml/min with HCS containing 100 nM ATP. As expected, their fluorescence increased within 2 minutes of perfusion (Figure 3.10 C).

Comparing these results with those of the previous section, it is apparent that the underlying increase in cytosolic Ca^{2+} was solely due to the action of ATP on the P2Y2R expressed by the ATP-BCs.

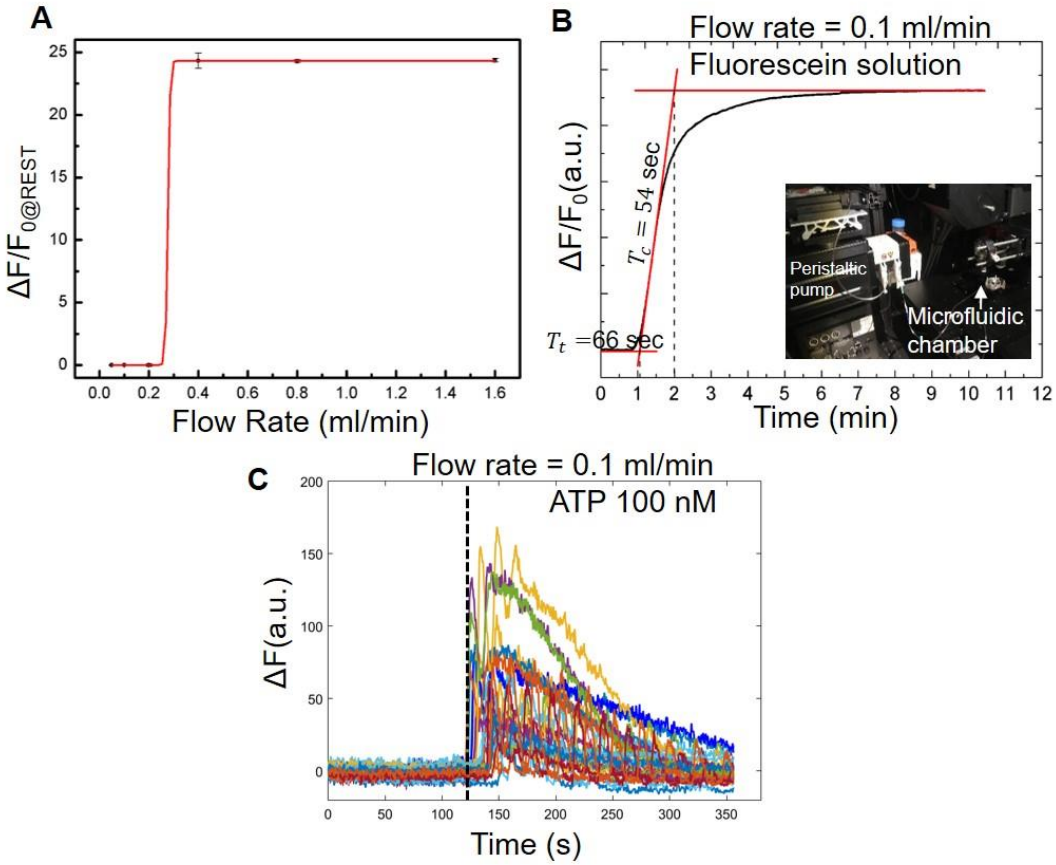

Figure 3.10: Characterization of microfluidic chamber and flow rate effect on ATP-BCs in the closed microfluidic chamber: (A) Responses of ATP-BCs to shear stress due to the flow rates (from 0.05 to 1.6 ml/min) in the closed microfluidic chamber. The graph represents the Ca^{2+} fluorescence changes ($\Delta F/F_{0@REST}$) on cells (n=100) vs. flow rate (ml/min). Note the abrupt transition from no effect to maximal effect at flow rates in excess of 0.2 ml/min. (B) Time constants of the microfluidic chamber at 0.1 ml/min (the flow rate selected for physiological experiments). The graph shows the emission of a fluorescein solution (120 µM) vs. time. T_t is the time required to fill the tubes; T_c is the time required to replace the fluid in the chamber. The insert shows the chamber placed in the sample holder of the multiphoton microscope, highlighting the positions of the microfluidic chamber, tubes and peristaltic pump. (C) Responses of ATP-BCs to exogenous ATP (100 nM) perfused in the closed microfluidic chamber at a flow rate of 0.1 ml/min. Based on the data in A, these responses were not due to fluid shear stress effects but were genuinely induced by ATP.

3.4 Discussion

Live cell-based sensors are promising tools for real time observations at single-cell level to test drugs and pollutants [126, 127]. Moreover, measurements of Ca^{2+} and cyclic adenosine monophosphate (cAMP) for biomedical research are being attempted with this method [128, 129].

The present thesis fits in this area. Combining the ability of the generated ATP-BCs together with microfluidic chamber, we were able to detect low (< 10 nM) concentrations of ATP in the extracellular environment. We also established experimental conditions that permit to perform these assays. By testing two different cell lines, our results suggest the better suitability of HEK293T-P2Y2R cells as ATP biosensors for the study of ATP pathways in different biological systems without altering the physiology of the tissue of interest. The P2Y2 receptors overexpressed by ATP-BCs have a high ATP affinity, consistent with previous reports [9]. Because of its metabotropic nature [1], the increase of intracellular Ca^{2+} concentration is due to release from intracellular storages [22]. This makes our ATP-BCs compliant varying Ca^{2+} concentration in the extracellular solutions (e.g. HCS, LCS).

We also tested the responses of ATP-BCs in presence of different inhibitors of pannexin 1 channels (Probenecid, DIDS and Fast Green FCF) and of an ecto-ATPase inhibitor (ARL67156). We demonstrated that ARL does not interfere with ATP-BCs responses whereas DIDS and Fast Green FCF interfere with the ATP-dependent Ca^{2+} signaling of the ATP-BCs mediated by P2Y2R, in great accordance with the literature [122, 130]. Screening of these compounds was crucial to exclude their direct effects on ATP-BCs which will provide a solid basis to investigate the role of connexin hemichannels and pannexin channels in the ATP release in complex environments such as cochlear organotypic cultures and tumor microenvironments.

Thanks to the high sensitivity of our ATP-BCs and to the architecture of the microfluidics chamber, in Chapter 4 we will prove the hypothesis proposed in previous studies suggesting the predominance of ATP release mediated by connexin hemichannels for the development of the auditory system [3, 4, 60, 131, 132] and in Chapter 5 we will confirm the evidences of the presence of ATP in the tumor microenvironment (TME) [36, 133, 134].

4. Relation between ATP release and calcium signaling in the mouse developing cochlea

4.1 Introduction to Ca^{2+} signaling in the developing cochlea

The cochlea is the inner ear structure where auditory processing is initiated. In the cochlear duct (CD), the basilar membrane supports a polarized sensory epithelium (the organ of Corti) which is responsible for sound transduction; it is composed by highly specialized sensory inner hair cells (IHCs) and outer hair cells (OHCs) characterized by a mechanosensory organelle composed of stereocilia (Figure 4.1) [135]. Different regions of the cochlear basilar membrane vibrate at different frequencies due to a complex interaction between fluid dynamics and variations in membrane thickness and width from the base (high frequencies) to the apex (low frequencies) of the cochlea [136, 137].

The IHCs and the OHCs are mechanically supported by inner and outer phalangeal cells that are flanked by various types of epithelial cells [107]. In the following, supporting and epithelial cells will be collectively named as cochlear non-sensory cells. An unusual extracellular fluid, the endolymph, bathes the apical pole of epithelium and it is characterized by low concentration of sodium (Na^+) and calcium (Ca^{2+}) ions, but rich in potassium (K^+) ions, which are the main charge carriers for sensory transduction.

During the period of time that precedes the acquisition of hearing, which in most rodents occurs around the second week after birth, the sensory epithelium is formed by the juxtaposition of the greater epithelial ridge (GER, which gives rise to the IHCs and medial non–sensory cells) and the adjacent lesser epithelial ridge (LER, which is thought to give rise to the OHCs and lateral non–sensory cells) [138, 139], as shown in Figure 4.1 C, D. Hearing acquisition relies not only on the functional maturation of hair cells but also on differentiation and proper organization of non–sensory cell networks that couple transfer ions, signaling and nutrient molecules through gap junction channels [140]. In the mammalian cochlea gap junction channels are formed primarily by connexin 26 (Cx26) and connexin 30 (Cx30) protein subunits [141, 142]. In this scenario ionized calcium (Ca^{2+}) plays numerous and fundamental roles in the inner ear for the correct development of the cochlea and for the acquisition of hearing [3].

It is generally thought that extracellular ATP modulates the function of both sensory and non-sensory cells in the inner ear [143, 144, 145, 146]. In the developing cochlea, ATP triggers cytosolic calcium concentration oscillations and propagation of intercellular Ca^{2+} waves that carry crucial biochemical information to the cochlear sensory epithelium [131, 147, 148]. Ca^{2+} wave propagation requires ATP binding to P2Y receptors that activate a canonical intracellular signal transduction cascade leading to diacylglycerol and inositol-1,4,5-trisphosphate (IP3) generation. Intracellular diffusion of IP3 and its subsequent binding to IP3 receptors, triggers Ca^{2+} release from the endoplasmic reticulum raising the cytosolic Ca^{2+} to peak levels of ~500 nM [3, 148]. This increase of Ca^{2+} concentration in the cytoplasm leads to an increased probability of opening for connexin hemichannels [57, 149, 150]. A wealth of experimental data and modeling efforts support the notion that open hemichannels release ATP from

the cytosol ($[ATP]_i$ in the range of mM) to the extracellular milieu ($[ATP]_e$ in the range of nM) [3, 43, 151].

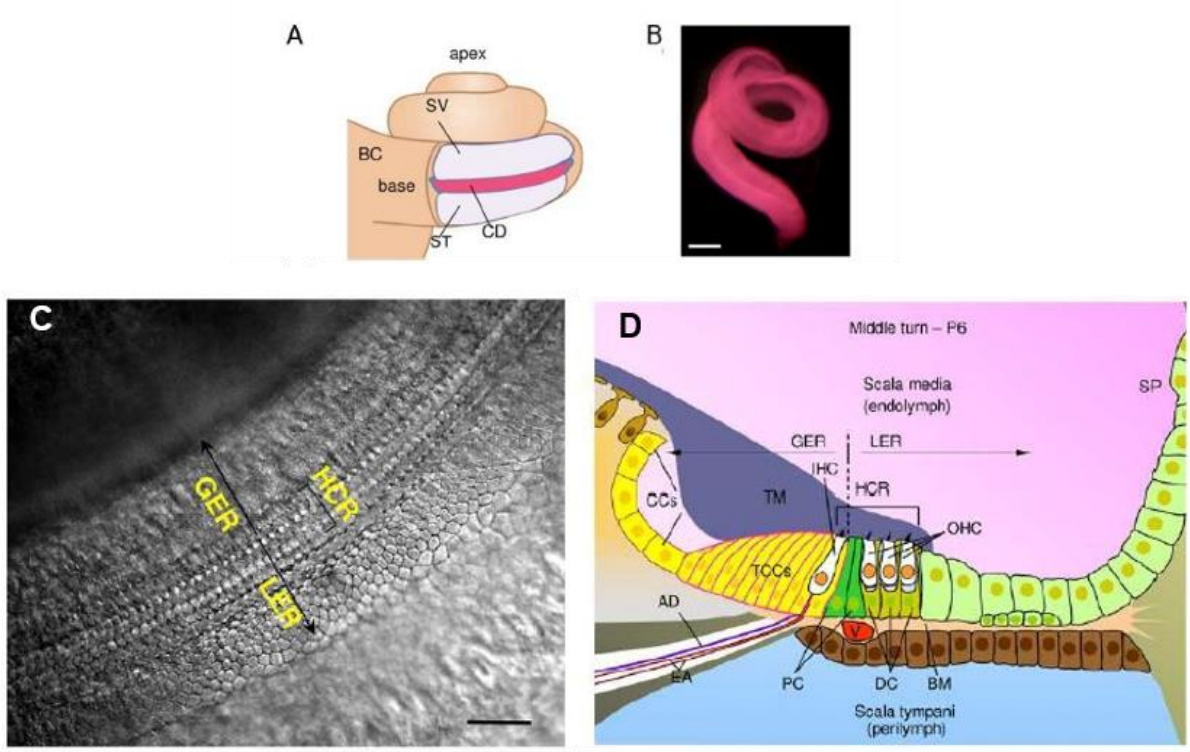

Figure 4.1: Anatomy of the cochlea and cochlear duct: from [107]. (A) Schematic drawing of the cochlea: BC, bony capsule shown fenestrated near the base to expose scala vestibuli (SV) and scala tympany (ST), both filled with perilymph; CD, cochlear duct (or scala media), filled with endolymph. (B) CD from a P5 mouse after removal of the bony capsule; scale bar, 1 mm. (C) Differential interference contrast (DIC) micrograph of the sensory epithelium in the basal turn of an organotypic cochlear culture, viewed from the scala media. LER, lesser epithelial ridge; GER, greater epithelial ridge; HCR, hair cell region; scale bar, 50 µm. (D) Schematic diagram of the epithelium viewed in transverse section (i.e. along the black line in (C)) The organ of Corti rests on the basilar membrane (BM) surmounted by the tectorial membrane (TM). The organ of Corti contains inner and outer hair cells (IHC, OHC), separated by pillar cells (PC). Each outer hair cell is supported by supporting cell of Deiters (DC). In the mature mouse cochlea afferent synapses typically have a single ellipsoid ribbon per active zone in both inner and outer hair cells. Inner hair cells form afferent synapses only with afferent dendrites (AD) of type I spiral ganglion neurons. The vas spiralis (V) is a blood vessel running in the tympanic layer of the basilar membrane just beneath the tunnel of Corti.

According to this scheme, ATP-dependent ATP release enables the regenerative cell-to-cell propagation of Ca^{2+} signals across the network of cochlear non-sensory cells by exploiting a cascade of biochemical reactions governed by critical phenomena that control also the frequency of intracellular Ca^{2+} oscillation [3].

In the GER of the developing cochlea, spontaneous Ca^{2+} transients arise periodically and propagate as Ca^{2+} waves [131]. It has been shown that flufenamic acid, a nonspecific blocker of connexin channels

[152], and the AbEC1.1 antibody, a specific blocker of Cx26 and Cx30 hemichannels [153], block spontaneous Ca^{2+} signaling activity in the GER [4, 132, 153]. The periodic Ca^{2+} signals can be blocked also by apyrase, an enzyme that catalyzes the hydrolysis of ATP to yield AMP and inorganic phosphate [147]. Moreover, Ca^{2+} waves failed to propagate in the developing sensory epithelium of $Cx30^{-/-}$ mice (which are global knockout for Gjb6) and $Cx26^{-/-}$ mice (which target Gjb2 expression in the sensory epithelium of inner ear) [43, 60, 154], both of which failed to acquire hearing [155]. On the contrary, Ca^{2+} waves propagated normally in mice that are global knockouts for molecular components of alternative ATP release conduits [81, 156, 157], such as $P2X7^{-/-}$ mice and $Panx1^{-/-}$ mice, both of which had hearing thresholds indistinguishable from those of their wild type siblings [4]. Altogether these data support the hypothesis that in the developing cochlea ATP is released through connexin hemichannels, however a direct proof is lacking.

In the first part of this Chapter, to test the hypothesis that ATP release is mediated by connexin hemichannels, we focus on the correlation between Ca^{2+} signaling and ATP release in the developing cochlea of wild type and pannexin 1 knock out ($Panx1^{-/-}$) mice using the ATP-BCs (widely described in the previous Chapter) coupled with the microfluidic chamber. In the second part, we concentrate on Ca^{2+} signaling in the network of non-sensory cells in the developing cochlea of two different mutant mice $Cx30^{-/-}$ and $Cx30^{A88V/A88V}$ underling the importance of connexin hemichannels and their relation with Ca^{2+} signaling in GER, ATP release and the acquisition of auditory function.

4.2 Materials and methods

4.2.1 Multiphoton microscopy

In order to distinguish Ca^{2+} signals from two focal planes few micron apart [158], a multi-photon (MP) partly custom-made microscope was used. The optical architecture shown in Figure 4.2 and Figure 4.3 was based on a customized Bergamo II Multiphoton microscope (Thorlabs Imaging System, Sterling, VI, USA).

Light input to the multiphoton microscope was provided by a femtosecond pulsed Titanium Sapphire (Ti:Sa) Laser (Chameleon Ultra II, Coherent, Santa Clara, CA, USA) coupled to a compact Optical Parametric Oscillator (OPO) (Chameleon MPX, Coherent) to extend the range of excitation wavelengths available. The dual output of the MPX OPO, driven by the a Ti:Sa laser (pump), provided two distinct pulsed laser beams: one, whose wavelength ranged from 680 nm to 1080 nm (corresponding to the Ti:Sa output), and the other one ranging from 1000 nm to 1340 nm (OPO output).

The pump beam was controlled by a LM0202 Electro Optical Modulator (EOM) (Qioptic, Waltham, MA, USA), a high frequency intensity modulator made of two crystals of potassium di-deuterium phosphate (DKDP). Since this modulator is based on a birefringent crystal, the modulation efficiency depends on the input polarization. The intrinsic divergence of the Ti:Sa beam was corrected by a motorized 1x telescope made of two 50 mm achromatic focal lenses whose distance could be adjusted remotely by the user. After collimation, the beam was combined with the OPO beam (as shown in Figure 4.2).

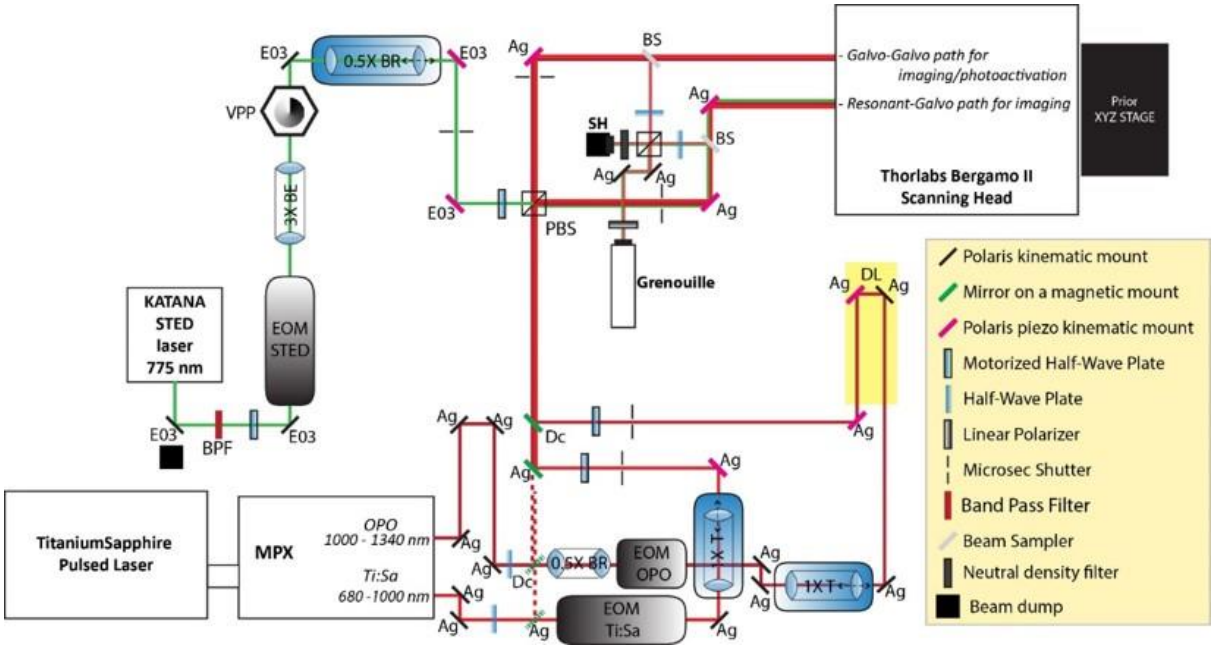

Figure 4.2: Simplified optical scheme of the multi-photon custom made microscope: Ag: Silver Mirror, Dc: Dichroic Mirror; BR: Beam Reducer; EOM: Electro-Optic Modulator; BE Beam Expander; T: Telescope; DL: Delay line; PBS: Polarizing beam splitter; E03: Near infrared dielectric mirror; VPP: Vortex Phase Plate; BS: Beam Sampler; SH: Shack Hartmann.

The OPO beam diameter was reduced in size by means of a 0.5X Beam Reducer (Leica Microsystems, Wetzlar, Germany) to fit the dimensions of the $LiTaO_3$ crystal of the LM 13 LT-P EOM (Qioptic, Waltham, MA, USA) and optimize the modulation efficiency. The conditioned OPO beam was then passed through a 1x motorized telescope like the one described above in order to correct beam divergence as a function of the OPO wavelength, and also to modify the Z position of the focal spot created by the objective. The OPO beam was then directed to an optical delay line, made of a pair of silver mirrors mounted in a retro-reflector configuration on a motorized high precision linear stage (Cat. N. 8MTL140C-300, STANDA, Vilnius, Lithuania). This device enables computer controlled micrometric variation of the optical path length and was used to temporally synchronize the pulsed OPO output to the Ti:Sa one. The possibility to synchronize the two beams is essential to perform sum frequency generation and stimulated emission depletion (STED) (as shown in Figure 4.2).

The pump and the OPO beams were merged by means of a 1000 nm short pass dichroic mirror (DMSP1000, Thorlabs). The polarizing beam splitter (PBS) placed in the shared path, split each output in two beams, whose relative powers were modulated by the rotation of two motorized half-wave plates (one for each beam). The two components of each beam were then fed to each one of the two scanning heads of the Thorlabs microscope, named resonant-galvo (RG) and the galvo-galvo (GG) scanning head, respectively (Figure 4.3).

A beam sampler (BSF10-B, Thorlabs GmbH Europe, Dachau/Munich, Germany) was inserted in each (RG and GG) beam path to select 5% of the light in order to check beam quality. Each 5% component was further split in two equal components by means of a half-wave plate followed by a PBS. One component was dimmed by a neutral density filter and directed to a Shack-Hartmann sensor to

visualize the shape of beam wavefront. The other component was polarized and fed to an auto-correlator (Grenouille 8- 50-USB, Swamp Optics LLC, USA) to check the temporal and spatial profile of the pulsed beams, as well as their mutual spatial alignment.

As shown in Figure 4.3, the beam in the GG scanning head was direct to the sample by two galvanometer mirrors (one for each axis). The GG solution was used to perform high-resolution morphological imaging and, more generally, when it was not necessary to follow dynamical processes at the millisecond time scale. The GG scanning head also provides full flexibility for arbitrary scan geometries.

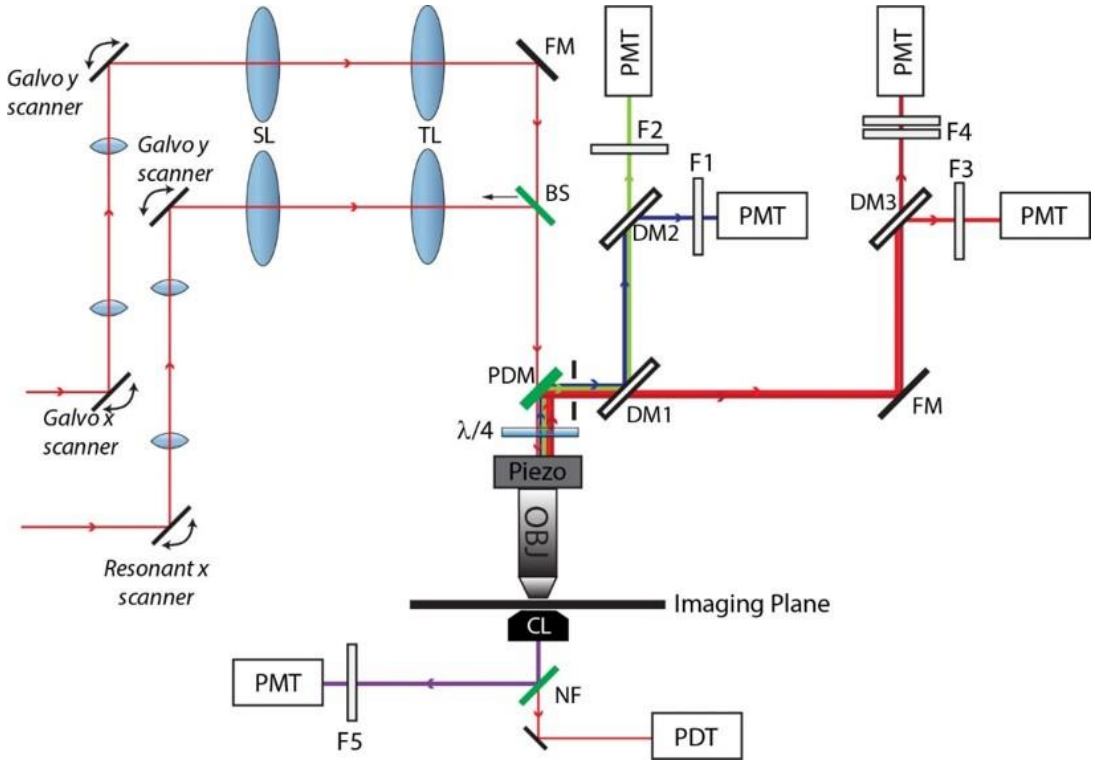

Figure 4.3: Schematic representation of the Scanning heads of the Thorlabs microscope: SL: Scan Lens; TL: Tube Lens; FM: Full Mirror; BS: 50/50 Beam splitter; PDM: Primary Dichroic Mirror; λ/4: Quarter wave plate; Piezo: Piezo Objective Scanner; Obj: Objective; DM1: 565 nm long pass filter (T565lpxr); DM2: 495 nm longpass filter (T495lpxru); DM3: a 652 long pass filter (FF652- Di01-25x36); F1: 460/50 nm band pass filter (ET460/50m-2p); F2: 525/40 nm band pass filter (FF02-525/40-25); F3: 612/69 band pass filter (FF01-612/69-25); F4: combination of 647 nm long pass filter (BLP01-647R-25) and 770 nm short pass filter (FF01-770/SP-25); NF: Notch Filter; PMT: photomultiplier tube; PDT: photodiode tube.

In the RG scanning head, the scan along the x-axis was provided by a special resonant mirror that oscillates at the fixed frequency of 12 kHz. This allowed us to scan full field frames (512x512 pixels) at a maximum frame rate of 45 frame per second (fps). However, with the RG scan head, the user can image only rectangular region of interest (ROI) because it does not allow scanning different

geometries. RG scanning head was used for milliseconds real-time functional imaging, such as Ca^{2+} imaging, using genetically encoded indicators (e.g. GCaMP). Importantly, we also used the GG scan head to photo-stimulate/photoactivate/uncage the molecules in a selected ROI in the field of view while we imaging the preparation with the RG scan head.

In both scanning heads, laser beams passed through a scan lens and a tube lens and were then directed to the objective. In the GG path, the light was reflected towards the sample by a full mirror. In the RG path, we used a 50/50 beam splitter (50/50 BS NIR, Chroma) with a 50% reflection efficiency. This optical element combined the beams from the two pathways and was placed on a motorized holder that allowed the user to exclude it from the light path when the GG scanning head was used. Before entering the objective, light from either scan head passed through a rotating quarter-wave plate in order to obtain circularly polarized light. Finally, a 25 X water immersion objective (XLPlanN25XWMP2, Olympus Corporation, Tokyo, Japan) mounted on a piezoelectric Z-scanner (PFM450E, Thorlabs) focused the light from each beam onto the sample. The piezoelectric actuator enabled fine focus adjustment (down to 3 nm) and fast Z-stack volume acquisition (400 nm range). The signal emitted by the sample was collected in an upright configuration by the same objective and was filtered by the use of a 735 long pass primary dichroic mirror (PDM, model FF735-Di02- 30x42, Semrock) to separate the emission in the visible (VIS) range from excitation in the infrared (IR) range. The VIS signal was further split using a combination of dichroic mirrors and bandpass filters and then collected by four different GaAsP photomultiplier tubes (PMTs).

4.2.2 Transgenic mice and genotyping

All mouse manipulations were performed in accordance with protocol approved by the Italian Ministry of Health (Prot. n.1005/2016-PR). Animals were bred and genotyped in the CNR Monterotondo node of the European Mouse Mutant Archive (EMMA), an ESFRI/INFRAFRONTIER Distributed Research Infrastructure.

The background strains of the transgenic mice used in this study are as follows: Panx1 knock out (KO) ($Panx1^{-/-}$) [43], Cx30 KO ($Cx30^{-/-}$) [155] and wild type littermates ($Panx1^{+/+}$, $Cx30^{+/+}$), C57BL/6; $Cx30^{A88V/A88V}$, CD-1 [159].

Mice used for this study were post-natal day 5 (P5) or post-natal day 3 (P3) pups, both male and female.

Mice were genotyped according to published protocols by standard PCR [43]. Primers for Panx1 were as follows:

- Panx1 f: 5’ – GGAAAGTCAACAGAGGTACCC – 3’
- Panx1 r: 5’ – CTTGGCCACGGAGTATGTGTT – 3’
- LacZ: 5’ – GTCCCTCTCACCACTTTTCTTACC – 3’

The $Panx1^{+/+}$ allele was targeted by the above f and r primers and identified by a 330 bp band, whereas $Panx1^{-/-}$ was targeted by primers Panx1 f and LacZ, and was identified by a 630 bp band. $Panx1^{+/-}$ was identified by the simultaneous presence of a 330 bp and a 630 bp band.

Primers for Cx30 were as follows:

- Cx30 f: 5’ – GGTACCTTCTACTAATTAGCTTGG – 3’;
- Cx30 r: 5’ – AGGTGGTACCCATTGTAGAGGAAG – 3’.

Primers for $Cx30^{A88V/A88V}$ were as follows:

- Cx30 A88V f: 5’ – GGTCGAAGGAACCTTTCACAGG – 3’;
- Cx30 A88V r: 5’ – GCTACCATCACGTGCTCTTTGG – 3’;

4.2.3 Cochlear organotypic cultures

Cochleae from post-natal day 5 (P5) or day 3 (P3) mice were quickly dissected in ice-cold Hepes buffered (pH 7.2) HBSS (Gibco, Cat.N. 14025050) and placed onto glass coverslips coated with Cell-Tak (Corning, Cat.N. 354240). The size of the coverslip was different depending on the experiment (5 mm glass coverslips for ATP release measurement, 12 mm glass coverslips for other experiments). The cochleae were incubated overnight at 37°C in DMEM/F12 (Gibco, Cat.N. 11320074) supplemented with 5% FBS (Gibco, Cat.N. 10270106) and 100 g/ml ampicillin (Sigma-Aldrich, Cat.N. A9518).

For Ca^{2+} signaling measurements, after overnight incubation, cochlear cultures were maintained for 45 min at 37°C in DMEM/F12, supplemented with Fluo-Forte (16 µM, ENZO, Cat.N. ENZ-52014) or Fluo-8 AM (20 µM). The incubation medium contained also pluronic F-127 (0.1%, w/v), and sulfinpyrazone (250 µM) to prevent dye sequestration and secretion. Samples were then transferred on the stage of the multi-photon microscope and perfused with extracellular solution (EXM) for 15 min at 1 ml/min to allow for de-esterification. The perfusion medium (EXM) contained (in mM): NaCl 135, KCl 5.8, CaCl2 1.3, NaH2PO4 0.7, MgCl2 0.9, Hepes-NaOH 10, d-glucose 6, pyruvate 2, amino acids, and vitamins (pH 7.48, 307 mOsm). Fluo-Forte was excited at 940 nm, whereas Fluo-8 was excited at 920nm. In either case, dye excitation was achieved by focusing the pump beam onto the sample through the 25X water-immersion objective. Fluorescence emission was selected in the range 435–485 nm by a single band-pass filter (ET460/50m-2p, Chroma Technology) placed in front of a non-descanned GaAsP detector. Mechanical ultra-fast shutters were used to limit light exposure to bear the minimum required for image acquisition. Images were acquired at 5 fps.

For experiments in the microfluidic chamber, 5 mm glass coverslips were used to plate the cochlear organotypic cultures. For recording, EXM was substituted by ECM, a medium obtained by replacing 2 mM Ca^{2+} in EXM with an endolymph-like concentration (20 µM) supplemented with the ectonucleotidase inhibitor ARL67156 100 µM or with apyrase (40U/ml, Sigma-Aldrich, Cat.No. A2230), an enzyme that catalyzes the hydrolysis of ATP. All experiments were performed at room temperature (22-25 °C). Illumination intensity, frame average, frame rate and the number of pixels in each frame were adjusted to minimize photobleaching and phototoxicity, while achieving sufficient signal to noise ratio and temporal resolution. Sequences of frames (512 × 512 pixels per frame) were acquired at a final rate of 1 fps (after frame averaging). Using the ThorImage LS 3.2 software (Thorlabs) in Z-Stack acquisition modality, it was possible to focus alternatively on the cochlea or the ATP-BCs. The distance between the two focal planes depended on the thickness of the cochlea and the assembly of the microfluidic chamber (ranging from 14 to 120 µm).

4.2.4 Quantitative measurement of ATP release with a standard bio-luminescence ATP assay

After the overnight incubation, cochlear cultures plated on 5 mm glass coverslips were transferred into a black 96-well plate with 200 µl serum- free DMEM/F12 in each well. Plates were then incubated for 30 minutes at 37°C and 5% CO_2. Immediately before starting the ATP release-stimulation protocol, cochleae were washed twice with a High Calcium Solution (HCS) containing a normal (1.8 mM) Ca^{2+} concentration (for detailed on HCS see Section 3.2.2). ATP release was stimulated by incubating the samples in HCS supplemented with ARL67156 (100 µM final concentration) for 20 minutes at 37 °C. After the incubation time, supernatant was collected and place in ice. The same organotypic cultures were then washed with Zero Calcium Solution (ZCS) containing a nominally zero calcium concentration and (in mM): 137 NaCl, 5.36 KCl, 0.44 KH2PO4, 0.18 Na2HPO4, 0.1 EGTA, 25 Hepes and 5.55 Glucose (pH 7.3). The same protocol of ATP release stimulation was repeated also in ZCS supplemented with ARL67156 (100 µM final concentration), the supernatant was collected and place in ice.

The amount of ATP release in these conditions was measured by using a bio-luminescent ATP assay kit (Molecular Probes-A22066) and the bio-luminescence was read by a luminometer (Perkin Elmer Victor Light 1420). For each experiment, ATP standard curves were generated using serially-diluted concentrations of ATP and used to convert measurements of luminescence signals into ATP concentrations (as described in the kit protocol).

4.3 Results

4.3.1 Responses of ATP-BCs evoked by photodamaging cochlear organotypic cultures of wild type mice

To test the hypothesis that Ca^{2+} wave propagation in the non-sensory cells of the GER correlate with ATP release through connexin hemichannels, we measured the ATP-dependent Ca^{2+} response of the ATP-BCs in correspondence of stimulated Ca^{2+} signals. We performed a set of experiments photodamaging a single non-sensory GER cell of a wild type (WT) cochlear organotypic cultures facing with ATP-BCs in the microfluidic chamber. The focal photodamage (at 920 nm, power 150 mW for 100 ms) generated a massive and time-controlled ATP release in a specific area (as shown in Figure 4.4 A). The released ATP was detected by the overlying ATP-BCs which responded with clearly detectable Ca^{2+} signals. Ca^{2+} imaging from the two types of cells was performed using a piezoelectric actuator couple with the water immersion objective that permitted us to step up and down repeatedly from one focal plane to the other at one frame per second, as described in Section 4.2.3 and shown in Figure 4.4 A.

As reported in Figure 4.4 B, replacing ARL67156 with 40 U/ml apyrase in the extracellular medium (LCS) reduced the propagation of intercellular Ca^{2+} waves in the GER [160, 161] after a photodamage. The time integral of the Ca^{2+} signals in WT cochleae in both conditions (LCS+ARL67156 and LCS+apyrase) yielded an area of 4.44 A.U. and 0.50 A.U., respectively. As shown in the left panel of Figure 4.4 C, D, we consistently recorded robust Ca^{2+} signals from the ATP-BCs following photodamage the cochlear organotypic cultures in LCS + ARL67156, but failed to detect biosensors responses in LCS + apyrase (4.4 C, D, right panel). Summing the fluorescence traces of all cells in the field of view and computing the value of the area under the curves (Figure 4.4 D) yielded 3.36 x 10^6 A.U. in presence of ARL67156 vs. 7 x·10^4 in presence of apyrase (similar results were measured for n = 3 independent

experiments). These results confirmed that ATP-BCs could detect the ATP released within the microfluidic chamber from the GER in the underlying cochlear oganotypic culture.

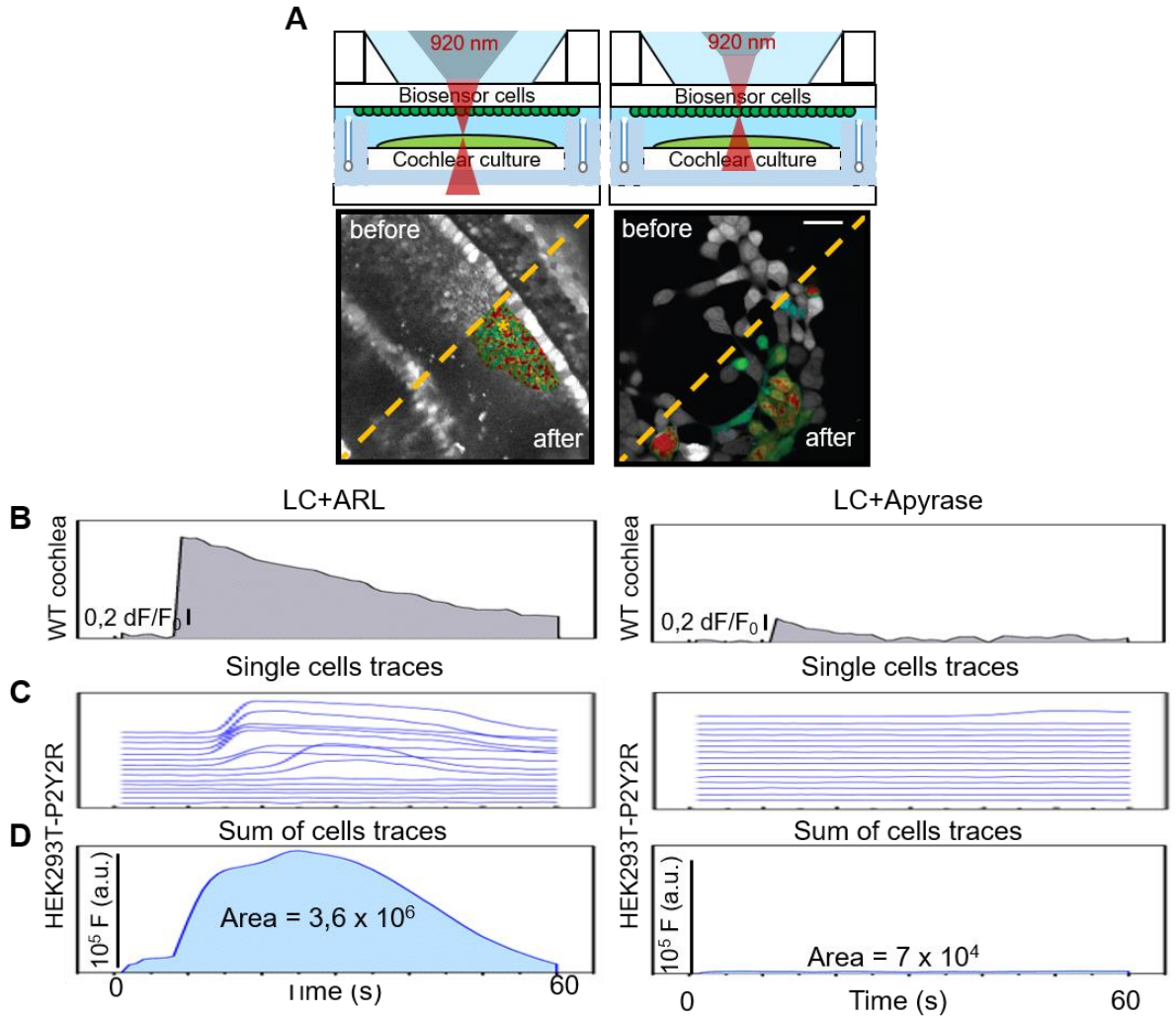

Figure 4.4: Specificity of ATP-BCs to ATP release from a wild type (WT) cochlea: (A) Top: Schematic representation of the microfluidic chamber during image acquisition with the multi-photon microscope of Ca^{2+} signals from the cochlea and from the biosensors cells both loaded with Fluo-8. The cochlear organotypic culture and the biosensor cells were mounted facing one another. Bottom: False-color images of each focal plane during the two steps of acquisition before and after the ATP-releasing stimulation (photodamaging). The yellow asterisk marks the photodamage point. Scale bar: 50 µm. (B) Representative time course of Fluo-8 traces generated as pixel averages from regions of interest (ROI) in the presence of ARL67156 (100 µM, left) or of apyrase (40 U/ml, right). The area under the curves of evoked Ca^{2+} waves in the GER is colored in grey. (C) Representative fluorescence signal changes (ΔF) of n= 15 cells (HEK293T-P2Y2R) in the field of view, used to detect local ATP release during photodamage of the cochleae in the presence of ARL67156 (100 µM, left) or apyrase (40 U/ml, right). (D) Fluorescence traces computed as the sum of single-cell fluorescence signals (F) detected in the biosensor cell population within the field of view.

4.3.2 Responses of ATP-BCs to spontaneous Ca^{2+} signaling in cochlear organotypic cultures of wild type and pannexin 1 knock out ($Panx1^{-/-}$) mice

To monitor the Ca^{2+} signals and to correlate them with the ATP release mediated by connexin hemichannels, we used the microfluidic chamber (for further details see Section 3.3.3) coupled with ATP-BCs (see Section 3.3) to compare ATP release in WT ($Panx1^{+/+}$) and $Panx1^{-/-}$ cochlear organotypic cultures (Figure 4.5 A). Both ATP-BCs and cochlear cultures were loaded with the Ca^{2+} selective dye Fluo-8 and multiphoton confocal Ca^{2+} imaging was performed by focusing alternatively (at 1 Hz rate) on the two preparations. In 7 independent experiments, we found that the distribution of intercellular Ca^{2+} fluorescence changes, integrated over time, was not significantly different between $Panx1^{-/-}$ cochlear cultures (mean = 3.60 A.U., median = 1.45, IQR = 2.77; n = 96 events) and $Panx1^{+/+}$ cultures (mean = 3.30 A.U., median = 1.89, IQR = 3.61; n = 104 events, p = 0.201, Mann-Whitney, U-test) (Figure 4.5 B, E). Similarly, in Figure 4.5 D it is reported the fluorescence trace computed as the sum of single fluorescence signal changes (some of them shown in Figure 4.5 C) detected in the whole biosensor cell population in the field of view. Moreover, the distribution of ATP-triggered Ca^{2+} responses detected in ATP-BCs overlying $Panx1^{-/-}$ cochlear organotypic cultures (mean = 2.38×10^4 A.U., median = 7.33×10^3, IQR = 2.19×10^4, n = 1695 cells) was not distinguishable (p = 0.105, Mann-Whitney, U-test) from the distribution of responses elicited by ATP released from $Panx1^{+/+}$ cochlear cultures (mean = 2.07×10^4 A.U., median = 3.88×10^3, IQR = 1.74×10^4, n = 1695 cells) (Figure 4.5 F).

To further validate the results reported above, we used the classical luciferin-luciferase ATP bioluminescence assay [162] to compare ATP release in cochlear organotypic cultures isolated from $Panx1^{+/+}$ and $Panx1^{-/-}$ P5 mouse pups (Figure 4.6). In cochleae isolated from both $Panx1^{+/+}$ and $Panx1^{-/-}$ mice, ATP release in the extracellular milieu was modulated by variations in the extracellular Ca^{2+} concentrations: in ZCS, the amount of ATP released from $Panx1^{-/-}$ cochleae was equal 8.14 nM ± 1.19 nM vs. 3.96 nM ± 0.70 nM in HCS (p = 0.015, t-test), and equal to 8.32 nM ± 1.68 nM vs. 3.09 nM ± 0.21 nM in HCS (p = 0.011, t-test) in Panx1 wild type mice. Thus, the amount of ATP released was not significantly different between the two genotypes, either in ZCS (p = 0.26, t-test) or in HCS (p = 0.93, t-test, n=6 cultures of either genotype). As Panx1 gating mechanisms are insensitive to change of extracellular divalent cation concentrations [70], our results strengthen further the hypothesis according to which connexin hemichannels are the sole conduits responsible for ATP release in the developing mouse cochlea.

These finding are in accordance with our previous results reported in Ref [83] where multiphoton microscopy was used to monitor spontaneous Ca^{2+} activity in cochlear organotypic cultures from P5 mice loaded with the Ca^{2+} indicator Fluo-Forte AM. Specifically, these results indicate that spontaneous ICS activity in the GER of the postnatal cochlea is not affected by Panx1 ablation and the absence of detectable defects in auditory function of $Panx1^{-/-}$ mice.

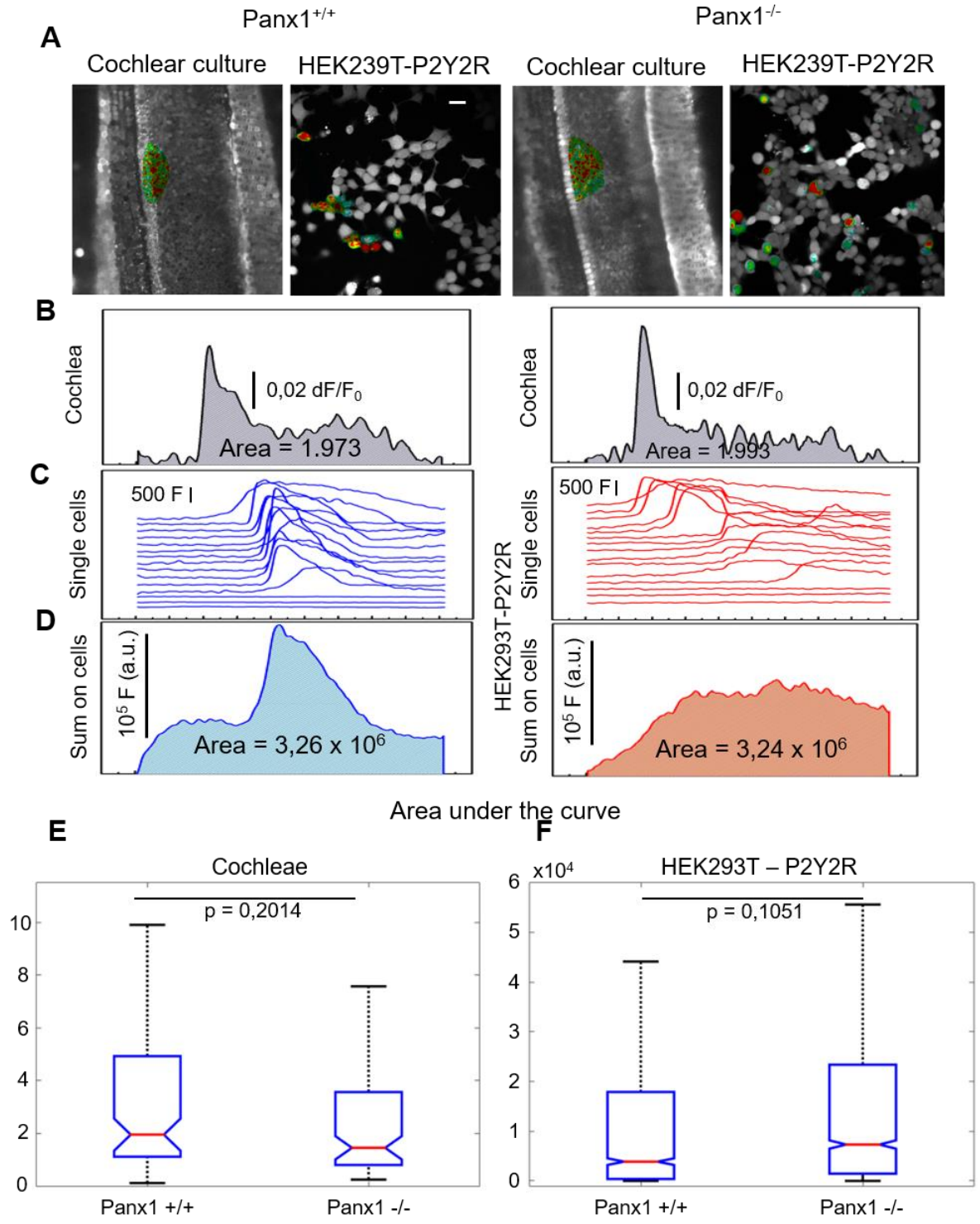

Figure 4.5: (Caption on the following page)

Figure 4.5: Pannexin1 (Panx1) channels are not involved in the generation of spontaneous ATP-mediated Ca^{2+} waves in the mouse developing cochlea: (A) Representative frames obtained while performing simultaneous two focal planes imaging to detect spontaneous Ca^{2+} signals in non-sensory cells of the GER of postnatal cochleae from $Panx1^{+/+}$ (wild type; left) and $Panx1^{-/-}$ (right) mice and activation of ATP-BCs, triggered by local release of ATP molecules. False-color images represent Fluo-8 fluorescence changes ($\Delta F/F_0$) obtained as maximal projection rendering of all frames recorded in cochlear organotypic cultures from P5 $Panx1^{+/+}$ and $Panx1^{-/-}$ transgenic mice. Scale bars: 50 µM. (B) Representative time course of Fluo-8 traces generated as pixel averages from regions of interest (ROI) relative to experiments in (A). The area under the curve of spontaneous cytosolic Ca^{2+} waves in the GER is colored in grey. (C) Representative fluorescence signals (*F*) of n = 15 cells (ATP-BCs) in the field of view shown in (A) and used to detect local ATP release during ATP-dependent Ca^{2+} oscillations in the cochleae. (D) Fluorescence trace computed as the sum of single fluorescence signal changes (*F*) detected in the whole biosensor cell population in the field of view in (A). (E) Box plots showing the distribution of intercellular Ca^{2+} fluorescence changes in developing cochleae of $Panx1^{+/+}$ and $Panx1^{-/-}$ mice, integrated over time. Data were obtained from n = 7 animals of each genotype and computed on n = 104 and n = 96 Ca^{2+} events for $Panx1^{+/+}$ and $Panx1^{-/-}$, respectively. (F) Distributions of ATP-triggered Ca^{2+} responses, integrated over time, measured in ATP-BCs during spontaneous Ca^{2+} oscillations in $Panx1^{+/+}$ (n= 1695 cells) and $Panx1^{-/-}$ (n = 1695 cells) developing cochleae.

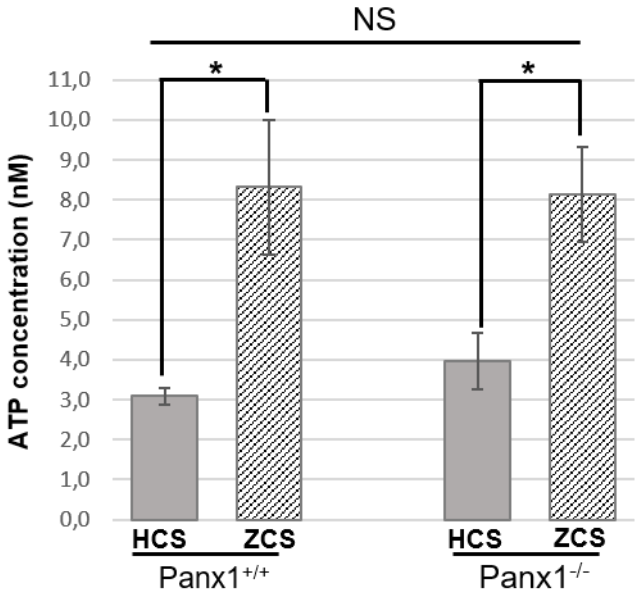

Figure 4.6: Quantification of spontaneous ATP release in cochlear organotypic cultures: ATP release from cochlear cultures obtained from Panx1 wild type mice ($Panx1^{+/+}$) and Panx1 knock out mice ($Panx1^{-/-}$) was quantified using a standard ATP bioluminescence assay kit. The same cochleae were incubated first with a High Calcium Solution (HCS = 2 mM Ca^{2+}) and then with a Zero Calcium Solution (ZCS). Data are mean and s.e.m. for independently repeated experiments on n=6 cultures (*$p < 0.05$, NS, p=0.94 between ZCS for the two genotypes; NS, p=0.26 between HCS for the two genotypes; Student t test.)

4.3.3 Strongly reduced ATP-dependent Ca^{2+} signaling in cochlear organotypic cultures of connexin 30 knock out ($Cx30^{-/-}$) mice

In the previous Section we have shown that Panx1 channels are not involved in ATP release in the developing cochlea and these data corroborate the hypothesis of other works that claimed that Panx1 is not involved in hearing acquisition [83, 154]. In contrast, connexins are known to be crucial for hearing and, mutation or deletion of Cx26 or Cx30, causes hearing loss in mice and humans [132, 163]. As a matter of fact, both $Cx30^{-/-}$ mice [155] and mice with targeted ablation of Cx26 in the inner ear [164, 165] are profoundly deaf. Moreover, deletion of Cx30 is associated with substantial downregulation of Cx26 expression in $Cx30^{-/-}$ mice [154, 166].

Of note, it has been proposed that ATP release from connexin hemichannels expressed in the cochlear non-sensory epithelium is important for the correct maturation of inner and outer hair cells (IHC and OHC respectively) which are responsible for the mechanoelectrical trasduction of sound signals [167, 168]. In particular, the release of ATP from non-sensory cells could affect the IHC firing activity directly, via the reduced activation of P2 receptors present in these cells, or indirectly via the elevation of K^+ around the IHCs following the activation of ATP autoreceptors in neighboring non-sensory cells [167]. The absence of connexins in non-sensory cells, which reduces the frequency and spatial extent of the Ca^{2+} waves and OHC synchronization, has been proposed to lead to a reduced number of ribbon synapses and type II afferent fibres [168].

To corroborate these conclusions, we analyzed ATP-BCs Ca^{2+} responses in the microfluidic chamber stimulated by spontaneous Ca^{2+} waves from $Cx30^{-/-}$ cochlea cultures. In Figure 4.7 A, B were reported representative Ca^{2+} response of the ATP-BCs coupled with $Cx30^{+/+}$ (in blue) or $Cx30^{-/-}$ (in red) cochlear cultures. The integration over time of the fluorescence traces measured on ATP-BCs coupled with $Cx30^{+/+}$ or $Cx30^{-/-}$ cochlear organotypic cultures (from at least 3 different mice) were significantly different ($p < 0.001$, Mann-Whitney U-test). From the distribution of Figure 4.7 C, we calculated the mean area under the fluorescence curves extrapolated from the ATP-dependent Ca^{2+} responses of the ATP-BCs that was equal to 2.30×10^4 for the cells coupled with $Cx30^{+/+}$ cochlear cultures vs. 2.90×10^3 for the cells coupled with $Cx30^{-/-}$, lending further support to the notion that ATP release is mediated by connexin hemicannels.

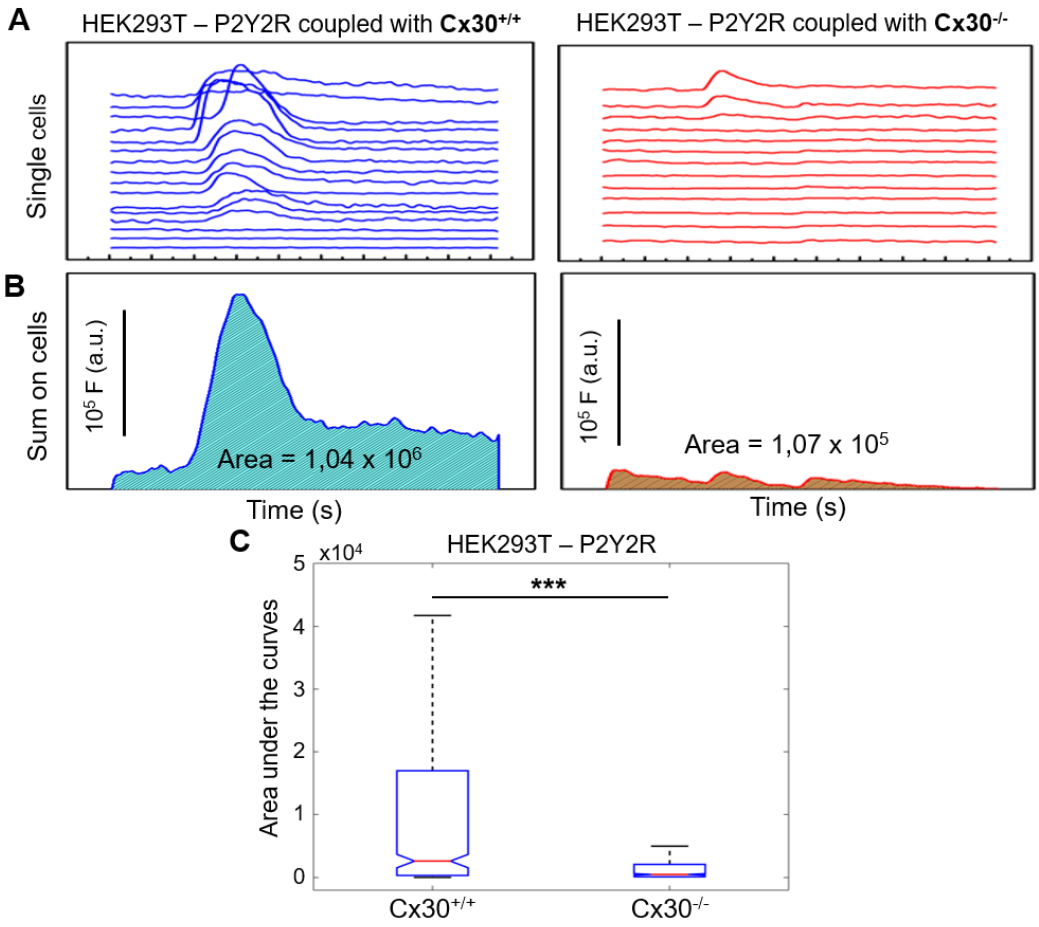

Figure 4.7: Connexin30 (Cx30) hemichannels are involved in the generation of spontaneous ATP-mediated Ca2+ waves in the mouse developing cochlea: (A) Representative fluorescence signals (F) of n = 15 cells (ATP-BCs) used to detect local ATP release during ATP-dependent Ca^{2+} oscillations in the $Cx30^{+/+}$ (blue) and $Cx30^{-/-}$ (red) cochleae. (B) Fluorescence trace computed as the sum of single fluorescence signal changes (F) detected in the whole biosensor cell population of a single experiment. (C) Distributions of ATP-triggered Ca^{2+} responses measured in ATP-BCs (n = 606 cells) during spontaneous Ca^{2+} oscillations in $Cx30^{+/+}$ and $Cx30^{-/-}$ developing cochleae, integrated over time.

In addition, we expanded the work of Rodriguez et al. [60], by using multiphoton microscopy to monitor spontaneous ICS activity in cochlear organotypic cultures obtained from P5 pups loaded with the Ca^{2+} indicator Fluo-Forte AM. As shown in Figure 4.8 A, B the frequency and the amplitude of spontaneous Ca^{2+} signaling in GER was strongly reduced in $Cx30^{-/-}$ cochlear organotypic cultures compared with $Cx30^{+/+}$ mice. Specifically, we examined the frequency of occurrence of spontaneous Ca^{2+} transients (events) in the apical cochlear turn by counting all occurrences within the portion of the GER in the field of view from P5 $Cx30^{-/-}$ mice and age–matched wild type siblings (Figure 4.8 C). The frequency of occurrence in $Cx30^{+/+}$ cochlear organotypic cultures was 18.30 ± 7.97 events/min and 5.61 ± 2.14 events/min in $Cx30^{-/-}$ cultures. The value of the median and the IQR (inter-quartile range) were respectively 0,0260 and 0,0321 for the $Cx30^{+/+}$ mice and 0,0241 and 0,0235 for the $Cx30^{-/-}$ mice (Figure 4.8 D). Statistical analysis of the event frequency distribution showed that the two pooled data were significantly different ($p < 0,001$, Mann-Whitney, U-test).

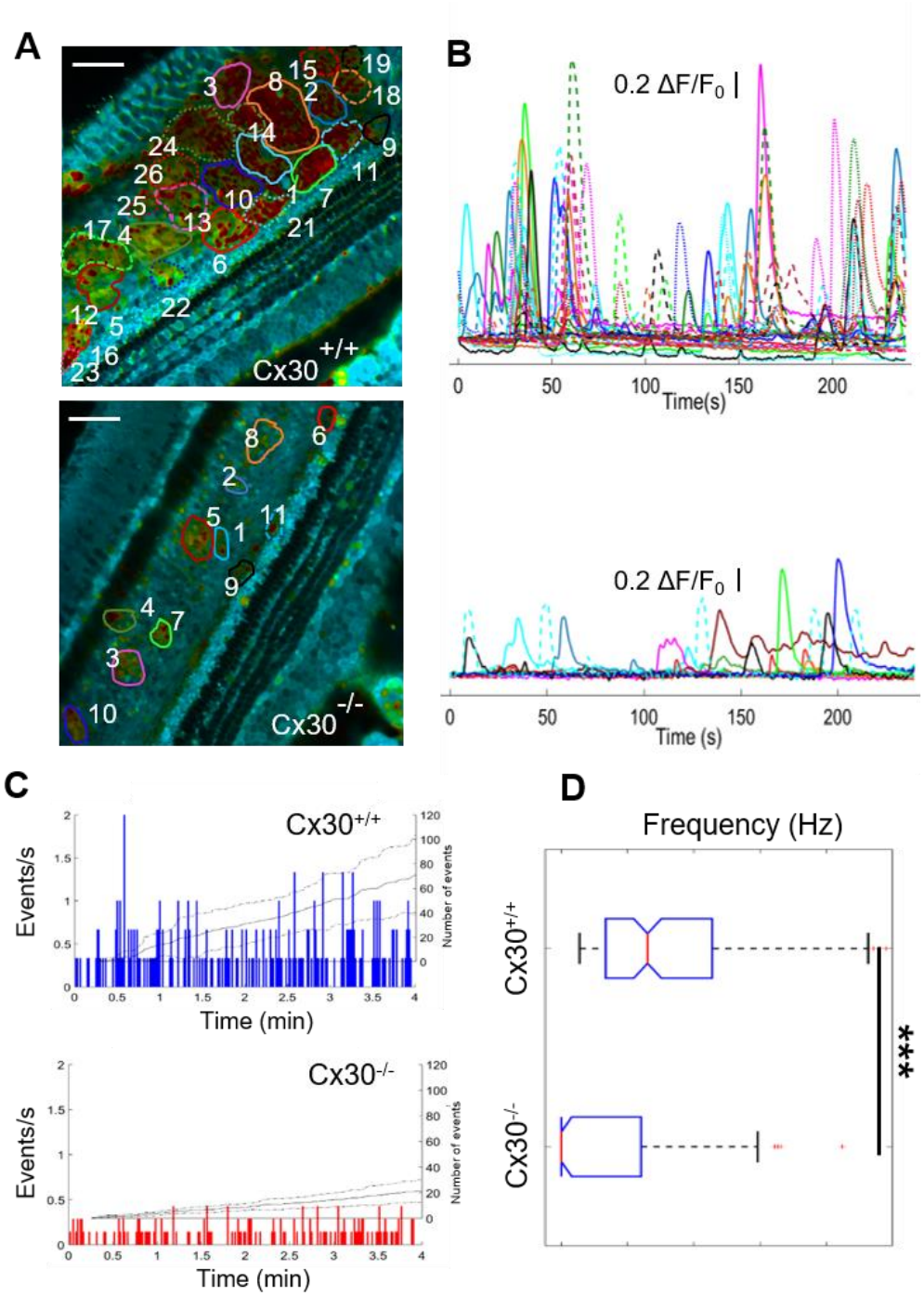

Figure 4.8: Spontaneous Ca^{2+} transients in the GER of wild type ($Cx30^{+/+}$) and connexin 30 knock out ($Cx30^{-/-}$) postnatal cochlear cultures: (A) Representative false-color image of Fluo-Forte fluorescence changes ($\Delta F/F_0$) in an apical-middle turn culture from $Cx30^{+/+}$ and $Cx30^{-/-}$ P5 mice. Each image was obtained as maximal projection rendering of all frames recorded over a 4 min time interval at five frames per second. The shown ROIs are superimposed on different Ca^{2+} hot spots. Scale bar, 50 µm. (B) Fluo-forte traces generated as pixel averages from the color-matched ROIs shown in (A). (C) Frequency histograms of spontaneous Ca^{2+} transients (events) in cultures from P5 WT (in blue) and P5 Cx30 KO (in red) mice (pooled data). (D) Distribution of the frequency between consecutive events. The value of the median and the IQR are respectively 0,0260 and 0,0321 ($Cx30^{+/+}$), 0,0241 and 0,0235 ($Cx30^{-/-}$) (***p < 0, 001, Mann-Whitney, U-test).

To consolidate these findings, we measured ATP release in cochlear organotypic cultures isolated from $Cx30^{+/+}$ and $Cx30^{-/-}$ transgenic P5 mouse pups (Figure 4.9) through a standard luminescence assay (n=6 mice for each genotype; for detailed protocol see Section 4.2.4). These results provide compelling evidence that connexin hemichannels play a pivotal role in ATP release, as (i) ATP release from $Cx30^{+/+}$ mouse cochleae was modulated by changes of extracellular Ca^{2+} concentrations (10.95 nM ± 0.87 nM in ZCS vs. 4.85 nM ± 0.68 nM in HCS, $p < 0.001$, t-test) and (ii) deletion of Cx30 significantly hampered ATP release in ZCS ($p = 0.001$, t-test), with respect to $Cx30^{+/+}$ cochleae. In particular, we found that the amount of ATP released from $Cx30^{-/-}$ cochlear cultures bathed in ZCS was equal to 6.40 nM ± 0.74 nM with respect to the amount detected in HCS (4.39 nM ± 0.69 nM, $p = 0.066$, t-test).

Altogether, these results support our working hypotheses that (i) connexin hemichannels are the major contributors to ATP release during the development of the cochlea and (ii) both Ca^{2+} signaling in the GER and ATP release mediated by connexin hemichannels are fundamental for hearing acquisition [163].

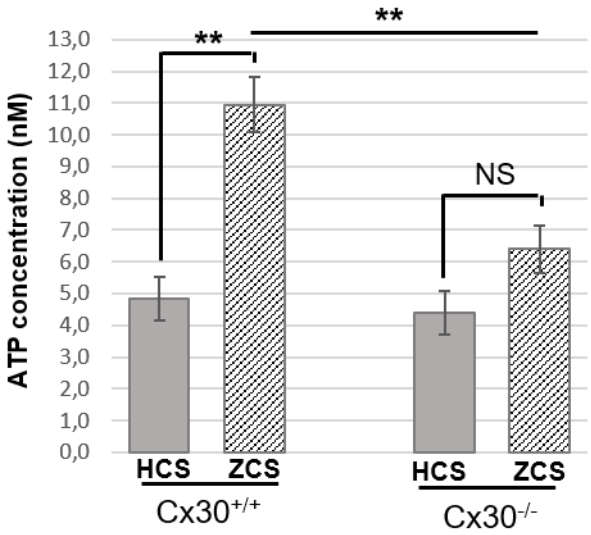

Figure 4.9: Quantitative ATP released by cochlear organotypic cultures measured with a bioluminescence ATP assay kit: (A) ATP release from cochlea cultures obtained from WT ($Cx30^{+/+}$) and Cx30 KO ($Cx30^{-/-}$) mice. The same cochlea was incubated at first with a High Calcium Solution (HCS) and then with a Zero Calcium Solution (ZCS) to promote hemichannel opening. Data are mean ± s.e.m. from n=6 different animals (**$p < 0.01$, NS $p = 0.066$, Student t test).

4.3.4 Enhanced ATP-dependent Ca^{2+} signaling in cochlear organotypic cultures of Cx30 $^{A88V/A88V}$ knock in mice

Mice expressing the A88V Cloustron syndrome mutant isoform of Cx30 [159], which leads to the formation hyperactive hemichannels [169], have been shown to exhibit better high-frequency hearing profiles with respect to their wild-type and heterozygous age-matched littermates at 6 to 9 months of age [159, 170]. We sought to corroborate and extend these surprising results. Thus, we initially recorded the auditory brainstem response (ABR). In humans and mice alike, sound-evoked ABR potentials appear as a series of consecutive relative maxima (peaks), termed Waves and labelled with Roman numerals, which arise from the synchronous short-latency synaptic activity of successive nuclei along the peripheral afferent auditory neural pathway [171, 172, 173]. Hearing threshold estimates

from clicks (namely the ability to detect broadband noise) were indistinguishable in both mutant and wild type mice aged 3 to 4 weeks. In contrast, thresholds for pure tone auditory stimulation at low frequencies (4 kHz and 8 kHz) were significantly higher in homozygous Cx30 $^{A88V/A88V}$ mutant mice compared to age-matched wild type littermate controls. Conversely, thresholds were significantly lower at 24 kHz and 32 kHz in homozygous Cx30 $^{A88V/A88V}$ mutant mice compared to age-matched wild type littermate controls (Figure 4.10). Of note, at 3 to 6 month of age Cx30 $^{A88V/A88V}$ mutant mice showed significantly better hearing profiles in response to both clicks and pure tone stimulation at 16 kHz, 24 kHz and 32 kHz, compared to age-matched WT controls (CD-1, genetic background) which are known to suffer from age- related hearing loss (ARHL) (data and statistical analysis shown in Figure 4.11).

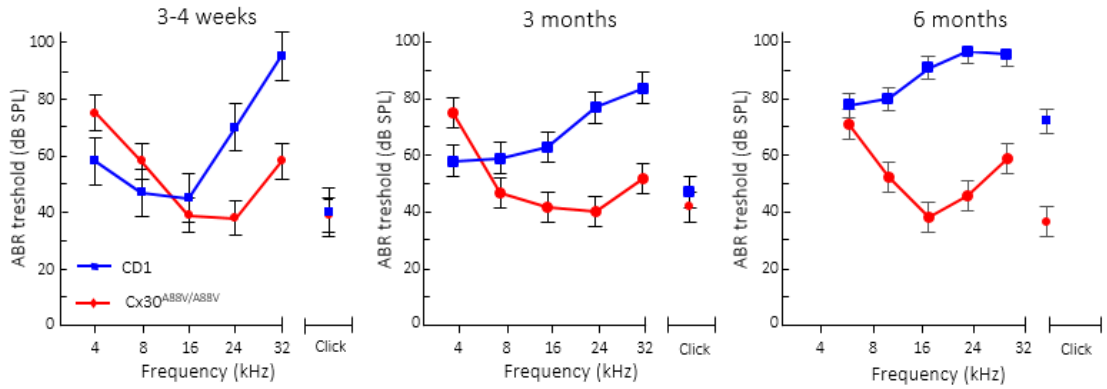

Figure 4.10: Auditory Brainstem Response (ABR) profiles of CD1 and Cx30 $^{A88V/A88V}$ mice: Hearing threshold estimated from Wave II for broadband (clicks) and tone bursts at 4, 8, 16, 32 kHz obtained from Cx30 $^{A88V/A88V}$ mice at 3-4 weeks, 3 months and 6 months of age, and from age-matched CD1 wild type littermates.

	3-4 weeks		3 months		6 months	
	CD1	Cx30$^{A88V/A88V}$	CD1	Cx30$^{A88V/A88V}$	CD1	Cx30$^{A88V/A88V}$
Click	40 (5.0)	39 (5.34) [*P*=0.900]	47 (17.32)	42 (10.14)[*P*=0.712]	74 (3.54)	35 (4.0) [*P*=0.062]
4 kHz	58 (5.83)	75 (1.58) [*P*=0.062]	58 (6.04)	75 (3.67) [*P*=0.092]	79 (1.99)	72 (1.22) [*P*=0.013]
8 kHz	47 (7.51)	58 (3.74) [*P*=0.130]	59 (17.31)	47 (10.14) [*P*=0.208]	82 (4.52)	52 (3.39) [*P*<0.001]
16 kHz	45 (9.31)	39 (3.67) [*P*=0.189]	63 (18.88)	42 (6.01) [*P*=0.237]	94 (3.09)	37 (4.36) [*P*<0.001]
24 kHz	70 (10.36)	38 (3.39) [*P*=0.046]	77 (21.17)	40 (10.41) [*P*=0.238]	100 (1.0)	45 (8.51) [*P*<0.001]
32 kHz	95 (5.0)	58 (4.64) [*P*=0.002]	84 (1.67)	52 (15.90) [*P*=0.147]	99 (0.81)	59 (8.21) [*P*=0.003]

Figure 4.11: Auditory brainstem response (ABR) thresholds for click stimuli and for tone bursts at 4, 8, 16, 24, 32 kHz obtained from CD1 and Cx30 $^{A88V/A88V}$ mice: Shown are mean values in dB SPL, rounded to nearest integer, with s.e.m. (in round brackets) for n = at least 6 mice per each genotype for each age set, and paired t-test p-values of each group relative to CD1 controls (in square brackets).

Several lines of evidence support the notion that connexin-depended Ca^{2+} signaling activity in the pre-hearing mouse cochlea conditions hearing performance in the adult stage [163]. Therefore, to investigate spontaneous calcium signaling in the non-sensory cells of the GER of $Cx30^{A88V/A88V}$ mice,we performed two-photon imaging in cochlear oganotypic cultures isolated from n = 5 P3 pups of each genotype and loaded with Fluo-8 (Figure 4.12). In the apical cochlear turn, the mean frequency of occurrence of spontaneous Ca^{2+} waves was 5.05 ± 4.00 events/min in WT CD-1 cultures (n = 322 events) vs 7.4 ± 3.00 events/min in Cx30 $^{A88V/A88V}$ cultures (n= 629 events). In the basal turn, the corresponding figures were 9.1 ± 4.2 events/min (n = 422) in WT CD-1 vs. 4.2 ± 1.3 events/min in mutant mice (n = 357) (Figure 4.13). Likewise, inter-peak interval distributions of spontaneous Ca^{2+} transients in Cx30 $^{A88V/A88V}$ apical turns were significantly higher (median = 0,0253; interquartile range (IQR) = 0,0286, $p < 0.001$, Mann-Whitney, U-test) with respect to those of wild type cultures (median = 0.01283; IQR = 0.0213), whereas in the basal turn the median and IQR values were equal to: 0.0152 and 0.0192 in mutant mice, and 0.0273 and 0.0264 in wild type mice ($p < 0.001$, Mann-Whitney, U-test).

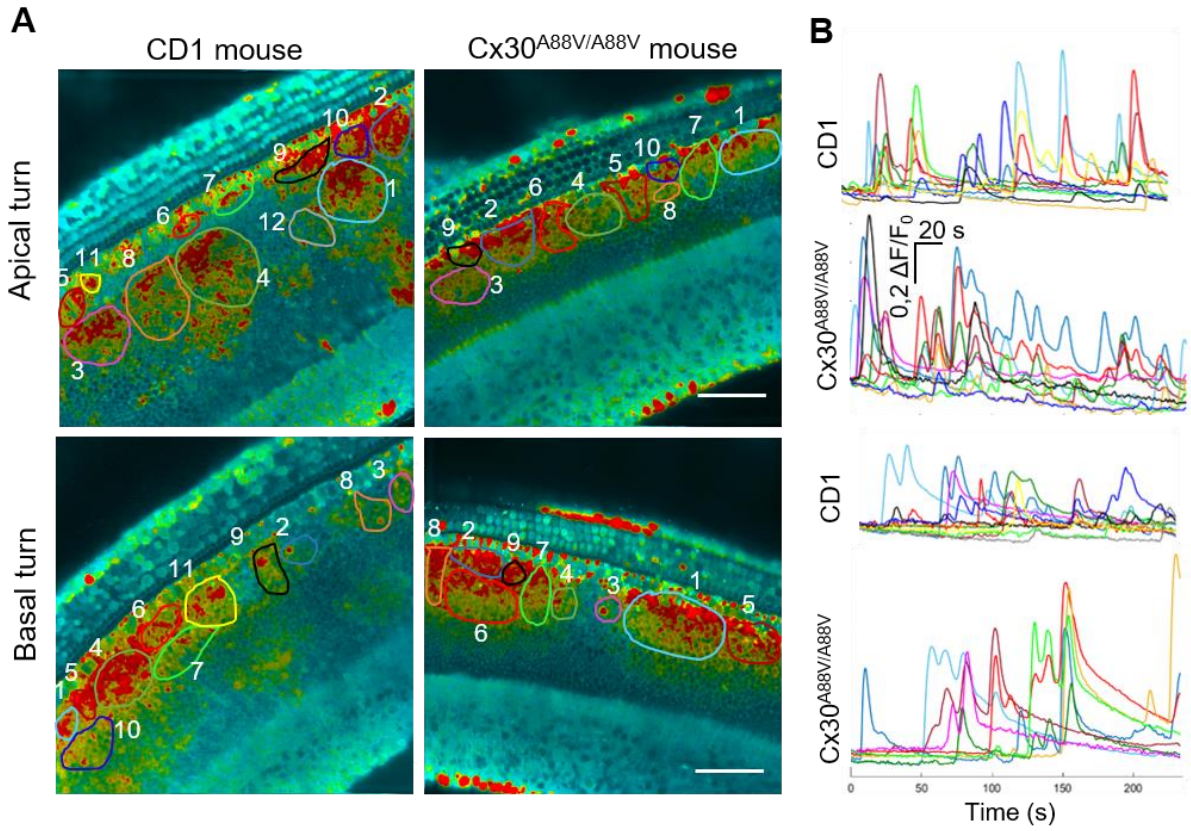

Figure 4.12: Spontaneous Ca^{2+} transients in the GER of CD1 and Cx30 $^{A88V/A88V}$ postnatal cochlear cultures: (A) Representative false-color image of Fluo-8 fluorescence changes ($\Delta F/F_0$) obtained as maximal projection rendering of all frames recorded in an apical and in a basal turn cochlear culture from a Cx30 $^{A88V/A88V}$ P3 mouse and its littermate (CD1) imaged for 4 min at five frames per second. ROIs are shown superimposed on different Ca^{2+} hot spots. Scale bar, 50 µm. (B) Fluo-8 traces generated as pixel averages over the color-matched ROIs shown in (A).

Furthermore, the mean peak amplitude of Ca^{2+} events in the apical and basal turn of Cx30 $^{A88V/A88V}$ cochlear organotypic cultures was 0.24 ± 0.08 $\Delta F/ F_0$ and 0.25 ± 0.12 $\Delta F/F_0$, respectively (Figure 4.14), where $\Delta F/F_0$ indicates Fluo-8 fluorescence emission change vs. baseline fluorescence. Mean peak amplitude values calculated for wild type littermates were 0.28 ± 0.18 $\Delta F/F_0$ in the apical turn and 0.16 ± 0.05 $\Delta F/F_0$ in the basal turn. Statistical analysis of the same pool of data revealed significant difference ($p < 0.001$) both in apical (median = 0.1889; IQR = 0.2004 for Cx30 $^{A88V/A88V}$ and median = 0.1068; IQR = 0.1088 for wild type mice) and basal turns (median = 0.2284; IQR = 0.2362 for mutant mice and median = 0.1109; IQR = 0,1013 for wild type) of postnatal cochlear cultures.

Summarizing, these results confirm that CD-1 WT mice exhibit early- onset, high frequency hearing loss whereas expression of the Cx30A88V in this genetic background resulted in extended hearing protection and overall better hearing profiles starting from 3 months. These auditory features correlate with enhanced spontaneous Ca^{2+} activity in the GER of pre-hearing Cx30 $^{A88V/A88V}$ mice compared to their WT siblings.

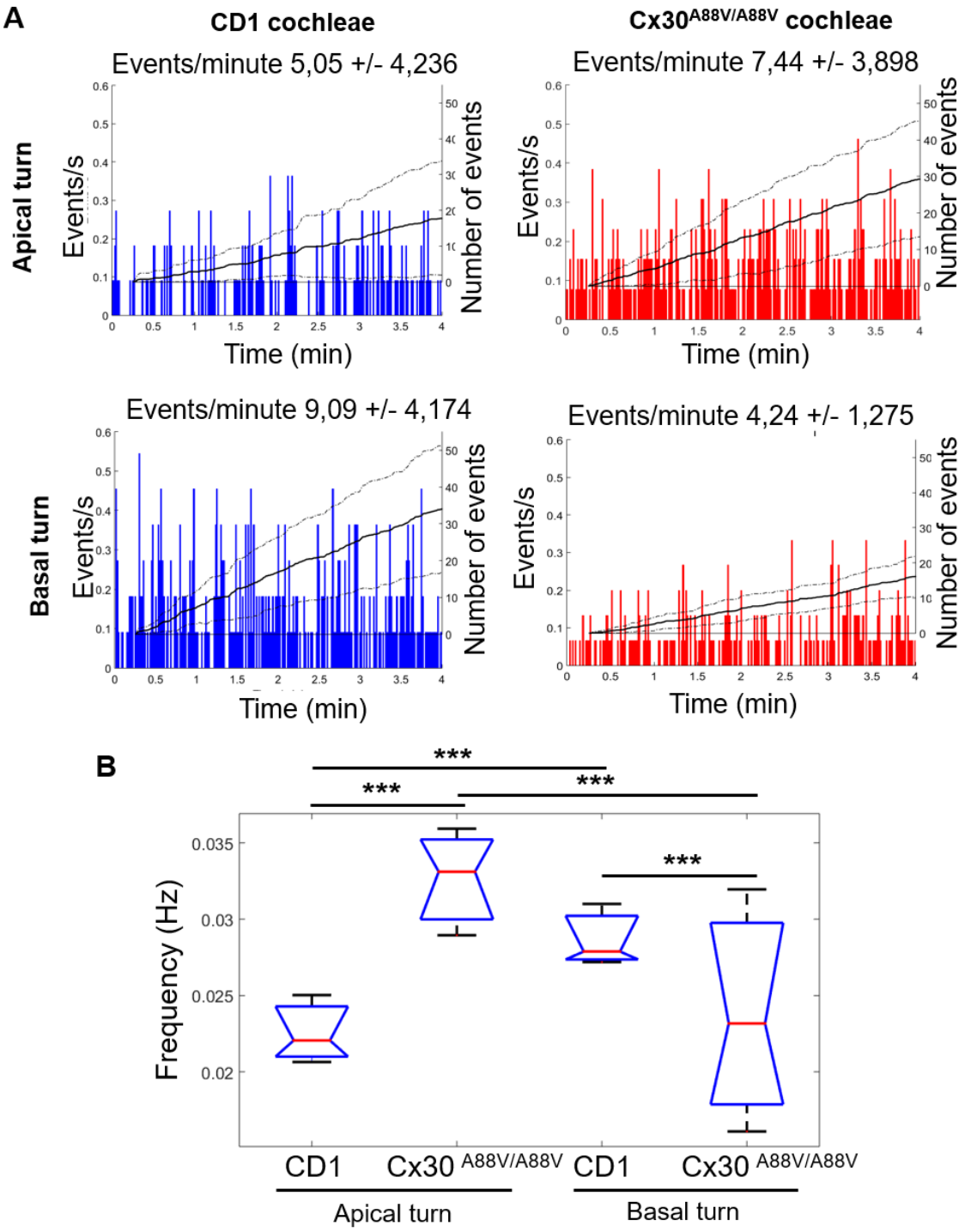

Figure 4.13: Frequency histograms of spontaneous Ca^{2+} transients (events) in cultures from CD1 mice (in blue) and Cx30 $^{A88V/A88V}$ mice (in red) and events' frequency distributions: (A) Frequency histograms from CD1 mice of apical turn and basal turn (in blue) and from Cx30 $^{A88V/A88V}$ mice of apical turn and basal turn (in red). (B) Box plots of event's frequency, computed as the inverse of the time interval between consecutive events occurring in the same hot spot. The value of the median and the IQR (inter-quartile range) for the apical turn are respectively 0,0183 and 0,0213 (CD1), 0,0253 and 0,0286 (Cx30 $^{A88V/A88V}$). The value of the median and the IQR (inter-quartile range) for the basal turn are respectively 0,0273 and 0,0264 (CD1), 0,0153 and 0,0192 (Cx30 $^{A88V/A88V}$). (***p < 0.001, Mann-Whitney, Utest).

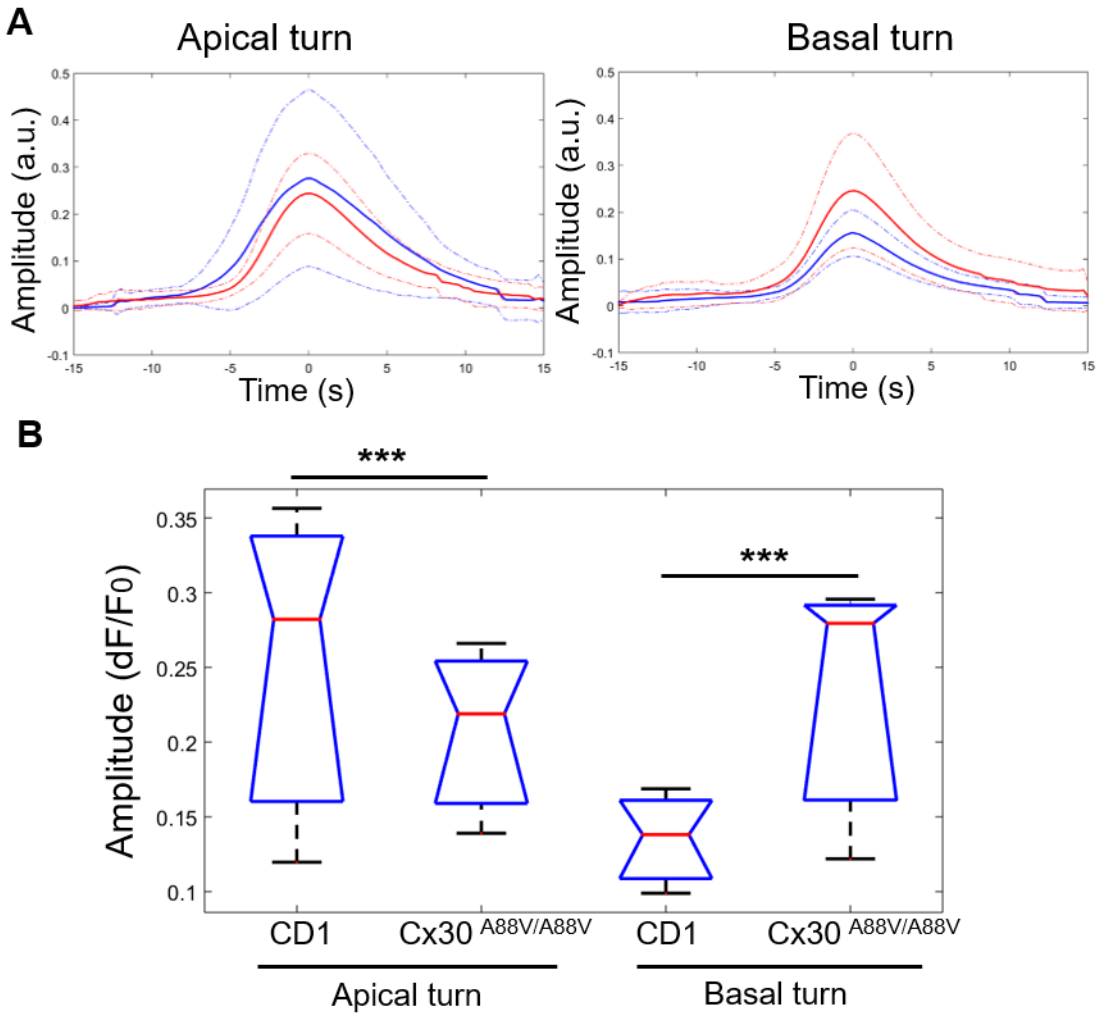

Figure 4.14: Average peaks of the overall Ca^{2+} events and distribution of events' amplitude in CD1 and Cx30 $^{A88V/A88V}$ developing cochleae: (A) Average peaks (solid line) and s.e.m. (dashed lines) computed in apical turn (left) and basal turn (right) of n=5 animals. Blue lines refer to CD1 WT mice; red lines refer to Cx30 $^{A88V/A88V}$. (B) Distribution of the events' amplitude. In the apical turn, the value of the median and the IQR (inter-quartile range) are respectively 0,1068 and 0,1088 (CD1), 0,1889 and 0,2004 (Cx30 $^{A88V/A88V}$). In the basal turn, the value of the median and the IQR (inter-quartile range) are respectively 0,1109 and 0,1013 (CD1), 0,2284 and 0,2362 (Cx30 $^{A88V/A88V}$). (*** $p < 0.001$, Mann-Whitney, U-test).

4.4 Discussion

ATP release in cochlear organotypic cultures is mediated by connexin hemichannels

Similarly to connexins, pannexins have been found to be extensively expressed in the mammalian inner ear [80], particularly in the cochlear spiral limbus, supporting cells of the organ of Corti and fibrocytes in the cochlear lateral wall [80]. However, the impact of Panx1 on auditory function remains unclear because of conflicts in published results [43, 82, 83, 174]. The Panx1$^{-/-}$ strain we have analyzed in this work was the first with a reported global ablation of Panx1 [43, 175]. Our published results [83] confirmed successful ablation of Panx1 both in the cochlea and in the brain of Panx1$^{-/-}$ mice. Our

analyses of auditory brainstem response (ABR) and distortion production otoacoustic emission (DPOAE) recordings indicate normal hearing sensitivity, normal function of the outer hair cell-based "cochlear amplifier" [176, 177, 178] and absence of cochlear nerve defects. In the same work [83] we confirmed that lack of Panx1 affects neither the expression of inner ear connexins nor gap junction communication in the organ of Corti. Moreover, our two-photon imaging experiments, performed to monitor cytosolic Ca^{2+} transients in the greater epithelial ridge (GER), revealed that there were no differences in the frequency of occurrence, mean amplitude and inter-peak interval distributions of spontaneous Ca^{2+} transients in the apical turn of organotypic cochlear cultures from P5 mice. These data lead to the conclusion that intercellular Ca^{2+} signal (ICS) activity in the postnatal cochlea are mediated by connexin hemichannels, ruling out a hypothetical contribution of Panx1 channels.

To validate and corroborate these data, in this work we spatially and temporally correlated the spontaneous ICS activity of cells in the GER and the ATP release mechanism, thanks to the ATP-BCs and the microfluidic chamber. Of note, the customized design of our microfluidic chamber allowed us to simultaneously monitor the spatial extent and propagation of intercellular Ca^{2+} waves and biosensor cells activation, confirming that ATP-induced ATP release is the primary mechanism underlying intercellular propagation of Ca^{2+} signals in the developing cochlea [3]. Therefore, this microfluidic chamber system represents a powerful tool to provide a real-time temporal and spatial correlation between spontaneous cytosolic Ca^{2+} oscillation, ATP release through Cx hemichannels and Ca^{2+} waves propagation. In particular, we experimentally proved the hypothesis that spontaneous Ca^{2+} transients in the GER have been attributed to the release of ATP [131, 179] through connexin hemicannels [60, 132]. Indeed, our experiments with cochlear organotypic cultures and ATP-BCs indicate that the ATP-release mechanism underlying the spontaneous ICS activity of cells in the GER was intact in Panx1 KO mice and impaired in Cx30 KO mice. Furthermore, the frequencies of spontaneous Ca^{2+} activity in the GER of the developing cochlea of $Cx30^{-/-}$ mice were strongly depleted and this mouse strain failed to acquired hearing [132]. Preservation of the ATP-induced ATP-release mechanisms and Ca^{2+} waves propagation are essential for hearing acquisition [4, 60, 132] and maturation of sensory hair cells [167]. In support of this claim by performing ATP release assays in cochlear organotypic cultures isolated from P5 mouse pups, we found that the amount of detectable ATP in the extracellular medium was comparable between $Panx1^{-/-}$ and $Panx1^{+/+}$, and was modulated by extracellular Ca^{2+} variation, a widely recognized mechanism to regulate hemichannel gating (see Introduction 1.2). Conversely, ATP release in cochleae isolated from Cx30 deficient mice was significantly abolished. In conclusion, our extended characterization of $Panx1^{-/-}$ and $Cx30^{-/-}$ mice provides strong evidence that ATP release is mediated by connexin hemichannels which are indispensable for cochlear tissue development, hearing acquisition and auditory function.

Enhanced ATP-dependent Ca^{2+} signaling and long-term protection against age-related hearing loss in $Cx30^{A88V/A88V}$ mice

The importance of Cx26 and Cx30 to hearing and cochlear homeostasis is highlighted by the fact that mutations in the genes that encode Cx26 (GJB2) and Cx30 (GJB6) in humans are the most common cause of inherited non- syndromic pre-lingual deafness [180, 181, 182]. Recently, it has been pointed out that the Cx30-A88V mutation, responsible for the onset of a rare autosomal dominant disorder named Clouston syndrome (OMIM #129500), is characterized by hearing preservation in mouse model [159, 170]. Specifically, $Cx30^{A88V/A88V}$ mice presented with elevated hearing thresholds within the lower

frequency ranges in the apical region of the cochlea (<10 kHz), but substantially improved hearing within the high frequency, basal region of the cochlea.

In this study we used auditory brainstem response (ABR), which is a measure of the electrical activity in the brainstem evoked by the presentation of given acoustic stimuli, in an attempt to determine whether A88V mutation confers long-term protection against hearing loss also in aged mutant mice. Our data are in accordance with the previously reported hearing preservation in young mice [159, 170] and extended those results by showing that this auditory phenotype at 40-60 dB SPL is even more pronounced in 6 months of age Cx30 A88V mutant mice with respect to their age-matched wild type controls. This might seem paradoxical, since *in vitro* studies have shown that the Cx30-A88V mutation can be highly toxic when overexpressed in certain cell lines [169, 183] because of the leaky hemichannels that increase the concentration of ATP into the extracellular medium [169].

To elucidate the mechanisms by which Cx30 $^{A88V/A88V}$ mutant mice showed unexpected hearing phenotype, we investigated intercellular Ca^{2+} activity in the developing cochlea of homozygous mutant mice. Our results show that there is a significant difference between the frequencies (inter-peak intervals) of Ca^{2+} signal events between the mutant and wild type mice, both in the apical and in the basal turn. Specifically, the Cx30 A88V mutation expressed in the developing cochlea caused Ca^{2+} events (i) to occur at higher frequency (number of events/s) in the apical turn than in the basal turn and (ii) the mean events amplitude is greater in the basal turn with respect to the apical turn. Of note, this trend was inverted for CD-1 wild type mice (i.e. genetic background), which conversely showed an overall lower occurrence of spontaneous Ca^{2+} events. The increase in the overall Ca^{2+} signaling in the cochlea could be explained by the hyperactivity of the Cx30-A88V hemichannels that released a higher concentration of ATP in the extracellular milieu. Our results indicate that the auditory phenotype of adult animals is related to the pattern of spontaneous cytosolic Ca^{2+} oscillation and ATP-dependent Ca^{2+} waves propagation within the GER in the developing cochlea.

It has been proposed [184, 185] that frequency of cytosolic Ca^{2+} oscillations regulate gene expression. Indeed, Kelly and co-workers [170] reported a reduction in the expression of the Cx30 in mutant mice (Cx30 $^{A88V/A88V}$) respect to WT (for both mRNA and protein). Moreover, their study showed an extensive loss of the OHCs on the basal turn of WT mice. Conversely Cx30 $^{A88V/A88V}$ mice were protected against hair cell loss and showed intact neurofilaments. Indeed, it has been postulated that oxidative stress lead to chronic inflammation and triggering of apoptotic cell death pathways, premature hearing loss and cochlear degeneration [186, 187]. Therefore, our on-going studies (not shown in this thesis work) strongly suggest that Cx30- A88V mutation in the epithelial gap junction network of the basal turns of cochlea may contribute to an augmented efficiency of the antioxidant defense system in Cx30 $^{A88V/A88V}$ mice, contributing somehow (among other molecular mechanisms that still need to be elucidated) to the prolonged high-frequency hearing protection compared to controls.

At present, however, it remains unknown whether the Cx30-A88V mutant confers long-term protection to high frequency hearing during aging and the preservation of hearing mechanism is unclear.

5. Study of ATP-dependent signaling in the tumor microenvironment

5.1 Introduction to the ATP in the tumor microenvironment and angiogenesis

As mentioned in the Introduction, ATP has the ability to finely tune physiologic and pathophysiologic responses such as neurosecretion, coagulation, smooth-muscle contraction, cell growth and apoptosis, or inflammation. In the tumor microenvironment (TME) purinergic signaling plays a crucial role for both immunosuppression and immunoactivation mainly focused on the concentration of adenine nucleosides (adenosine) and nucleotides (ADP and ATP) [37].

In recent years, the measurement of extracellular ATP concentration in intact tissues has become a major challenge. Different techniques measured this quantity and provided the same answer: ATP level in the interstitium of resting/healthy tissues is very low (order of nanomolar) whereas in stimulated or diseased tissues it can reach hundreds of µmol/l [5, 188, 189]. *Ex vivo* experiments clearly reported a higher adenosine concentration at least twice higher in tumors than in healthy tissues [190], but direct *in vivo* measurements of the adenosine concentration in tumors are not as yet available. These accumulations will turn out to be beneficial or detrimental for the host depending on (i) concentrations of ATP and adenosine, (ii) panel of P2 and P1 receptors expressed by the tumor cells and by the infiltrating inflammatory cells, (iii) level of expression of nucleotide-hydrolyzing enzymes (CD39 and CD73) that influence the rate of degradation from ATP to adenosine [191, 192]. Indeed, adenosine acts at P1 receptors, expressed on immune and cancer cells, causing immunosuppression and stimulation of cancer cell survival and proliferation [191]. The role of ATP in the complex dynamics of the host-tumor interaction is still unclear and ATP can act as an immunostimulant or an immunosuppressive agent causing cancer cell proliferation or even cancer cell death.

P2X7 receptor also has a dual role, because its activation may cause cytotoxicity as well as proliferation. This receptor is expressed predominately in cells of the immune system [106]. In particular ATP activates the P2X7 receptor of dendritic cells that potentiates immuno-responses [191]. On the other hand, it was observed that most malignant tumors overexpress P2X7 [193]. While cytotoxicity is most commonly triggered by millimolar ATP doses, P2X7 activation by endogenously released ATP produces a growth promoting effect [194, 195]. Accordingly, tumors engineered to overexpress P2X7 show an accelerated *in vivo* growth rate, higher VEGF release, thicker vascular networks, and an increased tendency to metastasize [6, 196].

To visualize the network of blood vessels and estimate tumor angiogenesis, micro-computed tomography (micro-CT, see Section 5.2.4) has become widely used because of the non-invasive 3D visualization and quantification of the morphology [197, 198] and its high spatial resolution. Micro-CT takes advantage of an x-ray source to penetrate soft-tissue without disrupting it. To evaluate blood vessels by x-ray imaging an application of radio-dense contrast agents is required. Microfil compounds are among the most used for *ex vivo* micro-CT measurements, consisting in a lead-containing silicon rubber that polymerizes within the vascular compartment, enabling the visualization of cardiovascular structures.

Nowadays purinergic receptors are considered a good target for anti- cancer therapy [90], but further studies on ATP metabolism in the TME must be carried out. Few techniques are able to measure ATP directly *in vivo* without altering the system [5] and less studies are focused on the mechanism of ATP release from cancer cells during tumor growth or therapy. Our ATP-BCs can be used as non-invasive probes to measure *in vivo* ATP in different conditions and to clarify the release mechanisms involved in tumor proliferation or regression mediated by extracellular ATP.

5.2 Materials and Methods

5.2.1 The mouse melanoma B16-F10 cell line

The B16-F10 mouse melanoma cell line was purchased from American Type Culture Collection (ATCC, Cat.N. CRL-6475). Cells were cultured in RPMI 1640-GlutaMAX (Thermo Fisher Scientific, Cat.N. 61870-010) supplemented with 10% heat-inactivated FBS and 1% penicillin/streptomycin.

B16-F10 P2X7R-silenced (shRNA P2X7R) cells were a gift of Professor Francesco Di Virgilio (Department of Morphology, Surgery and Experimental Medicine, Section of Pathology, Oncology and Experimental Biology, University of Ferrara) [199]. Gene silencing is considered a gene knock down mechanism since the methods used to silence genes generally reduce the expression of a gene [200]. B16 shRNA P2X7R were cultured in RPMI 1640-GlutaMAX supplemented with 10% heat-inactivated FBS and 1% penicillin/streptomycin and maintained at 37°C under controlled atmosphere of CO_2 (5%].

5.2.2 Transgenic mice and genotyping

All mouse manipulations were performed in accordance with a protocol approved by the Italian Ministry of Health (Prot. n.410/2016-PR). Animals are bred and genotyped in the CNR Monterotondo node of the European Mouse Mutant Archive (EMMA), an ESFRI/INFRAFRONTIER Distributed Research Infrastructure.

The background strains of the transgenic mice ($P2X7^{-/-}$) [201] and respective wild type ($P\ 2X7^{+/+}$) used in this study is C57BL/6.

Mice used for this study were female aged of 3-4 months.

Mice were genotyped according to published protocols by standard PCR [43]. Primers for P2X7 KO were as follows:

- P2X7 f: 5’ – TGCCCATCTTCTGAACACC – 3’;
- P2X7 r: 5’ – CTTCCTCTTACTGTTTCCTCCC – 3'.

5.2.3 Melanoma cell inoculation and tumor growth in the mouse dorsal skinfold chamber

The dorsal window chamber preparation, shown in Figure 5.1, consists of two complementary titanium alloy frames implanted onto WT and P2X7 KO mice. Detailed surgical procedures are described in Ref. [202]. The clear glass window permits direct observation of the tumor implant, surrounding vessels, and the host's subcutaneous tissues.

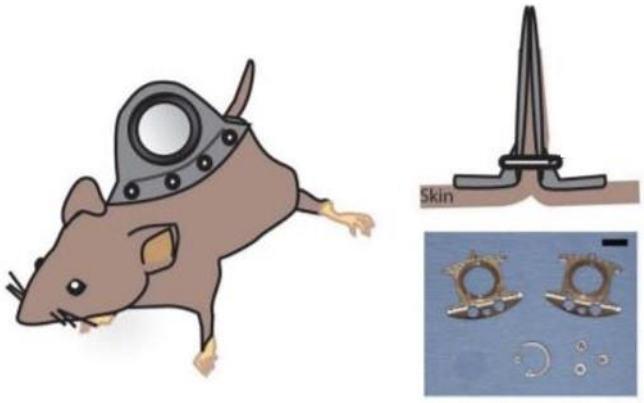

Figure 5.1: The mouse dorsal skinfold window chamber apparatus: adapted from [203]. The metal frame of the window is clamped surgically around the dorsal skinfold. Photograph shows the window chamber, retaining nuts and glass window. Scale bar, 1 cm.

To achieve stable and uniform expression of the GCaMP6s cytosolic Ca^{2+} biosensor, cultures of B16-F10 cells were infected with a lentiviral vector (pHAGE-RSV-GCaMP6s, a gift from Darrell Kotton, Addgene plasmid #80146). Lentivirus was produced using HEK293T packing cells according to a standard protocol described in Ref. [115]. B16-F10 cells, stably expressing GCaMP6s, were suspended in ice-cold HBSS at density of 16.7 x 10^6 cells/ml. The glass coverslip of the dorsal skinfold chamber was temporarily removed and 30 µl of cells suspension (containing ~ 5 x·10^5 cells) were deposited on the exposed dermal tissue to form a superficial tumor.

Experiments were performed 3-5 days after inoculation of the B16-F10- GCaMP6s cells. To detect the ATP released within the dorsal skinfold chamber, the empty glass coverslip of the chamber was replaced with another one in which ATP-BCs had been plated the day before at 70% density (Figure 5.2). The solution trapped between the tumor and this ATP-BCs-bearing coverslip was the LCS (20µM Ca^{2+}, described in Section 3.2.2) supplemented with ARL67156 (100 µM) or with apyrase (25U/ml).

5.2.4 Intravital imaging and ATP detection during photoactivation of a photosensitizer loaded in the tumor

Intravital imaging was performed using the multiphoton microscope described in Section 4.2.1. Fluorescence emission from either tumor or ATP- BCs (loaded with Fluo-8) was excited with the pump beam at 920 nm and collected through 525/40 nm bandpass filter. As described above (see Section 4.2.3), images from two different focal planes, one for the tumor and the other for the ATP-BCs, were collected sequentially and continuously by using the microscope objective mounted on a piezoelectric actuator, achieving a final acquisition rate of 0.5 fps.

To further test the ability of ATP-BCs to detect ATP release in the TME following an external stimulus, we performed photoactivation of a photosensitizer agent (PS) absorbed by tumor cells. PS molecules are promoted to a long-lived triplet state by absorption of light with specific wavelength. In this excited state, the "activated" PS molecule interacts with molecular oxygen present inside the cell and triggers a cascade of photochemical reactions leading to the production of extremely toxic reactive oxygen

species (ROS) [204]. Cytotoxic effects caused by PS excitation propagate from directly irradiated cells to surrounding non-exposed cells, a phenomenon called “bystander effect” [205, 206]. Exposure of cells to radiation induces ATP release towards the extracellular milieu [207]; moreover, ATP and purinergic signaling have been proposed as mediators of bystander signaling propagation both *in vitro* [208] and *in vivo* [209].

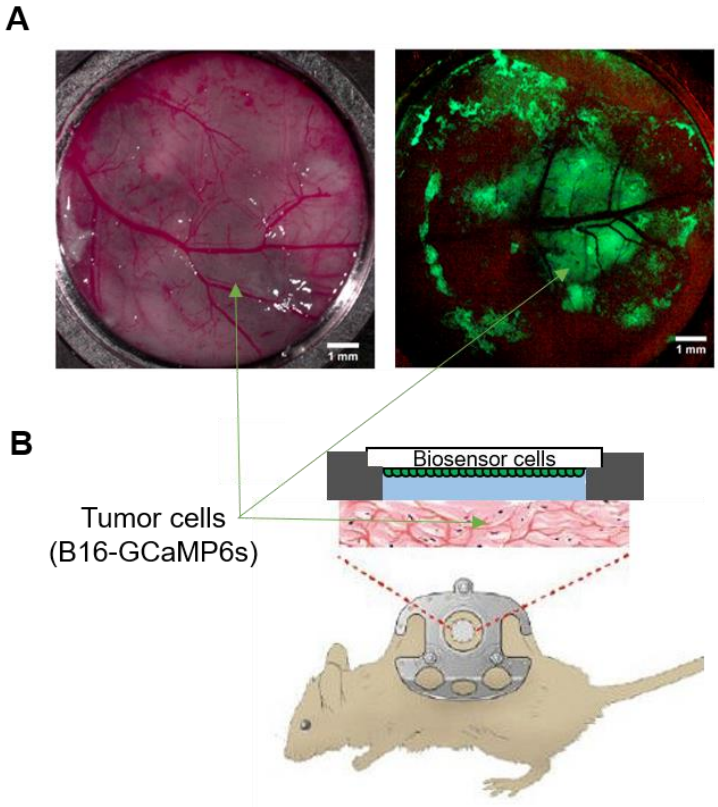

Figure 5.2: Two-dimensional melanoma derived from B16-F10 cells infected with GCaMP6s growth in the dorsal skinfold chamber: (A) Representative images of melanoma in the dorsal skinfold chamber. Left: bright field image; Right: fluorescence image of B16-F10 cells infected with the GCaMP6s cytosolic Ca^{2+} probe. Scale bars: 1 mm. (B) Sketch of the dorsal skinfold chamber coupled with ATP-BCs to detect ATP in the TME.

The tumor was first loaded with the PS incubating for 1hour with in extracellular medium containing PS (100 µM) and pluronic F-127 (0.1 % w/v). Then, the tumor was washed twice and the extracellular ATP measurement was repeated as described before simultaneously to focal PS activation.

We induced a massive ATP release in the TME in a spatiotemporally- controlled manner by photoactivating the PS Aluminum Phthalocyanine Chloride in a single cell of the tumor grown in the mouse dorsal skinfold chamber. For PS excitation, we used a 671 nm diode-pumped solid-state laser (Shanghai Dream Lasers Technology Co., Shanghai, China). The 671 nm laser light emitted from the multimode optics was collimated using an achromatic doublet and the beam was injected into the two-photon microscope optical path just above the objective via reaction at 45° of a dichroic mirror (600–750 nm notch dichroic custom-made by Semrock). The collimated laser beam was focused by the 60X objective into a 10 µm diameter spot (~80 µm2 area), which allowed spatially conned

irradiation of a single cell in the culture, i.e. "focal" irradiation, at an irradiance of $\sim 5 \times 10^6$ mW/cm^2 [210]. Photoactivation was performed with laser in continuous mode, while the objective was stepping up and down to record the signals from the two focal plane. Firstly, we controlled that this laser did not alter the ATP-BCs responses by performing the same experiment protocol in absence of PS.

5.2.5 Micro-Computed Tomography (micro-CT)

Micro-Computed Tomography (micro-CT) is a non-destructive imaging tool for the production of high-resolution three-dimensional (3D) images. Micro- CT equipment is composed of several components: x-ray tube, radiation filter and collimator (which focuses the beam), specimen stand, and phosphor-detector/charge-coupled device camera (Figure 5.3). Reconstruction of a 3D image is performed by rotating the sample to generate a series of 2D projections that will be transformed to a 3D representation by using a digital process called back-projection [198, 211]. This non-destructive imaging modality produces 3D images with volumetric pixel (voxel) approaching 1 µm.

The principle of micro-CT is based on the attenuation of an x-rays beam passing through the sample being imaged. As the beam passes through tissue, the intensity is diminished according to the absorption law $I_x = I_0 * e^{-\mu x}$, where I_0 is the intensity of the incident beam, x is the distance from the source, I_x is the intensity of the beam at distance x from the source, and µ is the linear attenuation coefficient [212]. Therefore, the attenuation depends both on the sample material and on the source energy and can be used to quantify the density of the tissues being imaged when the reduced intensity beams are collected by a detector array.

Samples for the visualization of vascular angiogenesis through micro-CT were obtained perfunding tumor-bearing mice with Microfil (a lead-containing silicon rubber, Flow Tech, Cat.N. MV-112) injected intra-cardially. Tumors were induced by inoculating 1 x 10^6 B16-F10 or shRNA P2X7R cells (see Section 5.2.1 for detailed description of the cells) subcutaneously into both the flank of female wild type (WT) mice and knock out mice for P2X7R gene (P2X7-KO). After 8 days from cells injection and before Microfil perfusion, mice were perfused with 20 mL of PBS supplemented with heparin 5U/ml, Sigma-Aldrich, Cat.N. H3149-50KU) for complete blood removal. Perfusion was performed at physiological pressures, using a peristaltic pump (Harvard Apparatus, Cat.N. P-70).

Samples collection was performed after 3 hours from the end of the perfusion to complete Microfil polymerization. Tumors were treated with paraformaldehyde (4%) and ethanol (from 50% to 100%) to fix and to dehydrate the samples. Once dehydration was completed, the tumors were scanned using a non–gantry-based SkyScan 1172 micro-CT system (Bruker). Tumors were positioned on a computer-controlled rotation platform and were scanned 200° around the vertical axis, in rotation steps of 0.7° at 39 kV. The generated isotropic pixel sizes were 8 µm. After volume rendering of reconstructed high-resolution micro-CT data sets, blood vessels were visualized and systematically analyzed using Analyze 12.0 software.

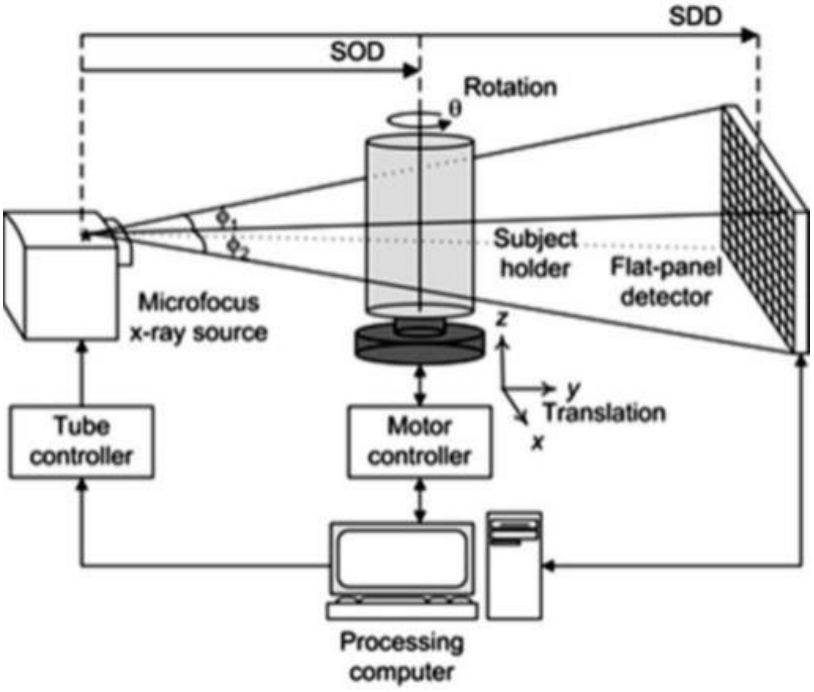

Figure 5.3: Schematic diagram of a micro-CT system: from [213]

5.3 Results

5.3.1 Response of ATP-BCs exposed to melanoma investigated by intravital multiphoton microscopy

It is well know that ATP is abundant in the TME [90, 190]. Pellegatti et al. [5] suggested a new probe (pmeLUC, plasma membrane luciferase) stably transfected in HEK293T cells to measure ATP concentration in the TME in *in vivo* experiments.

Here, we reported preliminary experiments to prove the ability of ATP- BCs to detect ATP release in TME under spontaneous condition and after photostimulation of the tumor cells pre-loaded with a PS (Aluminum Phthalocyanine Chloride). To this aim we used B16-F10 cells to induce melanoma in a dorsal skinfold chamber (see Section 5.2.3). Traditionally, the dorsal skinfold chamber technique in mouse models was used to visualize dynamic processes, e.g. cell migration, vascular growth, immune system infiltration and tumor response to therapy [214]. More recently, it has been exploited to study Ca^{2+} signaling in the tumor mass [215, 216]. Our future prospective is to use the dorsal skinfold chamber to study Ca^{2+} signalling in 2D melanoma and its correlation with ATP using the ATP-BCs in spontaneous condition and during the process of phototherapy. Our sensors are relatively easy to generate (lentiviral infection) and handle and they are easy to monitor through confocal microscopes. Moreover ATP-BCs are adapted to record real-time signals and to study metabolic mechanisms at cellular resolution, whereas the pmeLUC-HEK293T gives a macroscopic measure of ATP concentration through total body *in vivo* measurements.

As shown in Figure 5.4, ATP-dependent Ca^{2+} responses were measured in ATP-BCs loaded with Fluo-8 when they were mounted in the dorsal skinfold chamber as described in Section 5.2.3 (see also Figure 5.2). Interestingly, we were able to detect ATP spontaneously release from the tumor cells in the TME

(Figure 5.4 A). Similarly, more robust signals were recorded from ATP-BCs after photostimulation of the tumor cells and they are completely abolished when ARL was substituted by apyrase (25U/ml) (Figure 5.4 B, C). Further studies must be carried out to corroborate these data and to prove the relation between Ca^{2+} signals and ATP release mediated by connexins in the TME. However these preliminary measurements are very promising and prove the versatility of ATP-BCs.

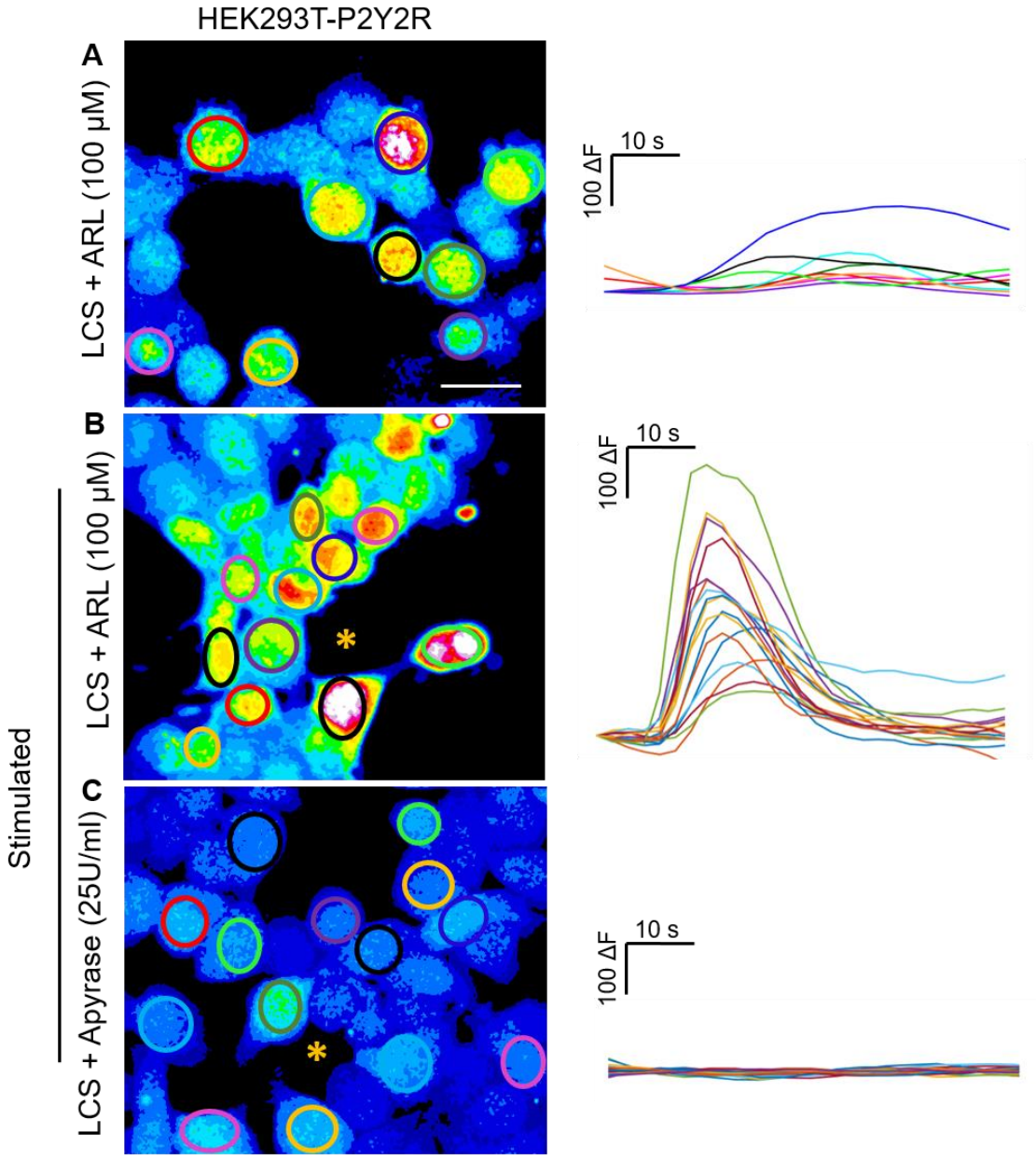

Figure 5.4: Spontaneous and photostimulated ATP release in the tumor microenvironment: Left: representative false-color image of biosensor cells mounted in the dorsal skin chamber facing B16-F10 melanoma cells. Right, ATP-dependent Ca^{2+} signaling traces generated as pixel averages over the color-matched ROIs (shown in the corresponding image at the left) in unstimulated conditions (A) or during photostimulation with a photosensitizer (PS) loaded in the tumor cells (B, C). The fluid filling the gap between tumor and ATP-BCs was a Low Calcium Solution (LCS) supplemented with ARL67156 (100 µM, A, B) or with apyrase (25U/ml, C). Yellow asterisks represent the photostimulated point in the tumor underneath the coverglass bearing the ATP-BCs. Scale bar: 20 µm.

5.3.2 A micro-CT-based study of melanoma-driven angiogenesis in wild type and P2X7R KO mice

Microfil perfusion combined with *ex vivo* micro-CT imaging allowed highly detailed 3D visualization of blood vessels as well as systematic and quantitative analysis of vascular parameters such as vessel size, vessel distribution, and vessel branching (Figures 5.5). This technique allowed to assess these parameters within intact tumors, holding great potential for the better understanding of tumor angiogenesis.

In order to understand the role of P2X7 in tumor growth and angiogenesis, we injected parental B16-F10 (B16 WT) or B16 shRNA-P2X7R cells in WT and P2X7 KO mice. After 8 days from the inoculation the mouse was perfused with Microfil and the tumors were collected. We can notice from Figure 5.5 that the vasculatures of the tumors derived from B16 WT cells showed a more chaotic pattern of vessels and blunt ends compared to tumors derived from B16-shRNA cells.

From the micro-CT dataset we first evaluated the total volume of different samples and the relative volume of the blood vessels. Surprisingly, the total volume of tumors generated with B16 WT were lower compared to tumors generated with B16-shRNA (Figure 5.6 A,C). In particular the mean values of tumor volumes were 68.91 ± 14.70 mm^3 and 77.16 ± 15.92 mm^3 for the B16 WT cells inoculated in WT or KO mice respectively (the pooled data were not statistically different, p = 0.71, t-test), while the volumes were 122.31 ± 14.56 mm^3 in WT mice and 112.10 ± 7.27 mm^3 in KO mice for tumors derived from B16-shRNA cells (p = 0.51, t-test). All data were generated from at least n = 5 tumors. Furthermore, comparing the pooled data of tumor volumes from the tumors induced with the two different cell lines (B16 WT or B16-shRNA) on mice with the same genetic background, we noticed that they were significantly different (p = 0.009 for WT mice and p = 0.044 for KO mice, t-test). These data suggests that at this stage the P2X7 receptors, expressed by the tumor cells and by the immune system of the host, were not crucial for tumor growth.

We next evaluated the vascular volume, that correspond to the volume filled with the Microfil (Figure 5.6 B), and we compared it with the total volume of the same sample (Figure 5.6 C). The mean value of the vessel volume percentages of vessel volumes were equal to 11.59 ± 2.24 mm^3 (that correspond to 16.82% ± 0.06% of total volume) for B16-WT tumors grown in WT mice and equal to 10.41 ± 1.81 mm^3 (that correspond to 13.50% ± 0.051% of total volume) for B16-WT tumors grown in KO mice. Our data were in great accordance with the literature and showed statistical difference (p = 0.025, t-test) between B16-WT tumor grown in WT or KO because of a decrease in vascular endothelial growth factor (VEGF) reported in KO mice [6, 217]. Conversely, the percentages of mean vessel volumes for B16-shRNA tumors were 3.98% ± 0.60% and 4.19% ± 0.31% for WT and KO mice, respectively (p = 0.32, t-test), whereas the actual vessels volume were 4.88 ± 0.15 mm^3 and 4.70 ± 0.04 mm^3. As previously reported, the comparisons of the percentage of vessel volumes between tumors induced with B16-WT or B16-shRNA in mice with the same genetic background were statistically different (p = 5.5 x 10^{-5} for WT mice and p = 5.5 x 10^{-6} for KO mice, t-test).

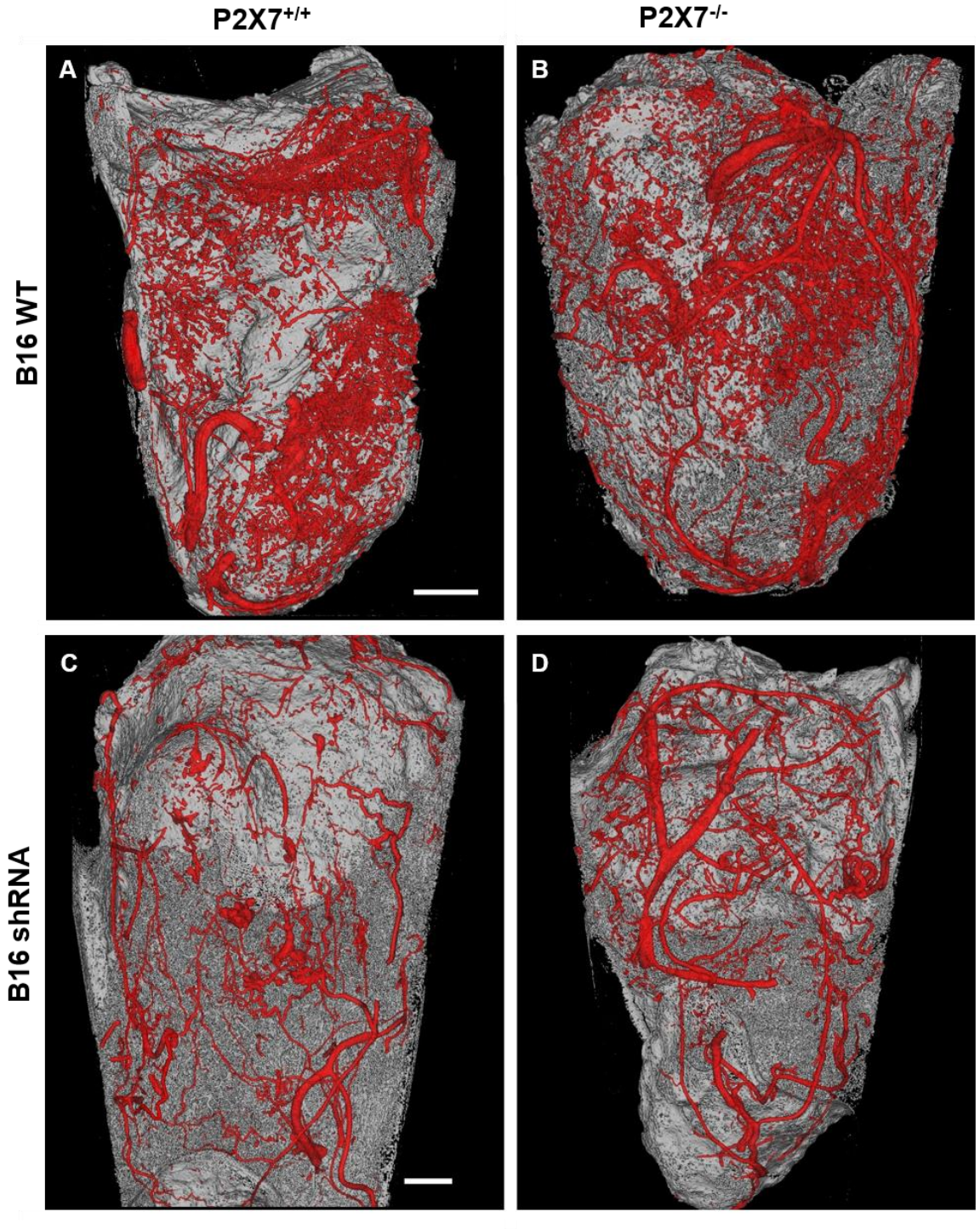

Figure 5.5: MicroCT imaging of tumor angiogenesis derived from B16 WT (A,B) or shRNA-P2X7R (C,D) cells injected in WT ($P2X7^{+/+}$, A,C) or KO ($P2X7^{-/-}$, B,D) mice: Mice were humanely euthanized and perfused with Microfil (a microCT contrast agent) 8 days after the injection of 10^6 cells in the right hip. The three-dimensional micromorphology of tumor blood vessels was visualized at a resolution of approximately 8 µm. Scale bar: 2 mm. Videos of the volume renderings can be downloaded from https://www.dropbox.com/sh/i23yczdv502a0w1/AADH2tCGiid66eutC073HMSZa?dl=0

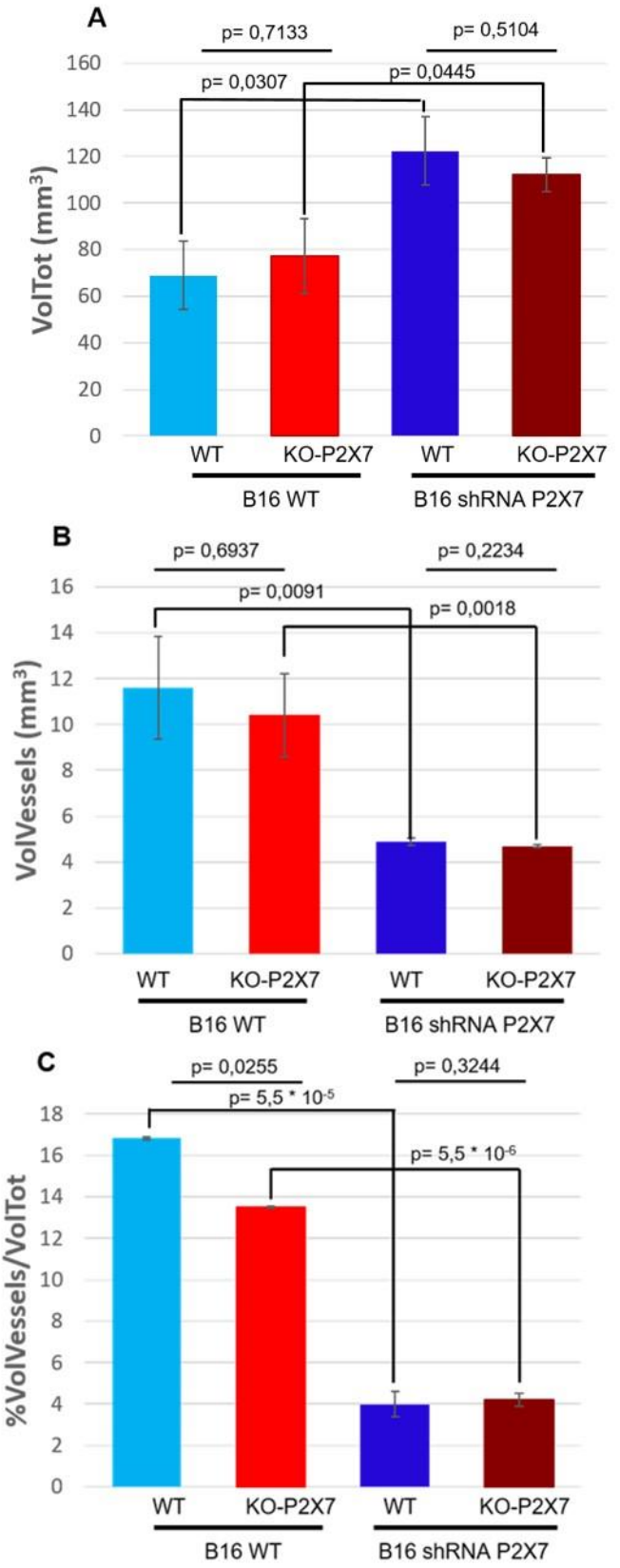

Figure 5.6: Tumor volumes (A), vessel volume (B) and percentage of vessels volume (C) of the tumors 8 days after injection of B16 WT or shRNA P2X7 cells in WT or P2X7 KO mice: Histograms show data from at least n = 5 sample for each conditions. Data were generated with Analyze 12.0.

Consistently with the increased vascular volume and higher degree of angiogenesis [199] in tumor-bearing mice induced with B16 WT cells, a clear tendency towards increased vessel size was observed (Figure 5.7). Comparing vessel diameters obtained by *ex vivo* micro-CT confirmed the significant difference between the two distributions ($p < 0.001$, Fisher F-test, Figure 5.7). The most probable diameter observed in tumors grown in WT mice and derived from B16 WT cells were 40 µm < d ≤ 50 µm (23.24 ± 3.36 counts) compared to tumors derived from B16 shRNA cells 30 µm < d ≤ 40 µm (20.94 ± 1.36 counts). Similarly for KO tumor-bearing mice inoculated with B16 WT or B16-shRNA cells (Figure 5.7 B) the most frequent diameters ranged between 40 µm and 50 µm (25.16 ± 4.53 counts) and between 20 µm and 30 µm (23.39 ± 1.56 counts) respectively (Figure 5.7 B).

Altogether this data demonstrated that in the chosen stage of the tumor progression (around 8 days) through the high resolution and accuracy of *ex vivo* micro-CT measurement, it was possible to measure tumor angiogenesis before the occurrence of conformational and volumetric differences and validate the hypothesis that the receptor P2X7 expressed by the tumor cells released VEGF.

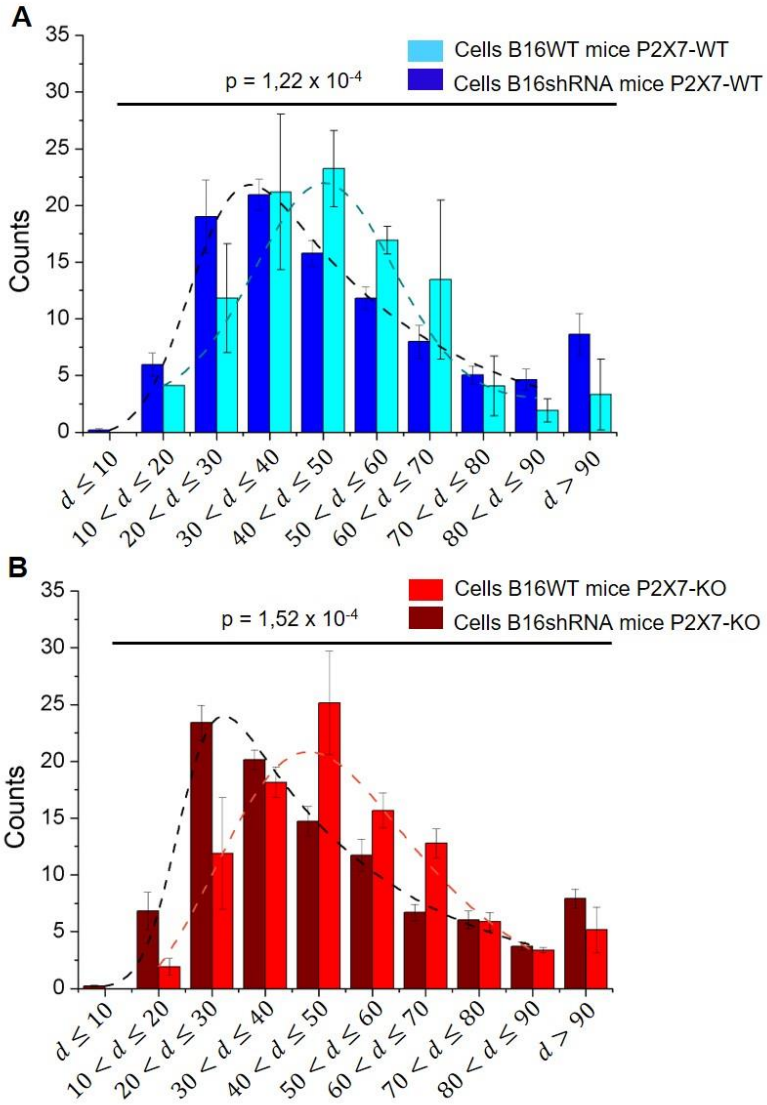

Figure 5.7: Distribution of vessel diameter 8 days after injection of B16 WT or shRNA P2X7 cells: (A) Quantification of blood vessel sorted by diameter in tumor derived by the injection in WT mice of B16 WT (in cyan) and shRNA-P2X7 (in blue) cells. (B) Quantification of blood vessel sorted by diameter in tumor derived by the injection in P2X7 KO mice of B16 WT (in red) and shRNA-P2X7 (in bordeaux) cells. Data were obtained with Analyze 12.0 and are expressed as mean counts ± s.e.m. from n = 4 different tumors for each conditions. Dashed lines are the fit of the distributions obtained with the *GaussMod* model of Analyze 12.0 ($p = 1.22 \times 10^{-4}$ and $p = 1.52 \times 10^{-4}$, Fisher F-test).

5.4 Discussion

The TME is the site where tumor cells are in close contact with host cells and is a dynamic environment. The understanding of the biochemical composition and molecular mechanisms of the TME that regulates tumor cells metabolism, proliferation and motility or host immune responses are crucial to develop new anti-cancer therapies that are more effective on the tumor cells and preserve the host cells integrity.

The biochemical composition of the TME is the result of the activity of both the tumor and host cells. Cancer cells release metabolites that acidify the TME and enzymes that degrade the extracellular matrix [218, 219]. Likewise, host cells release cytokines, growth factors, cytotoxic molecules [220]. Nucleotides, mainly ATP, are also released into the TME by both tumor and host cells. The effects of nucleotides in the TME are countless, they can affect migration and activation of immune cells as well as growth and aggressiveness of tumor cells, and a deep understanding of purinergic signaling in the TME may offer novel therapeutic prospects.

The most obvious suitable target would be extracellular ATP itself. The concentration of this nucleotide is markedly increased in tumor sites and therefore decreasing its levels might be beneficial; alternatively, it might be possible to further increase the TME ATP concentration to exploit ATP-dependent cytotoxicity [221]. The *in vivo* administration of ATP has been explored as an anticancer therapy in tumor-bearing mice with conflicting results [222, 223]. Recent studies have proposed as therapeutic strategies targeting: (i) purinergic receptors overexpressed by most tumor cells [90], (ii) ectonucleotidases that increase ATP degradation and adenosine accumulation with the consequent inhibition of immune responses [224, 225] or (iii) ATP release mechanisms [226, 227] that however are poorly investigated.

Mechanisms of ATP release are not completely characterized and it has been hypothesized that in the TME they could be whether passive, such as stressed or dying cells or hypoxia [228], or active through conductive channels, vesicles, or plasma membrane proteins forming non-selective pores (e.g. connexins, pannexins, P2X7R) [40].

The challenge of measuring extracellular ATP concentration in intact tissues has been addressed in different ways. Promising *in vitro* methods have been developed, but only few *in vivo* techniques have been proposed. Dubyak and co-workers [229] developed a chimeric protein that consists of the IgG-binding domain fused in-frame with the complete sequence for firefly luciferase that specifically bind the cell surface; recently Tantama and co-workers [230] provided a ratiometric FRET-based fluorescence indicator able to detect extracellular ATP. However no *in vivo* data are available for these two probes. Other more sophisticated techniques based on atomic force microscopy [231], patch-clamp [232] or tandem enzyme reactions [233] have also been proposed, but these techniques are complex to use. Micro- electrode recording has also been applied to extracellular ATP measurement in tissue slices and *in vivo* [234]. This technique suffers of an intrinsic limit: the insertion of the electrode tip into the tissue causes by itself tissue damage with consequent ATP release. As already mentioned only Di Virgilio and co-workers [5] proved the abilities of their developed luciferase probes to measure *in vivo* extracellular ATP.

In this frame, dorsal skinfold chamber coupled with our ATP-BCs could be a powerful tool to reveal the mechanisms of ATP release in the TME both in spontaneous condition or during therapies. Indeed,

thanks to our preliminary results, we can assess that ATP-BCs are sensitive enough to detect extracellular ATP accumulated in the TME of 2D melanoma and are able to investigate molecular pathways at cellular level. Moreover, we proved the possibility to use ATP-BCs also during therapy such as photodynamic therapy. The results shown in this thesis are really promising and further experiments must be carried out, in particular in presence of inhibitors of plasma membrane channels (e.g connexins blocker) to gain more insight into the molecular mechanism.

Nowadays, the most validated candidates for anti-cancer therapies are the purinergic receptors [90]. In order to fully recognise the potential of purinergic signaling in cancer therapy, an in-depth characterization of P2 receptors is needed. We focused on the relation between P2X7R and the angiogenetic process. It is known that ATP has a strong angiogenic effect on the intratumour vessel network. Specifically, stimulation of P2Y1R, known to be expressed by endothelial cells [235], activates P2X7R that triggers VEGF release [6, 236, 237].

For this study we used micro-CT measurement and we selected Microfil, an x-ray contrast agent that offers several advantages including: its wide use, ease of administration and tissue preparation, high contrast of vasculature structure and long-term sample stability [238]. Using this technique it was possible to identify clear differences in tumor vessel structure and density that were characteristic and consistent within the tumor lines evaluated. In great accordance with the literature [6], our results showed that tumors derived from B16 WT cells are more angiogenetic compared to tumors derived from B16-shRNA, proving that vessel architecture among the different tumor models were reflective of their relative abilities to engage host cells in the angiogenic process [239]. The relative vessels volumes and differences in diameter offer the potentiality to correlate tumor angiogenesis patterns with tumor progression and severity. This promising model can be used to validate the response of the tumors to a given anti-angiogenic agent and to test the P2X7 receptors as potential target for cancer therapy.

Conclusions

In this thesis work, we have investigated the correlation between Ca^{2+} signaling and ATP release in developing cochlear organotypic cultures and tumor microenvironment to better understand their molecular pathway and to develop new therapeutic strategies. To this end, we designed and characterized a new powerful tool for the detection of sub-micromolar concentrations of extracellular ATP based on live-cells biosensors, called ATP-BCs. We demonstrated the high sensitivity, selectivity and versatility of the ATP-BCs. Most importantly, the ATP-BCs are one of the few available probe for *in vivo* detection of ATP. Combining this tool with a new designed microfluidic chamber, we were able to measure ATP in two different environments (cochlear organotypic cultures and tumor microenvironment).

In the developing cochleae, we highlighted the pivotal roles played by connexin 26 and connexin 30 hemichannels as mediators of ATP-dependent intercellular Ca^{2+} signals activity in the developing cochlea. Furthermore, our extended characterization of $Panx1^{-/-}$ mice finally provides strong evidence that, unlike Cx26 and Cx30, Panx1 is dispensable for cochlear tissue development, hearing acquisition and auditory function. These data afford an additional fundamental piece of information in an attempt to address the still critically debated question about the plausible roles played by Panx1 in the physiology and pathology of the inner ear.

Thanks to the non-invasiveness of ATP-BCs, it was possible to investigate ATP release during photodynamic therapy in *in vivo* tumor. Although further studies are required, these results are promising to study purinergic signaling in tumors and to investigate new therapeutic strategies.

Our results and the above considerations have widened the knowledge on the mechanisms of ATP release in developing cochlea and encourage further studies to characterize purinergic signaling in the tumor microenvironment as potential therapeutic target.

Bibliography

[1] Ralevic, Vera, and Geoffrey Burnstock. Receptors for purines and pyrimidines. Pharmacological reviews 50.3 (1998): 413-492.

[2] Burnstock, Geoffrey. Purinergic signaling: therapeutic developments. Frontiers in pharmacology 8 (2017): 661.

[3] Ceriani, Federico, Tullio Pozzan, and Fabio Mammano. Critical role of ATP-induced ATP release for Ca2+ signaling in nonsensory cell net- works of the developing cochlea. Proceedings of the National Academy of Sciences 113.46 (2016): E7194-E7201.

[4] Mammano, F. and M. Bortolozzi, Ca2+ signaling, apoptosis and autophagy in the developing cochlea: Milestones to hearing acquisition. Cell Calcium, 2018. 70: p. 117-126.

[5] Pellegatti, Patrizia, et al. Increased level of extracellular ATP at tumor sites: in vivo imaging with plasma membrane luciferase. PloS one 3.7 (2008): e2599.

[6] Adinolfi, Elena, et al. Expression of P2X7 receptor increases in-vivo tumor growth. Cancer research 72.12 (2012): 2957-2969.

[7] Drury, A. N., and A. V. Szent-Gy¨orgyi. The physiological activity of adenine compounds with especial reference to their action upon the mammalian heart 1. The Journal of physiology 68.3 (1929): 213-237.

[8] Burnstock, G. Purinergic nerves. Pharmacological reviews 24.3 (1972): 509-581.

[9] Bours, M. J. L., et al. Adenosine 5J-triphosphate and adenosine as endogenous signaling molecules in immunity and inflammation. Pharmacology & therapeutics 112.2 (2006): 358-404.

[10] Abbracchio, Maria P., and Geoffrey Burnstock. Purinoceptors: are there families of P2X and P2Y purinoceptors? Pharmacology & therapeutics 64.3 (1994): 445-475.

[11] Jacobson, Kenneth A., Michael F. Jarvis, and Michael Williams. Purine and pyrimidine (P2) receptors as drug targets. Journal of medicinal chemistry 45.19 (2002): 4057-4093.

[12] Burnstock, Geoffrey, and Gillian E. Knight. Cellular distribution and functions of P2 receptor subtypes in different systems. Int Rev Cytol 240.1 (2004): 31-304.

[13] Khakh, Baljit S., et al. International union of pharmacology. XXIV. Current status of the nomenclature and properties of P2X receptors and their subunits. Pharmacological reviews 53.1 (2001): 107-118.

[14] North, R. Alan. Molecular physiology of P2X receptors. Physiological reviews 82.4 (2002): 1 013-1067.

[15] von Kugelgen, Ivar, and Axel Wetter. Molecular pharmacology of P2Y- receptors. Naunyn-S chmiedeberg's archives of pharmacology 362.4-5 (2000): 310-323.

[16] Boeynaems, Jean-Marie, et al. P2Y receptors: new subtypes, new functions. Drug development research 59.1 (2003): 30-35.

[17] Zimmermann, Herbert. 5J-Nucleotidase: molecular structure and functional aspects. Biochemical Journal 285.Pt 2 (1992): 345.

[18] Zimmermann, H. Extracellular purine metabolism. Drug Development Research 39.3-4 (1996): 337-352.

[19] Gendron, F. P., et al. Purine signaling and potential new therapeutic approach: possible outcomes of NTPDase inhibition. Current drug targets 3.3 (2002): 229-245.

[20] Fuentes, Eduardo, and Ivan Palomo. Extracellular ATP metabolism on vascular endothelial cells: A pathway with pro-thrombotic and anti- thrombotic molecules. Vascular pharmacology 75 (2015): 1-6.

[21] Fields, R. Douglas, and Geoffrey Burnstock. Purinergic signaling in neuronglia interactions. Nature Reviews Neuroscience 7.6 (2006): 423.

[22] Burnstock, Geoffrey. Short-and long-term (trophic) purinergic signalling. Philosophical Transactions of the Royal Society B: Biological Sciences 371.1700 (2016): 20150422.

[23] La Sala, Andrea, et al. Alerting and tuning the immune response by extracellular nucleotides. Journal of leukocyte biology 73.3 (2003): 339- 343.

[24] Di Virgilio, Francesco. Purinergic mechanism in the immune system: a signal of danger for dendritic cells. Purinergic signaling 1.3 (2005): 205.

[25] Chen, Jiang-Fan, Holger K. Eltzschig, and Bertil B. Fredholm. Adenosine receptors as drug targets—what are the challenges? Nature reviews Drug discovery 12.4 (2013): 265.

[26] de Lera Ruiz, Manuel, Yeon-Hee Lim, and Junying Zheng. Adenosine A2A receptor as a drug discovery target. Journal of medicinal chemistry 57.9 (2013): 3623-3650.

[27] Layland, Jamie, et al. Adenosine: physiology, pharmacology, and clinical applications. JACC: Cardiovascular Interventions 7.6 (2014): 581- 591.

[28] Liu, Hong, and Yang Xia. Beneficial and detrimental role of adenosine signaling in diseases and therapy. Journal of applied physiology 119.10 (2015): 1173-1182.

[29] Borea, Pier Andrea, et al. Adenosine as a multi- signaling guardian angel in human diseases: when, where and how does it exert its protective effects? Trends in pharmacological sciences 37.6 (2016): 419-434.

[30] Burnstock, G., and C. Kennedy. P2X receptors in health and disease. Advances in pharmacology. Vol. 61. Academic Press, 2011. 333-372.

[31] Bartlett, Rachael, Leanne Stokes, and Ronald Sluyter. The P2X7 receptor channel: recent developments and the use of P2X7 antagonists in models of disease. Pharmacological reviews 66.3 (2014): 638-675.

[32] Ford, Anthony P., et al. P2X3 receptors and sensitization of autonomic reflexes. Autonomic Neuroscience 191 (2015): 16-24.

[33] Arulkumaran, Nishkantha, Robert J. Unwin, and Frederick WK Tam. A potential therapeutic role for P2X7 receptor (P2X7R) antagonists in the treatment of inflammatory diseases. Expert opinion on investigational drugs 20.7 (2011): 897-915.

[34] Junger, Wolfgang G. Immune cell regulation by autocrine purinergic signaling. Nature Reviews Immunology 11.3 (2011): 201.

[35] Hansson, Elisabeth, et al. Therapeutic innovation: inflammatory- reactive astrocytes as targets of inflammation. IBRO reports 1 (2016): 1-9.

[36] Burnstock, Geoffrey, and Francesco Di Virgilio. Purinergic signaling and cancer. Purinergic signaling 9.4 (2013): 491-540.

[37] Di Virgilio, Francesco, and Elena Adinolfi. Extracellular purines, purinergic receptors and tumor growth. Oncogene 36.3 (2017): 293.

[38] Romagnoli, Romeo, et al. The P2X7 receptor as a therapeutic target. Expert opinion on therapeutic targets 12.5 (2008): 647-661.

[39] Sawynok, J. Adenosine receptor targets for pain. Neuroscience 338 (2016): 1-18.

[40] Lazarowski, Eduardo R. Vesicular and conductive mechanisms of nucleotide release. Purinergic signaling 8.3 (2012): 359-373.

[41] Bennett, Michael VL, et al. Gap junctions: new tools, new answers, new questions. Neuron 6.3 (1991): 305-320.

[42] Harris, Andrew L. Emerging issues of connexin channels: biophysics fills the gap. Quarterly reviews of biophysics 34.3 (2001): 325-472.

[43] Anselmi, Fabio, et al. ATP release through connexin hemichannels and gap junction transfer of second messengers propagate Ca2+ signals across the inner ear. Proceedings of the National Academy of Sciences 105.48 (2008): 18770-18775.

[44] Laird, Dale W. Life cycle of connexins in health and disease. Biochemical Journal 394.3 (2006): 527-543.

[45] S´aez, Juan C., and Luc Leybaert. Hunting for connexin hemichannels. FEBS letters 588.8 (2014): 1205-1211.

[46] Beyer, Eric C., David L. Paul, and Daniel A. Goodenough. Connexin family of gap junction proteins. Journal of Membrane Biology 116.3 (1990): 187-194.

[47] Bruzzone, Roberto, Thomas W. White, and David L. Paul. Connections with connexins: the molecular basis of direct intercellular signaling. European Journal of Biochemistry 238.1 (1996): 1-27.

[48] Bukauskas, Feliksas F., and Vytas K. Verselis. Gap junction channel gating. Biochimica et Biophysica Acta (BBA)-Biomembranes 1662.1-2 (2004): 42-60.

[49] Muller, Daniel J., et al. Conformational changes in surface structures of isolated connexin 26 gap junctions. The EMBO journal 21.14 (2002): 3598-3607.

[50] Valiunas, Virginijus, and Robert Weingart. Electrical properties of gap junction hemichannels identified in transfected HeLa cells. Pflugers Archiv 440.3 (2000): 366-379.

[51] Beahm, Derek L., and James E. Hall. Hemichannel and junctional properties of connexin 50. Biophysical journal 82.4 (2002): 2016-2031.

[52] G´omez-Hern´andez, Juan M., et al. Molecular basis of calcium regulation in connexin-32 hemichannels. Proceedings of the National Academy of Sciences 100.26 (2003): 16030-16035.

[53] Lopez, William, et al. Insights on the mechanisms of Ca2+ regulation of connexin26 hemichannels revealed by human pathogenic mutations (D50N/Y). The Journal of general physiology 142.1 (2013): 23-35.

[54] Cotrina, Maria Luisa, et al. Connexins regulate calcium signaling by controlling ATP release. Proceedings of the National Academy of Sciences 95.26 (1998): 15735-15740.

[55] De Vuyst, Elke, et al. Intracellular calcium changes trigger connexin 32 hemichannel opening. The EMBO journal 25.1 (2006): 34-44.

[56] De Vuyst, Elke, et al. Ca2+ regulation of connexin 43 hemichannels in C6 glioma and glial cells. Cell calcium 46.3 (2009): 176-187.

[57] Carrer, A., et al., Cx32 hemichannel opening by cytosolic Ca2+ is inhibited by the R220X mutation that causes Charcot-Marie-Tooth disease. Human molecular genetics, 2017. 27.

[58] Dale, Nicholas, and Bruno G. Frenguelli. Release of adenosine and ATP during ischemia and epilepsy. Current neuropharmacology 7.3 (2009): 160-179.

[59] Huckstepp, Robert TR, et al. Connexin hemichannel-mediated CO2- dependent release of ATP in the medulla oblongata contributes to central respiratory chemosensitivity. The Journal of physiology 588.20 (2010): 3901-3920.

[60] Rodriguez, L., et al., Reduced phosphatidylinositol 4,5-bisphosphate synthesis impairs inner ear Ca2+ signaling and high-frequency hearing acquisition. Proceedings of the National Academy of Sciences of the United States of America, 2012. 109(35): p. 14013-14018.

[61] Garcia, Isaac E., et al. ”From hyperactive Connexin26 hemichannels to impairments in epidermal calcium gradient and permeability barrier in the keratitis-ichthyosis-deafness syndrome.” Journal of Investigative Dermatology 136.3 (2016): 574-583.

[62] Eltzschig, Holger K., et al. ATP release from activated neutrophils occurs via connexin 43 and modulates adenosine-dependent endothelial cell function. Circulation research 99.10 (2006): 1100-1108.

[63] Chen, Yu, et al. Purinergic signaling: a fundamental mechanism in neutrophil activation. Sci. Signal. 3.125 (2010): ra45-ra45.

[64] Scemes, Eliana, David C. Spray, and Paolo Meda. Connexins, pannexins, innexins: novel roles of “hemi-channels”. Pflugers Archiv- European Journal of Physiology 457.6 (2009): 1207.

[65] Sosinsky, Gina E., et al. ”Pannexin channels are not gap junction hemichannels.” Channels 5.3 (2011): 193-197.

[66] Boassa, Daniela, et al. Pannexin1 channels contain a glycosylation site that targets the hexamer to the plasma membrane. Journal of Biological Chemistry 282.43 (2007): 31733-31743.

[67] Bruzzone, Roberto, et al. Pannexins, a family of gap junction proteins expressed in brain. Proceedings of the National Academy of Sciences 100.23 (2003): 13644-13649.

[68] Baranova, Ancha, et al. The mammalian pannexin family is homologous to the invertebrate innexin gap junction proteins. Genomics 83.4 (2004): 706-716.

[69] Penuela, Silvia, Ruchi Gehi, and Dale W. Laird. The biochemistry and function of pannexin channels. Biochimica et Biophysica Acta (BBA)- Biomembranes 1828.1 (2013): 15-22.

[70] Patel, Dakshesh, Xian Zhang, and Richard D. Veenstra. Connexin hemichannel and pannexin channel electrophysiology: how do they differ?. FEBS letters 588.8 (2014): 1372-1378.

[71] Bruzzone, Roberto, et al. Pharmacological properties of homomeric and heteromeric pannexin hemichannels expressed in Xenopus oocytes. Journal of neurochemistry 92.5 (2005): 1033-1043.

[72] Bao, Li, Silviu Locovei, and Gerhard Dahl. Pannexin membrane channels are mechanosensitive conduits for ATP. FEBS letters 572.1-3 (2004): 65-68.

[73] Seminario-Vidal, Lucia, et al. Rho signaling regulates pannexin 1- mediated ATP release from airway epithelia. Journal of Biological Chemistry 286.30 (2011): 26277-26286.

[74] Chekeni, Faraaz B., et al. Pannexin 1 channels mediate ‘find-me’signal release and membrane permeability during apoptosis. Nature 467.7317 (2010): 863.

[75] Qiu, Feng, et al. Two non-vesicular ATP release pathways in the mouse erythrocyte membrane. FEBS letters 585.21 (2011): 3430-3435.

[76] Li, Ang, et al. Mechanisms of ATP release by human trabecular meshwork cells, the enabling step in purinergic regulation of aqueous humor outflow. Journal of cellular physiology 227.1 (2012): 172-182.

[77] Qiu, Feng, and Gerhard Dahl. A permeant regulating its permeation pore: inhibition of pannexin 1 channels by ATP. American Journal of Physiology-Cell Physiology 296.2 (2009): C250-C255.

[78] Akopova, Irina, et al. Imaging exocytosis of ATP-containing vesicles with TIRF microscopy in lung epithelial A549 cells. Purinergic signalling 8.1 (2012): 59-70.

[79] Tang, Wenxue, et al. Pannexins are new molecular candidates for assembling gap junctions in the cochlea. Neuroreport 19.13 (2008): 1253.

[80] Wang, Xiao-Hui, et al. Identification and characterization of pannexin expression in the mammalian cochlea. Journal of Comparative Neurology 512.3 (2009): 336-346.

[81] Zhao, Hong-Bo. Expression and function of pannexins in the inner ear and hearing. BMC cell biology 17.1 (2016): 16.

[82] Chen, Jin, et al. Pannexin1 channels dominate ATP release in the cochlea ensuring endocochlear potential and auditory receptor potential generation and hearing. Scientific reports 5 (2015): 10762.

[83] Zorzi, Veronica, et al. Mouse Panx1 is dispensable for hearing acquisition and auditory function. Frontiers in molecular neuroscience 10 (2017): 379.

[84] Abitbol, Julia M., et al. Differential effects of pannexins on noise- induced hearing loss. Biochemical Journal 473.24 (2016): 4665-4680.

[85] Rassendren, Fran¸cois, et al. The permeabilizing ATP receptor, P2X7 cloning and expression of a human cDNA. Journal of Biological Chemistry 272.9 (1997): 5482-5486.

[86] Surprenant, A., et al. The cytolytic P2Z receptor for extracellular ATP identified as a P2X receptor (P2X7). Science 272.5262 (1996): 735-738.

[87] Suadicani, S.O., C.F. Brosnan, and E. Scemes, P2X7 receptors mediate ATP release and amplification of astrocytic intercellular Ca2+ signaling. The Journal of neuroscience: the official journal of the Society for Neuroscience, 2006. 26(5): p. 1378-1385.

[88] Brandao-Burch, Andrea, et al. The P2X7 receptor is an important regulator of extracellular ATP levels. Frontiers in endocrinology 3 (2012): 41.

[89] Di Virgilio, Francesco, et al. The P2X7 receptor in infection and inflammation. Immunity 47.1 (2017): 15-31.

[90] Di Virgilio, Francesco, et al. Extracellular ATP and P2 purinergic signalling in the tumour microenvironment. Nature Reviews Cancer 18.10 (2018): 601.

[91] Lazarowski, Eduardo R., et al. Molecular mechanisms of purine and pyrimidine nucleotide release. Advances in pharmacology. Vol. 61. Academic Press, 2011. 221-261.

[92] Kanner, B. I., and S. Schuldiner. Mechanism of storage and transport of neurotransmitters. CRC Crit. Rev. Biochem 22 (1987): 1-38.

[93] Zimmermann, Herbert. ATP and acetylcholine, equal brethren. Neurochemistry international 52.4-5 (2008): 634-648.

[94] Reimer, Richard J., and Robert H. Edwards. Organic anion transport is the primary function of the SLC17/type I phosphate transporter family. Pflugers Archiv 447.5 (2004): 629-635.

[95] Bankston, Laurie A., and Guido Guidotti. Characterization of ATP Transport into Chromaffin Granule Ghosts SYNERGY OF ATP AND SEROTONIN ACCUMULATION IN CHROMAFFIN GRANULE GHOSTS. Journal of Biological Chemistry 271.29 (1996): 17132- 17138

[96] Sawada, Keisuke, et al. Identification of a vesicular nucleotide transporter. Proceedings of the National Academy of Sciences 105.15 (2008): 5683-5686.

[97] Rettig, Jens, and Erwin Neher. Emerging roles of presynaptic proteins in Ca++-triggered exocytosis. Science 298.5594 (2002): 781-785

[98] Zhang, Xiaodong, et al. Ca2+-dependent synaptotagmin binding to SNAP-25 is essential for Ca2+-triggered exocytosis. Neuron 34.4 (2002): 599-611.

[99] Berridge, Michael J., Martin D. Bootman, and H. Llewelyn Roderick. Calcium: calcium signaling: dynamics, homeostasis and remodelling. Nature reviews Molecular cell biology 4.7 (2003): 517.

[100] Giorgi, Carlotta, et al. Calcium dynamics as a machine for decoding signals. Trends in cell biology 28.4 (2018): 258-273.

[101] Bernardi, Paolo, et al. The mitochondrial permeability transition pore: channel formation by F-ATP synthase, integration in signal transduction, and role in pathophysiology. Physiological reviews 95.4 (2015): 1111-1155.

[102] Rizzuto, Rosario, et al. Ca2+ transfer from the ER to mitochondria: when, how and why. Biochimica et Biophysica Acta (BBA)- Bioenergetics 1787.11 (2009): 1342-1351.

[103] Clapham, David E. Calcium signaling. Cell 131.6 (2007): 1047-1058.

[104] White, Steven M., et al. Calcium signaling pathways utilized by P2X receptors in freshly isolated preglomerular MVSMC. American Journal of Physiology-Renal Physiology 280.6 (2001): F1054-F1061.

[105] Surprenant, Annmarie, and R. Alan North. ”Signaling at purinergic P2X receptors.” Annual review of physiology 71 (2009): 333-359.

[106] Burnstock, Geoffrey, and Jean-Marie Boeynaems. Purinergic signalling and immune cells. Purinergic signaling 10.4 (2014): 529-564.

[107] Mammano, Fabio. ATP-dependent intercellular Ca2+ signaling in the developing cochlea: facts, fantasies and perspectives. Seminars in cell and developmental biology. Vol. 24. No. 1. Academic Press, 2013.

[108] Burnstock, Geoffrey, and Michael Williams. P2 purinergic receptors: modulation of cell function and therapeutic potential. Journal of Pharmacology and Experimental Therapeutics 295.3 (2000): 862-869.

[109] Bjorkgren, Ida, and Polina V. Lishko. Purinergic signaling in testes revealed. The Journal of general physiology 148.3 (2016): 207-211.

[110] Berridge, Michael J. Inositol trisphosphate and calcium signaling mechanisms. Biochimica et Biophysica Acta (BBA)-Molecular Cell Research 1793.6 (2009): 933-940.

[111] Gui, Qingyuan, et al. The application of whole cell-based biosensors for use in environmental analysis and in medical diagnostics. Sensors 17.7 (2017): 1623.

[112] Taniguchi, Akiyoshi. Live cell-based sensor cells. Biomaterials 31.23 (2010): 5911-5915.

[113] Ceriani, Federico, et al. Design and construction of a cost-effective spinning disk system for live imaging of inner ear tissue. Auditory and Vestibular Research. Humana Press, New York, NY, 2016. 223-241.

[114] Gibson, Daniel G., et al.Enzymatic assembly of DNA molecules up to several hundred kilobases. Nature methods 6.5 (2009): 343.

[115] Wang, Xiaoyin, and Michael McManus. Lentivirus production. JoVE (Journal of Visualized Experiments) 32 (2009): e1499.

[116] Erb, Laurie, and Gary A. Weisman. Coupling of P2Y receptors to G proteins and other signaling pathways. Wiley Interdisciplinary Reviews: Membrane Transport and Signaling 1.6 (2012): 789-803.

[117] Merten, Marc D., et al. Characterization of two distinct P2Y receptors in human tracheal gland cells. European journal of biochemistry 251.1-2 (1998): 19-24.

[118] Schachter, Joel B., et al. HEK293 human embryonic kidney cells endogenously express the P2Y1 and P2Y2 receptors. Neuropharmacology 36.9 (1997): 1181-1187.

[119] Levesque, S. A., et al. Specificity of the ecto-ATPase inhibitor ARL 67156 on human and mouse ectonucleotidases. British journal of pharmacology 152.1 (2007): 141-150.

[120] Willebrords, Joost, et al. Inhibitors of connexin and pannexin channels as potential therapeutics. Pharmacology & therapeutics 180 (2017): 144-160.

[121] Silverman, William, Silviu Locovei, and Gerhard Dahl. Probenecid, a gout remedy, inhibits pannexin 1 channels. American Journal of Physiology-Cell Physiology 295.3 (2008): C761-C767.

[122] Ma, Weihong, et al. Pharmacological characterization of pannexin-1 currents expressed in mammalian cells. Journal of Pharmacology and Experimental Therapeutics 328.2 (2009): 409-418.

[123] Wang, Junjie, David George Jackson, and Gerhard Dahl.The food dye FD&C Blue No. 1 is a selective inhibitor of the ATP release channel Panx1. The Journal of general physiology 141.5 (2013): 649-656.

[124] Romanello, Milena, et al. Mechanically induced ATP release from human osteoblastic cells. Biochemical and biophysical research communications 289.5 (2001): 1275-1281.

[125] Frangos, J. A., L. V. McIntire, and S. G. Eskin. Shear stress induced stimulation of mammalian cell metabolism. Biotechnology and bioengineering 32.8 (1988): 1053-1060.

[126] Wada, Ken-Ichi, et al. Live cells-based cytotoxic sensorchip fabricated in a microfluidic system. Biotechnology and bioengineering 99.6 (2008): 1513-1517.

[127] Notingher, Ioan. Raman spectroscopy cell-based biosensors. Sensors 7.8 (2007): 1343-1358.

[128] Azpiazu, Inaki, and N. Gautam. A fluorescence resonance energy transfer-based sensor indicates that receptor access to a G protein is unrestricted in a living mammalian cell. Journal of Biological Chemistry 279.26 (2004): 27709-27718.

[129] Rich, Thomas C., and Jeffrey W. Karpen. cyclic AMP sensors in living cells: what signals can they actually measure?. Annals of biomedical engineering 30.8 (2002): 1088-1099.

[130] Soltoff, Stephen P., et al. Blockade of ATP binding site of P2 purinoceptors in rat parotid acinar cells by isothiocyanate compounds. Biochemical pharmacology 45.9 (1993): 1936-1940.

[131] Tritsch, N.X., et al., The origin of spontaneous activity in the developing auditory system. Nature, 2007. 450: p. 50.

[132] Schutz, Melanie, et al. The human deafness-associated connexin 30 T5M mutation causes mild hearing loss and reduces biochemical coupling among cochlear non-sensory cells in knock-in mice. Human molecular genetics 19.24 (2010): 4759-4773.

[133] Spychala, Jozef. ”Tumor-promoting functions of adenosine.” Pharmacology & therapeutics 87.2-3 (2000): 161-173.

[134] White, Nicholas, and Geoffrey Burnstock. ”P2 receptors and cancer.” Trends in pharmacological sciences 27.4 (2006): 211-217.

[135] Lim, David J. Functional structure of the organ of Corti: a review. Hearing research 22.1-3 (1986): 117-146.

[136] Mammano, Fabio, and Renato Nobili. ”Biophysics of the cochlea: linear approximation.” The Journal of the Acoustical Society of America 93.6 (1993): 3320-3332.

[137] Nobili, R., and F. Mammano. ”Biophysics of the cochlea II: Stationary nonlinear phenomenology.” The Journal of the Acoustical Society of America 99.4 (1996): 2244-2255.

[138] Dedo, Herbert H., and Francis A. Sooy. XVI Endaural Encephalocele and Cerebrospinal Fluid Otorrhea: A Review. Annals of Otology, Rhinology & Laryngology 79.1 (1970): 168-177.

[139] Lim D, Rueda J:Structural development of the cochlea. In Development of Auditory and Vestibular Systems - 2. 1st edition. Edited by Romand R. New York: Elsevier Science Publishing Co., Inc; 1992:33–58. 655 Avenue of America New York, NY 10010. USA, Hardcover: 557 pages. ISBN 10: 0444812636, 13: 978-0444812636.

[140] Kelly, Michael C., and Ping Chen. Development of form and function in the mammalian cochlea. Current opinion in neurobiology 19.4 (2009): 395-401.

[141] Lautermann, Jurgen, et al. Expression of the gap-junction connexins 26 and 30 in the rat cochlea. Cell and tissue research 294.3 (1998): 415-420.

[142] Lautermann, Jurgen, et al. Developmental expression patterns of connexin26 and-30 in the rat cochlea. Developmental genetics 25.4 (1999): 306-311.

[143] Housley, G.D., A. Bringmann, and A. Reichenbach, Purinergic signaling in special senses. Trends in Neurosciences, 2009. 32(3): p. 128-141.

[144] Ashmore, J.F. and H. Ohmori, Control of intracellular calcium by ATP in isolated outer hair cells of the guinea-pig cochlea. The Journal of physiology, 1990. 428: p. 109-131.

[145] Yan, D., et al., Mutation of the ATP-gated P2X(2) receptor leads to progressive hearing loss and increased susceptibility to noise. Proceedings of the National Academy of Sciences of the United States of America, 2013. 110(6): p. 2228-2233.

[146] Frolenkov, G.I., Regulation of electromotility in the cochlear outer hair cell. The Journal of physiology, 2006. 576(Pt 1): p. 43-48.

[147] Gale, J.E., et al., A Mechanism for Sensing Noise Damage in the Inner Ear. Current Biology, 2004. 14(6): p. 526-529.

[148] Beltramello, M., et al., Impaired permeability to Ins(1,4,5)P3 in a mutant connexin underlies recessive hereditary deafness. Nat Cell Biol, 2005. 7(1): p. 63-9.

[149] De Vuyst, E., et al., Connexin hemichannels and gap junction channels are differentially influenced by lipopolysaccharide and basic fibroblast growth factor. Molecular biology of the cell, 2007. 18(1): p. 34-46.

[150] Leybaert, L., et al., Connexins in Cardiovascular and Neurovascular Health and Disease: Pharmacological Implications. Pharmacological reviews, 2017. 69(4): p. 396-478.

[151] Majumder, P., et al., ATP-mediated cell–cell signaling in the organ of Corti: the role of connexin channels. Purinergic signaling, 2010. 6(2): p. 167-187.

[152] Verselis, V.K. and M. Srinivas, Connexin channel modulators and their mechanisms of action. Neuropharmacology, 2013. 75: p. 517-524.

[153] Xu, Liang, et al. Design and characterization of a human monoclonal antibody that modulates mutant connexin 26 hemichannels implicated in deafness and skin disorders. Frontiers in molecular neuroscience 10 (2017): 298.

[154] Ortolano, S., et al., Coordinated control of connexin 26 and connexin 30 at the regulatory and functional level in the inner ear. Proceedings of the National Academy of Sciences of the United States of America, 2008. 105(48): p. 18776-18781.

[155] Teubner, Barbara, et al. Connexin30 (Gjb6)-deficiency causes severe hearing impairment and lack of endocochlear potential. Human molecular genetics 12.1 (2003): 13-21.

[156] Huang, Y.-J., et al., The role of pannexin 1 hemichannels in ATP release and cell-cell communication in mouse taste buds. Proceedings of the National Academy of Sciences of the United States of America, 2007. 104(15): p. 6436-6441.

[157] Pellegatti, P., et al., A novel recombinant plasma membrane-targeted luciferase reveals a new pathway for ATP secretion. Molecular biology of the cell, 2005. 16(8): p. 3659-3665.

[158] Diaspro, Alberto, et al. Multi-photon excitation microscopy. Biomedical engineering online 5.1 (2006): 36.

[159] Bosen, Felicitas, et al. The Clouston syndrome mutation connexin30 A88V leads to hyperproliferation of sebaceous glands and hearing impairments in mice. FEBS letters 588.9 (2014): 1795-1801.

[160] Ceriani, Federico, and Fabio Mammano. Calcium signaling in the cochlea–Molecular mechanisms and physiopathological implications. Cell Communication and Signaling 10.1 (2012): 20.

[161] Chan, Dylan K., and Stephanie L. Rouse. Sound-induced intracellular Ca2+ dynamics in the adult hearing cochlea. PloS one 11.12 (2016): e0167850.

[162] Braet, Katleen, et al. ”Pharmacological sensitivity of ATP release triggered by photoliberation of inositol-1, 4, 5-trisphosphate and zero extracellular calcium in brain endothelial cells.” Journal of cellular physiology 197.2 (2003): 205-213.

[163] Mammano, Fabio. ”Inner ear connexin channels: roles in development and maintenance of cochlear function.” Cold Spring Harbor Perspectives in Medicine 9.7 (2019): a033233.

[164] Cohen-Salmon, Martine, et al. Targeted ablation of connexin26 in the inner ear epithelial gap junction network causes hearing impairment and cell death. Current Biology 12.13 (2002): 1106-1111.

[165] Crispino, Giulia, et al. BAAV mediated GJB2 gene transfer restores gap junction coupling in cochlear organotypic cultures from deaf Cx26Sox10Cre mice. PloS one 6.8 (2011): e23279.

[166] Boulay, Anne-C´ecile, et al. Hearing is normal without connexin30. Journal of Neuroscience 33.2 (2013): 430-434.

[167] Johnson, Stuart L., et al. Connexin-mediated signaling in nonsensory cells is crucial for the development of sensory inner hair cells in the mouse cochlea. Journal of Neuroscience 37.2 (2017): 258-268.

[168] Ceriani, Federico, et al. Coordinated calcium signaling in cochlear sensory and non-sensory cells refines afferent innervation of outer hair cells. The EMBO Journal 38.9 (2019).

[169] Essenfelder, Guilherme Munhoz, et al. Connexin30 mutations responsible for hidrotic ectodermal dysplasia cause abnormal hemichannel activity. Human molecular genetics 13.16 (2004): 1703-1714.

[170] Kelly, John J., et al. The connexin 30 A88V mutant reduces cochlear gap junction expression and confers long-term protection against hearing loss. J Cell Sci 132.2 (2019): jcs224097.

[171] Zheng, Q.Y., K.R. Johnson, and L.C. Erway, Assessment of hearing in 80 inbred strains of mice by ABR threshold analyses. Hearing Research, 1999. 130(1): p. 94-107.

[172] Zhou, X., et al., Auditory brainstem responses in 10 inbred strains of mice. Brain Research, 2006. 1091(1): p. 16-26.

[173] Legatt, A.D., Mechanisms of intraoperative brainstem auditory evoked potential changes. Journal of clinical neurophysiology, 2002. 19(5): p. 396-408.

[174] Hanstein, R., et al., Promises and pitfalls of a Pannexin1 transgenic mouse line. Frontiers in pharmacology, 2013. 4: p. 61-61.

[175] Bargiotas, P., et al., Pannexins in ischemia-induced neurodegeneration. Proceedings of the National Academy of Sciences, 2011. 108(51): p. 20772-20777.

[176] Frolenkov, G.I., et al., The Membrane-based Mechanism of Cell Motility in Cochlear Outer Hair Cells. Molecular Biology of the Cell, 1998. 9(8): p. 1961-1968.

[177] Nobili, R., F. Mammano, and J. Ashmore, How well do we understand the cochlea? Trends in Neurosciences, 1998. 21(4): p. 159-167.

[178] Ashmore, J., Cochlear outer hair cell motility. Physiological reviews, 2008. 88(1): p. 173-210.

[179] Tritsch, Nicolas X., and Dwight E. Bergles. Developmental regulation of spontaneous activity in the Mammalian cochlea. Journal of Neuroscience 30.4 (2010): 1539-1550.

[180] Chan, Dylan K., and Kay W. Chang. GJB2-associated hearing loss: Systematic review of worldwide prevalence, genotype, and auditory phenotype. The Laryngoscope 124.2 (2014): E34-E53.

[181] Kenneson, Aileen, Kim Van Naarden Braun, and Coleen Boyle. GJB2 (connexin 26) variants and nonsyndromic sensorineural hearing loss: a HuGE review. Genetics in Medicine 4.4 (2002): 258.

[182] Snoeckx, Rikkert L., et al. GJB2 mutations and degree of hearing loss: a multicenter study. The American Journal of Human Genetics 77.6 (2005): 945-957.

[183] Berger, Amy C., et al. Mutations in Cx30 that are linked to skin disease and non-syndromic hearing loss exhibit several distinct cellular pathologies. J Cell Sci 127.8 (2014): 1751-1764.

[184] Dolmetsch, Ricardo E., Keli Xu, and Richard S. Lewis. Calcium oscillations increase the efficiency and specificity of gene expression. Nature 392.6679 (1998): 933.

[185] Li, Wen-hong, et al. Cell-permeant caged InsP 3 ester shows that Ca 2+ spike frequency can optimize gene expression. Nature 392.6679 (1998): 936.

[186] Fetoni, Anna Rita, et al. Cx26 partial loss causes accelerated presbycusis by redox imbalance and dysregulation of Nfr2 pathway. Redox biology 19 (2018): 301-317.

[187] Menardo, J., et al., Oxidative Stress, Inflammation, and Autophagic Stress as the Key Mechanisms of Premature Age-Related Hearing Loss in SAMP8 Mouse Cochlea. Antioxidants & Redox Signaling, 2011. 16(3): p. 263-274

[188] Falzoni, Simonetta, Giovanna Donvito, and Francesco Di Virgilio. Detecting adenosine triphosphate in the pericellular space. Interface focus 3.3 (2013): 20120101.

[189] Yegutkin, Gennady G. Enzymes involved in metabolism of extracellular nucleotides and nucleosides: functional implications and measurement of activities. Critical reviews in biochemistry and molecular biology 49.6 (2014): 473-497.

[190] Ohta, Akio, et al. A2A adenosine receptor protects tumors from anti-tumor T cells. Proceedings of the National Academy of Sciences 103.35 (2006): 13132-13137.

[191] Di Virgilio, Francesco. Purines, purinergic receptors, and cancer. Cancer research 72.21 (2012): 5441-5447.

[192] Ghiringhelli, Fran¸cois, et al. Activation of the NLRP3 inflammasome in dendritic cells induces IL-1β–dependent adaptive immunity against tumors. Nature medicine 15.10 (2009): 1170.

[193] Di Virgilio, Francesco, Davide Ferrari, and Elena Adinolfi. P2X7: a growth-promoting receptor—implications for cancer. Purinergic signalling 5.2 (2009): 251-256.

[194] Adinolfi, Elena, et al. Basal activation of the P2X7 ATP receptor elevates mitochondrial calcium and potential, increases cellular ATP levels, and promotes serum-independent growth. Molecular biology of the cell 16.7 (2005): 3260-3272.

[195] Adinolfi, Elena, et al. Trophic activity of a naturally occurring truncated isoform of the P2X7 receptor. The FASEB Journal 24.9 (2010): 3393-3404.

[196] Jelassi, B., et al. P2X 7 receptor activation enhances SK3 channels-and cystein cathepsin-dependent cancer cells invasiveness. Oncogene 30.18 (2011): 2108.

[197] Miller, Janet C., et al. Imaging angiogenesis: applications and potential for drug development. Journal of the National Cancer Institute 97.3 (2005): 172-187.

[198] Lee, T. Y., T. G. Purdie, and E. Stewart. CT imaging of angiogenesis. The Quarterly Journal of Nuclear Medicine and Molecular Imaging 47.3 (2003): 171.

[199] Adinolfi, Elena, et al. Accelerated tumor progression in mice lacking the ATP receptor P2X7. Cancer research 75.4 (2015): 635-644.

[200] Mocellin, Simone, and Maurizio Provenzano. ”RNA interference: learning gene knock-down from cell physiology.” Journal of translational medicine 2.1 (2004): 39.

[201] Sim, Joan A., et al. Reanalysis of P2X7 receptor expression in rodent brain. Journal of Neuroscience 24.28 (2004): 6307-6314.

[202] Makale, Milan. Intravital imaging and cell invasion. Methods in enzymology 426 (2007): 375-401.

[203] Alieva, Maria, et al. Imaging windows for long-term intravital imaging: General overview and technical insights. Intravital 3.2 (2014): e29917.

[204] Plaetzer, Kristjan, et al. ”Photophysics and photochemistry of photo-dynamic therapy: f undamental aspects.” Lasers in medical science 24.2 (2009): 259-268.

[205] Dahle, Jostein, et al. ”The bystander effect in photodynamic inactivation of cells.” Biochimica et Biophysica Acta (BBA)-General Subjects 1475.3 (2000): 273-280.

[206] Prise, Kevin M., and Joe M. O’sullivan. ”Radiation-induced bystander signaling in cancer therapy.” Nature Reviews Cancer 9.5 (2009): 351.

[207] Tsukimoto, Mitsutoshi, et al. ”Involvement of purinergic signaling in cellular response to γ radiation.” Radiation research 173.3 (2009): 298- 309.

[208] Ohshima, Yasuhiro, et al. ”Involvement of connexin43 hemichannel in ATP release after γ-irradiation.” Journal of radiation research 53.4 (2012): 551-557.

[209] Mancuso, M., et al. ”Role of connexin43 and ATP in long-range by- stander radiation damage and oncogenesis in vivo.” Oncogene 30.45 (2011): 4601.

[210] Nardin, Chiara, et al. ”Photosensitizer Activation Drives Apoptosis by Interorganellar Ca2+ Transfer and Superoxide Production in Bystander Cancer Cells.” Cells 8.10 (2019): 1175.

[211] Guldberg, R. E., et al. Analyzing bone, blood vessels, and biomaterials with microcomputed tomography. IEEE engineering in medicine and biology magazine 22.5 (2003): 77-83.

[212] Stauber, Martin, and Ralph Muller. Micro-computed tomography: a method for the non-destructive evaluation of the three-dimensional structure of biological specimens. Osteoporosis. Humana Press, 2008. 273-292.

[213] Lee, Sang Chul, et al. A flat-panel detector based micro-CT system: performance evaluation for small-animal imaging. Physics in Medicine and Biology 48.24 (2003): 4173.

[214] Conway, James RW, Neil O. Carragher, and Paul Timpson. Developments in preclinical cancer imaging: innovating the discovery of therapeutics. Nature Reviews Cancer 14.5 (2014): 314.

[215] Giorgi, Carlotta, et al. Intravital imaging reveals p53-dependent cancer cell death induced by phototherapy via calcium signaling. Oncotarget 6.3 (2015): 1435.

[216] Calì, Bianca, et al. Critical role of gap junction communication, calcium and nitric oxide signaling in bystander responses to focal photodynamic injury. Oncotarget 6.12 (2015): 10161.

[217] Bianchi, G., et al. ATP/P2X7 axis modulates myeloid-derived suppressor cell functions in neuroblastoma microenvironment. Cell death & disease 5.3 (2014): e1135.

[218] Quail, Daniela F., and Johanna A. Joyce. Microenvironmental regulation of tumor progression and metastasis. Nature medicine 19.11 (2013): 1423.

[219] Corbet, Cyril, and Olivier Feron. Tumour acidosis: from the passenger to the driver's seat. Nature Reviews Cancer 17.10 (2017): 577.

[220] Hanahan, Douglas, and Robert A. Weinberg. Hallmarks of cancer: the next generation. cell 144.5 (2011): 646-674.

[221] Kepp, Oliver, et al. Extracellular nucleosides and nucleotides as immunomodulators. Immunological reviews 280.1 (2017): 83-92.

[222] Shabbir, Majid, et al. Effect of extracellular ATP on the growth of hormone-refractory prostate cancer in vivo. BJU international 102.1 (2008): 108-112.

[223] Xie, Rui, et al. "The P2Y2 nucleotide receptor mediates the proliferation and migration of human hepatocellular carcinoma cells induced by ATP." Journal of Biological Chemistry 289.27 (2014): 19137-19149.

[224] Vijayan, Dipti, et al. Targeting immunosuppressive adenosine in cancer. Nature Reviews Cancer 17.12 (2017): 709.

[225] Marcus, Aaron J., et al. Metabolic control of excessive extracellular nucleotide accumulation by CD39/ecto-nucleotidase-1: implications for ischemic vascular diseases. Journal of Pharmacology and Experimental Therapeutics 305.1 (2003): 9-16.

[226] Furlow, Paul W., et al. Mechanosensitive pannexin 1 channels mediate microvascular metastatic cell survival. Nature cell biology 17.7 (2015): 943.

[227] Burma, Nicole E., et al. Blocking microglial pannexin-1 channels alleviates morphine withdrawal in rodents. Nature medicine 23.3 (2017): 355.

[228] Hatfield, Stephen M., et al. Immunological mechanisms of the antitumor effects of supplemental oxygenation. Science translational medicine 7.277 (2015): 277ra30-277ra30.

[229] Beigi, Reza, et al. Detection of local ATP release from activated platelets using cell surface-attached firefly luciferase. American Journal of Physiology-Cell Physiology 276.1 (1999): C267-C278.

[230] Conley, Jason M., et al. Imaging extracellular ATP with a genetically- encoded, ratiometric fluorescent sensor. PloS one 12.11 (2017): e0187481.

[231] Schneider, Stefan W., et al. Continuous detection of extracellular ATP on living cells by using atomic force microscopy. Proceedings of the National Academy of Sciences 96.21 (1999): 12180-12185.

[232] Hayashi, Seiji, et al. Detecting ATP release by a biosensor method. Science Signaling 2004.258 (2004): pl14-pl14.

[233] Corriden, Ross, Paul A. Insel, and Wolfgang G. Junger. A novel method using fluorescence microscopy for real-time assessment of ATP release from individual cells. American Journal of Physiology-Cell Physiology 293.4 (2007): C1420-C1425.

[234] Llaudet, Enrique, et al. Microelectrode biosensor for real-time measurement of ATP in biological tissue. Analytical chemistry 77.10 (2005): 3267-3273.

[235] Pirotton, Sabine, et al. Endothelial P2-purinoceptors: subtypes and signal transduction. Journal of autonomic pharmacology 16.6 (1996): 353-356.

[236] Hill, Lindsay M., et al. Extracellular ATP may contribute to tissue repair by rapidly stimulating purinergic receptor X7-dependent vascular endothelial growth factor release from primary human monocytes. The Journal of Immunology 185.5 (2010): 3028-3034.

[237] Amoroso, Francesca, et al. The P2X7 receptor is a key modulator of the PI3K/GSK3β/VEGF signaling network: evidence in experimental neuroblastoma. Oncogene 34.41 (2015): 5240.

[238] Nyangoga, Herv´e, et al. Three-dimensional characterization of the vascular bed in bone metastasis of the rat by microcomputed tomography (MicroCT). PLoS One 6.3 (2011): e17336.

[239] Downey, Charlene M., et al. Quantitative ex-vivo micro-computed tomographic imaging of blood vessels and necrotic regions within tumors. PloS one 7.7 (2012): e41685.